

# RCA REVIEW

*a technical journal*

RADIO AND ELECTRONICS  
RESEARCH • ENGINEERING

**VOLUME XVI**

**SEPTEMBER 1955**

**NO. 3**

RADIO CORPORATION OF AMERICA

DAVID SARNOFF, *Chairman of the Board*

FRANK M. FOLSOM, *President*

CHARLES B. JOLLIFFE, *Vice President and Technical Director*

JOHN Q. CANNON, *Secretary*

ERNEST B. GORIN, *Vice President and Treasurer*

---

RCA LABORATORIES

E. W. ENGSTROM, *Executive Vice President*

---

RCA REVIEW

C. C. FOSTER, *Manager*

CHARLES H. VOSE, *Business Manager*

---

*Copyright, 1955, by RCA Laboratories, Radio Corporation of America*

---

PRINTED IN U.S.A.

RCA REVIEW, published quarterly in March, June, September, and December by RCA Laboratories, Radio Corporation of America, Princeton, New Jersey. Entered as second class matter July 3, 1950 at the Post Office at Princeton, New Jersey, under the act of March 3, 1879. Subscription price in the United States and Canada; one year \$2.00, two years \$3.50, three years \$4.50; in other countries: one year \$2.40, two years \$4.30, three years \$5.70. Single copies in the United States, \$.75; in other countries, \$.85.

# RCA REVIEW

*a technical journal*

RADIO AND ELECTRONICS  
RESEARCH • ENGINEERING

*Published quarterly by*

RCA LABORATORIES

*in cooperation with all subsidiaries and divisions of*

RADIO CORPORATION OF AMERICA

---

---

VOLUME XVI

SEPTEMBER, 1955

NUMBER 3

---

---

## CONTENTS

	PAGE
A Beam Power Tube for Ultra-High-Frequency Service .....	321
W. P. BENNETT	
Simplified Design Procedures for Tuned Transistor Amplifiers .....	339
C. C. CHENG	
The Natural Equivalent Circuit of Junction Transistors .....	360
J. ZAWELS	
Frequency Characteristics of Local Oscillators .....	379
W. Y. PAN	
Methods for Revealing P-N Junctions and Inhomogeneities in Ger- manium Crystals .....	398
J. I. PANKOVE	
Stabilization of Pulse Duration in Monostable Multivibrators .....	403
A. C. LUTHER, JR.	
Periodic Magnetic Field Focusing for Low-Noise Traveling-Wave Tubes .....	423
K. K. N. CHANG	
System Parameters Using Tropospheric Scatter Propagation .....	432
H. H. BEVERAGE, E. A. LAPORT, AND L. C. SIMPSON	
Extension of "The Effect of Initial Noise Current and Velocity Cor- relation on The Noise Figure of Traveling-Wave Tubes".....	458
W. R. BEAM	
On the Problem of Optimum Detection of Pulsed Signals in Noise....	461
A. H. BENNER AND R. F. DRENICK	
RCA TECHNICAL PAPERS .....	480
AUTHORS .....	484

---

**RCA REVIEW** is regularly abstracted and indexed by *Industrial Arts Index*, *Science Abstracts* (I.E.E.-Brit.), *Electronic Engineering Master Index*, *Chemical Abstracts*, *Proc. I.R.E.*, and *Wireless Engineer*.

# RCA REVIEW

---

## BOARD OF EDITORS

### *Chairman*

R. S. HOLMES  
*RCA Laboratories*

M. C. BATSEL  
*Engineering Products Division*

G. L. BEERS  
*Radio Corporation of America*

H. H. BEVERAGE  
*RCA Laboratories*

G. H. BROWN  
*RCA Laboratories*

I. F. BYRNES  
*Radiomarine Corporation of America*

D. D. COLE  
*RCA Victor Television Division*

O. E. DUNLAP, JR.  
*Radio Corporation of America*

E. W. ENGSTROM  
*RCA Laboratories*

D. H. EWING  
*RCA Laboratories*

A. N. GOLDSMITH  
*Consulting Engineer, RCA*

O. B. HANSON  
*Radio Corporation of America*

E. W. HEROLD  
*RCA Laboratories*

R. F. HOLTZ  
*RCA International Division*

C. B. JOLLIFFE  
*Radio Corporation of America*

E. A. LAPORT  
*Radio Corporation of America*

C. W. LATIMER  
*RCA Communications, Inc.*

H. W. LEVERENZ  
*RCA Laboratories*

G. F. MAEDEL  
*RCA Institutes, Inc.*

H. B. MARTIN  
*Radiomarine Corporation of America*

H. F. OLSON  
*RCA Laboratories*

D. S. RAU  
*RCA Communications, Inc.*

D. F. SCHMIT  
*Radio Corporation of America*

S. W. SEELEY  
*RCA Laboratories*

G. R. SHAW  
*Tube Division*

R. E. SHELBY  
*National Broadcasting Company, Inc.*

A. W. VANCE  
*RCA Laboratories*

A. F. VAN DYCK  
*Radio Corporation of America*

I. WOLFF  
*RCA Laboratories*

### *Secretary*

C. C. FOSTER  
*RCA Laboratories*

---

## REPUBLICATION AND TRANSLATION

Original papers published herein may be referenced or abstracted without further authorization provided proper notation concerning authors and source is included. All rights of republication, including translation into foreign languages, are reserved by RCA Review. Requests for republication and translation privileges should be addressed to *The Manager*.

# A BEAM POWER TUBE FOR ULTRA-HIGH-FREQUENCY SERVICE\*

By

W. P. BENNETT

Tube Division, Radio Corporation of America  
Lancaster, Pa.

*Summary*—This paper describes a new beam power tetrode, the 6448, designed specifically for operation as a grid-driven (grounded-cathode) amplifier at frequencies up to 1000 megacycles. Although this type is specifically suited to meet the stringent requirements of television broadcast service, it is also useful in the generation of higher powers in almost all types of service at frequencies up to and above 1000 megacycles.

A combination of features in the 6448 makes satisfactory grid-driven performance, with its attendant low drive requirements, practical. In the cylindrically symmetrical electrode structure, a centrally located plate is surrounded by an array of unit tetrode electron-optical systems. The geometry of each tetrode unit is similar to that used in conventional beam power tubes. Effective internal bypass capacitors are provided in the screen-grid-to-cathode circuit. The arrangement of electrode supports and conducting leads provides isolated input and output circuits having no common current paths. This arrangement, in conjunction with a very low plate-to-control-grid capacitance, results in a virtual elimination of feedback effects. Consequently, neutralization is unnecessary.

Other noteworthy features of the 6448 such as the thoriated-tungsten filaments and the ceramic insulators are also discussed. Characteristics of the tube are presented, together with data showing performance in television and continuous-wave service. Circuits for use at 900 megacycles are described. Suitability of the tube for the transmission of color-television signals is discussed.

## INTRODUCTION

SHORTLY after World War II, it became evident that television broadcasting would eventually expand into the ultra-high-frequency (UHF) bands, and that the transmission of color as well as black-and-white pictures would eventually be required. Transmitting tubes available at that time were inadequate for the generation of the high-power signals required for UHF propagation. Although parallel operation of tubes could be used to obtain higher powers,<sup>1,2</sup> the use

\* Decimal Classification: R583.4.

<sup>1</sup>G. H. Brown, W. C. Morrison, W. L. Behrend and J. G. Reddeck, "Method of Multiple Operation of Transmitting Tubes Particularly Adopted for Television Transmission in the Ultra-High-Frequency Band," *RCA Review*, Vol. 10, p. 161, June, 1949.

<sup>2</sup>J. R. Bennett and L. S. Lappin, "A New Ultra-High-Frequency Television Transmitter," *RCA Review*, Vol. 11, p. 190, June, 1950.

of a single tube for each chosen power level was desirable technically, as well as economically sound. Development work was started, therefore, on a transmitting tube capable of delivering a power output of 5 to 10 kilowatts in UHF color or black-and-white television service.

In the early phases of the development, very little was known about the requirements for color-television transmission. Consequently, the major objective of the tube development program was versatility with regard to class of service, frequency coverage, and ability to operate in broadband circuits. High-quality performance, long and reliable service life, and simplicity for the end users were placed above all other considerations.

Desirable characteristics for r-f power amplifier tubes for UHF service include the following items:

- (1) Long, reliable service life.
- (2) Simple, trouble-free auxiliary circuits requiring only simple adjustments.
- (3) Coverage of the entire UHF band.
- (4) High power gain.
- (5) Very little coupling between input and output circuits.
- (6) Maximum versatility and high efficiency of operation in all classes of service.

For use in television service, a power amplifier should also have (a) ability to operate in broad-band circuits, (b) proper phase response, and (c) linearity. Phase response and linearity assume special importance for the faithful transmission of color signals under the present FCC standards.

## DESIGN CONSIDERATIONS

### *Cathode Structure*

Thoriated-tungsten filaments are used in the 6448 to provide long, reliable service life and high current capabilities. A mechanically stable support structure is provided by the use of a cooled, heat-resistant spring to apply tension to each filament as it is held in place in a V-groove. Because the array of directly heated filaments is divided into two sections, a simple 2-phase a-c supply may be used for filament excitation and, as a result, hum-free operation may be obtained.

### *Electron-Gun Structure*

Study of several types of electron-gun structures indicated that the gun used in beam power tubes provides the desirable characteristics

listed above. The fine-grain, closely spaced, aligned-wire geometry of the tetrode configuration has proven its ability to provide high power gain, low feedback effects, high efficiency, and versatility in small power tubes. The extension of this gun design for use at higher voltages, higher current densities, and ultra-high frequencies was limited only by mechanical problems encountered in the design of well-cooled, stable, electrically sound supporting structures.

The elements of the beam-power-tube electron gun, shown in Figure 1, are the cathode, the aligned lateral wires of the control grid

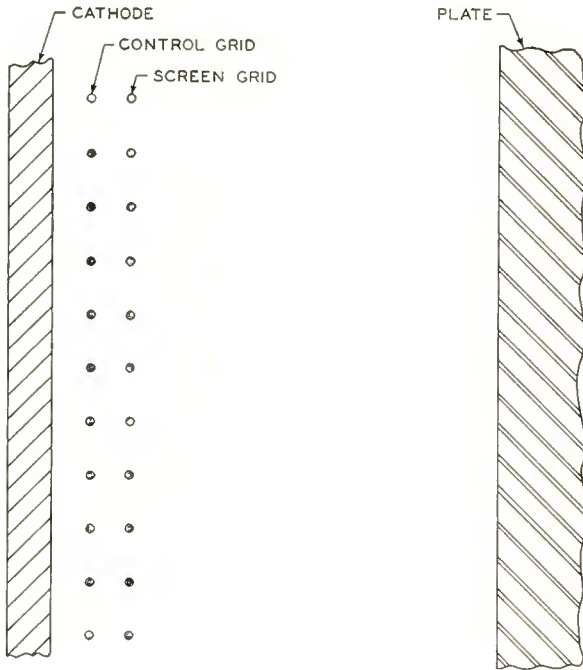


Fig. 1—Elements of the beam power tube gun as used in the 6448.

and screen grid, and the plate. It is of the utmost importance that these elements be supported to insure mechanical stability during thermal cycling under operating conditions. Furthermore, thermal isolation of the cathode is essential. Consideration must also be given to the provision of adequate cooling for all other elements of the gun.

#### *Tube Configuration*

The full benefits of this electron gun are realized only when the tube is operated as a grid-driven (grounded-cathode) device. For this type of operation, an internal r-f short-circuit path is provided between

the screen grid and cathode or ground. Feedback effects are minimized by the provision of separate circuits for input and output currents, i.e., a path for the r-f input circulating currents distinct from that used by the output currents. The tube configuration which combines these features and also satisfies the requirements listed previously is, in effect, built inside out. In this design, the plate is the centrally located member, which is surrounded, in turn, by the screen grid, control grid, and filament elements.

An important factor in the solution of the interrelated electrical, mechanical, and thermal problems is the special construction of the screen-grid and control-grid assemblies. A massive, water-cooled, copper ring clamped between two flat copper plates forms the support structure for the screen grid. The copper plates, which constitute the filament-supporting structure, are insulated from the screen-grid ring by means of mica sheets. These mica insulators act as the screen-to-cathode, or screen-to-ground, bypass capacitors. Copper fins brazed to the inner diameter of the massive, water-cooled, copper ring project radially inward and pass between adjacent individual filament strands and control-grid units. A continuous, cylindrical, screen-grid surface is provided by windows or frames brazed to the inner edges of the fins which contain the electron apertures in the form of lateral wires wound and peened in copper lands. The lateral screen wires are aligned with similar lateral wires on the control-grid units. This screen grid has exceptional heat-dissipation capabilities because the wires are connected by a short continuous path to a water-cooled copper ring.

The control-grid assembly consists of an array of 40 sturdy channel-shaped copper members brazed to a heavy copper base. The base, in turn, is bolted to a water-cooled copper member which constitutes the external control-grid terminal. Lateral wires are wound across the open side of the copper channels to form the control-grid apertures. The exceptional heat-dissipation capability of the control grid is evidenced by the absence of any observable grid emission, even at the highest operating levels to which the tubes have been subjected.

#### DESCRIPTION OF TUBE

This beam power tube, the 6448, meets all the requirements for the transmission of a high-quality 12-to-15-kilowatt color or black-and-white television signal over the entire UHF television band. In such service, the 6448 has a power gain greater than 15, and can be driven adequately by a single 6181<sup>3</sup> or similar 1-kilowatt tube. The 6448 is

---

<sup>3</sup> W. P. Bennett and H. F. Kazanowski, "One-Kilowatt Tetrode for UHF Transmitters," *Proc. I.R.E.*, Vol. 41, p. 13. January, 1953.

also well suited to all types of amplifier service at lower frequencies and at frequencies up to and above 1000 megacycles.

A photograph of the 6448 ceramic-seal, water-cooled UHF beam power tube is shown in Figure 2. Two ceramic vacuum seals are located at opposite ends of the central cylindrical metal housing. The lower or input end of the tube, which contains the cylindrical r-f control-grid terminal, is almost hidden from view at the bottom of the photograph. The upper or output end contains the plate and cathode terminals. The projections at the input end of the tube include the electrical and water connections for the screen grid and the filament. These connec-

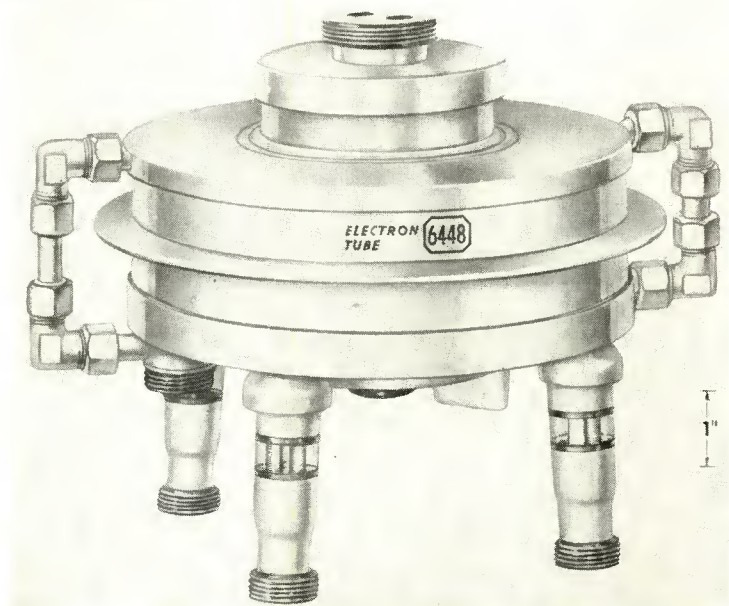


Fig. 2—6448 UHF ceramic-seal, water-cooled beam power tube.

tions project through the main metal housing on insulating bushings. The main metal housing of the tube is at cathode or ground potential.

The view of the input end of the tube in Figure 3 shows the cylindrical symmetry of the r-f terminals and the nature of the conveniently threaded combination electrical-and-water connectors provided for the screen grid, the two filament sections, the cathode, and the control grid. Water paths are provided in all the internal electrode-supporting parts, as well as in the two metal end plates, to provide complete and efficient cooling. The external metallic portions of the tube are silver-plated to provide high-conductivity r-f contact areas, as well as to maintain a good appearance.

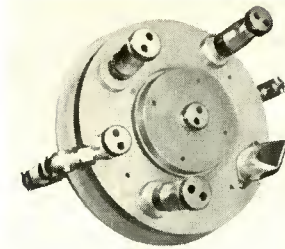


Fig. 3—Input end of 6448 showing r-f terminals and combination electrical and water connections for filament, cathode, and grids.

#### DESIGN FEATURES

In the photograph of the 6448 tube shown in Figure 4, a portion of the external shell has been cut away to show the internal construction. The most unusual feature about the construction of the 6448 is its "inverted" configuration. The internal plate is surrounded in turn by the screen grid, the control grid, and finally, the cathode elements. The active input-electrode region consists of an array of 40 identical unit tetrode electron-optical systems arranged in a cylindrical symmetrical array about the centrally located single cylindrical plate.

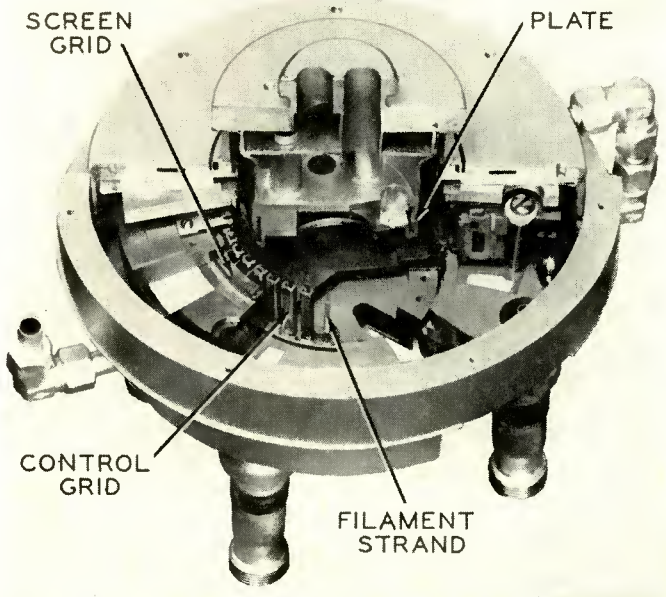


Fig. 4—Cutaway view of tube showing internal construction.

The internal screen bypass capacitors, in conjunction with the appropriate arrangement of the supporting structures and r-f terminals, make UHF grid-driven operation practical, without appreciable feedback or need for neutralization. Although one of the output terminals is conveniently at d-c ground or cathode potential, it is in effect the r-f screen grid connection as a consequence of the internal screen-to-cathode bypass capacitors. When this arrangement is used, there are no current paths common to both input and output circulating displacement currents.

Another important feature of the 6448 is the use of individually supported, directly-heated, thoriated-tungsten filaments. It is believed that this tube is the only large commercial UHF power tube which employs the type of emitter currently accepted as the standard of the industry for long service life.

The 40 tetrode units are disposed in a circular array about the central plate. The filaments of the 40 units are clipped into V-groove slots in a water-cooled copper ring which serves as the input cathode terminal of the tube. The filaments are supported at their upper ends by 40 individual spring members which maintain accurate positioning as the filaments contract and expand during operational cycling.

#### CERAMIC-TO-METAL SEALS

A further important feature of the tube construction is the use of high-strength, low-loss, alumina ceramics for the insulating members in the two envelope vacuum seals at which r-f voltages are applied. The ceramic-to-metal seals, similar to those developed by P. T. Smith,<sup>4</sup> are made as follows: A thin metal coating consisting of a finely powdered mixture of molybdenum and manganese is applied to the ends of the ceramic cylinders. High-temperature firing causes this metal coating to adhere to the ceramic. The ceramic is then nickel-plated, and is brazed to a 0.020-inch copper envelope part to complete the vacuum seal. Because the copper member is relatively thin and the ceramic is relatively strong, the difference in thermal expansion between the ceramic and copper is taken up by deformation of the copper. This type of seal provides an almost ideal circuit configuration having no discontinuous flanges.

#### UNIT ELECTRODES

Figure 5 is an enlarged scale drawing showing a cross section of

---

<sup>4</sup> P. T. Smith, "Some New Ultra-High-Frequency Power Tubes," *RCA Review*, Vol. 13, p. 224, June, 1952.

two of the 40 unit tetrodes. A detailed description of the internal construction of the tube must begin with the description of one of these units.

The unit filament is surrounded by the unit control-grid electrode. The grid consists of a channel-shaped copper member, across the open side of which 0.0036-inch-diameter platinum-clad molybdenum wires are wound at a pitch of 36 turns per inch and peened into place. The spacing between the grid wires and the cathode is about 0.020 inch. Because the open space in back of the cathode is about three times the space in front, and because the field from the screen voltage reaches

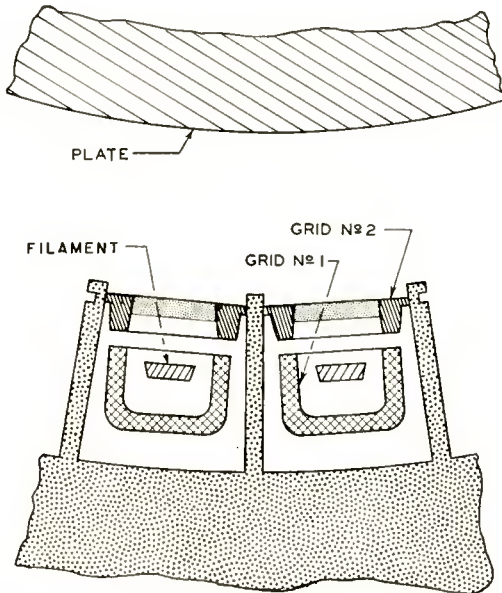


Fig. 5—Enlarged drawing of two unit tetrodes.

through the openings in the front wire section of the control grid, most electrons leave the wide face of the filament and pass through the grid and screen to the plate region. Very few electrons are drawn from the back of the cathode to the opaque grid box.

The unit screen grid, which surrounds the unit control grid, consists of radial fins attached to the massive water-cooled copper block and a front window panel on which the lateral wires are wound and peened, as in the control grid. During the assembly of the tube, the wires of each screen window are adjusted so that they are aligned with the wires of the corresponding control-grid unit. The screen-grid wires are then permanently brazed in place to the radial fins. The electrode

geometry of each of these units is similar to that of beam power tubes such as the 6L6 and 807.

The active unit electrode parts are shown in Figure 6. The thoriated-tungsten filaments contain a temperature-correction section at each end of the  $\frac{3}{4}$ -inch long central emitting portion. This end section has a reduced cross-sectional area which compensates for the heat conducted out at the ends of the filament in contact with the cooled supporting structure. Thus, a uniform temperature is maintained over

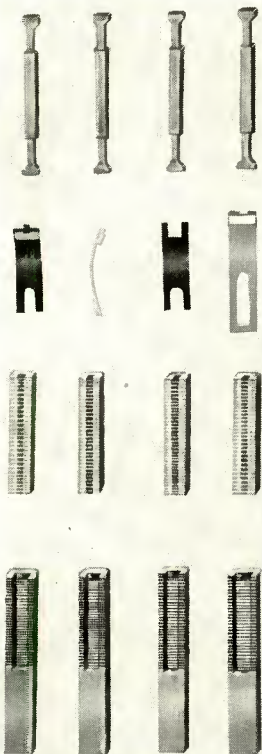


Fig. 6—Active unit electrode parts. Top to bottom: unit filament, filament springs, unit grid, unit screen.

the active emitting portion of the filament so that equal availability of electrons is provided.

The filament spring members, also shown in Figure 6, consist of copper strips having slots and V-grooves which hold the filaments, and steel spring members which maintain their spring action at the required elevated operating temperature. The majority of the metal parts in the tube are made of copper to provide high electrical and thermal conductivity.

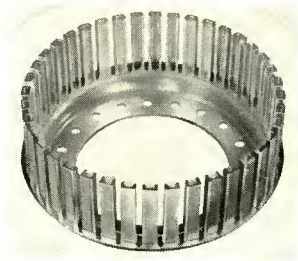


Fig. 7—Control-grid assembly.

#### ELECTRODE ASSEMBLIES

The control-grid assembly is shown in Figure 7. The 40 unit channels are brazed to a sturdy copper support which, during subsequent assembly of the tube, is bolted to the water-cooled copper member which forms the external r-f contact surface.

Figure 8 shows the complete screen-grid assembly. The massive outer copper ring is provided with a water channel for efficient removal of heat generated at the active wire surface of the screen. This heat is conducted through the copper fins to the main block.

A high-dissipation plate is required to handle the high unit plate losses associated with compact high-frequency tubes. Plate losses are normally higher in tubes for UHF service, especially when broadband operation is required.

A plate assembly is shown along with the complete tube mount in Figure 9. The 40 individual filament springs and the filament heads

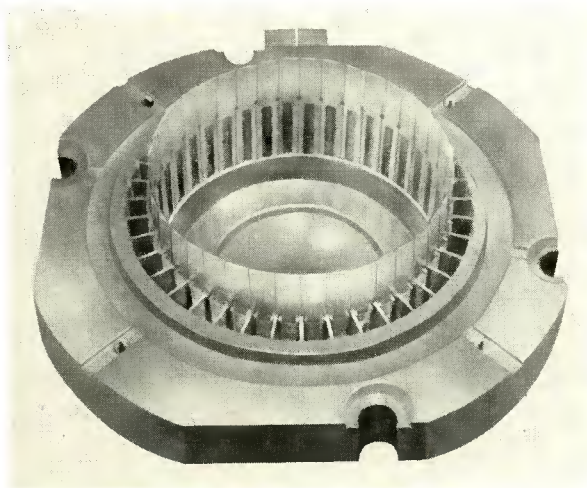


Fig. 8—Screen-grid assembly.

can be seen in the mount assembly. The flat copper ring in the center of the picture is the output screen-to-ground bypass capacitor which is fastened during final tube assembly to the 40 screen tabs projecting from the mount. This ring is held against the flat surface of the mica and plate header by means of springs.

Some design parameters for the 6448 are listed in Table I.

Table I—Design Parameters.

Control-grid-to-cathode spacing .....	0.020 inch
Control-grid-to-screen-grid spacing .....	0.020 inch
Screen-grid-to-plate spacing (total distance from inner diameter of lateral screen wires to plate surface) ...	0.300 inch
Active emitting length of filament .....	0.750 inch
Output strapped resonant frequency .....	850 Mc
Input strapped resonant frequency .....	300 Mc

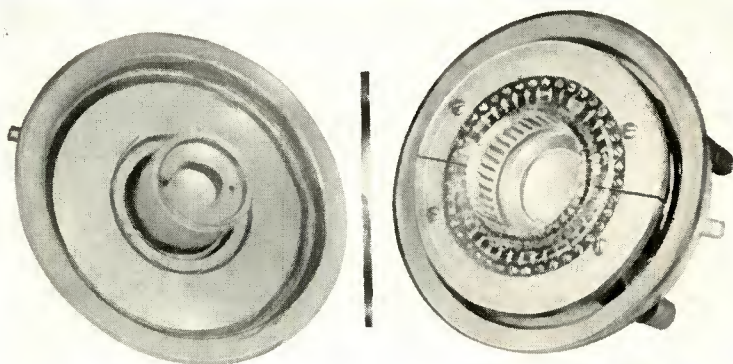


Fig. 9—Plate assembly and complete tube mount assembly.

#### PERFORMANCE DATA

Table II gives general tube data. The performance indicated in Table III is obtained under broad-band conditions suitable for transmission of color as well as black-and-white television signals. No neutralization is required. Extensive tests have proven the suitability of the 6448 for faithful transmission of a color television signal. These tests and their results have been reported.<sup>5</sup>

Typical operating conditions for Class C telegraphy or FM telephony service at a carrier frequency of 500 megacycles per second are given in Table IV. A power gain of 50 is easily obtained in this type of service.

<sup>5</sup> L. L. Koros, "A Novel UHF Television High-Power-Amplifier System," *RCA Review*, Vol. 16, pp. 251-280, June, 1955.

Table II—General Data.

## Electrical:

Filament (2-section multistrand thoriated-tungsten):	
voltage per section (a-c or d-c) .....	1.35 volts
current per section .....	975 amperes
Mu-Factor, Grid No. 2 to Grid No. 1 .....	7.5

## R-F Power Amplifier Class B Television Service—Up to 1000 Mc

## Maximum Ratings:

D-C Plate Voltage .....	7000 max. volts
D-C Grid-No. 2 (screen) voltage .....	1000 max. volts
D-C Plate Current .....	7 max. amperes
Plate Dissipation .....	26,000 max. watts

## Mechanical:

Over-all Length .....	7-11/32 inches
Maximum Diameter .....	11-3/8 inches
Weight .....	25 pounds

Table III — Typical Operation of R-F Power Amplifier in Class B Television Service—Color or Black-and-White

	<u>Synchronizing Level</u>	<u>Average Readings Corresponding to Indicated Synchronizing Level Values for Typical Picture Conditions</u>
D-C Plate Voltage .....	5600	5600 volts
D-C Grid-No. 2 Voltage...	975	975 volts
D-C Grid-No. 1 Voltage...	—140	—140 volts
D-C Plate Current .....	6.5	3.2 amperes
Driver Power Output .....	900	
Useful Power Output ....	15,000	

Table IV — Class C Telegraphy or FM Telephony at 500 Megacycles

D-C Plate Voltage .....	6900	5600 volts
D-C Grid-No. 2 Voltage .....	1000	975 volts
D-C Grid-No. 1 Voltage .....	—150	—180 volts
D-C Plate Current .....	6.5	3.6 amperes
D-C Grid-No. 2 Current .....	0.3	0.15 ampere
D-C Grid-No. 1 Current .....	0.3	0.01 ampere
Driver Power Output .....	400	250 watts
Useful Power Output .....	23,000	8,000 watts

The 6448 also performs well at the high-frequency end of the UHF band, and is being used in the highest-frequency, commercially operated, high-power UHF television stations. Typical operating conditions for Class C telegraphy or FM telephony service at a frequency of 900 megacycles are given in Table V.

Average plate characteristics for the 6448 are shown in Figure 10.

Table V—Class C Telegraphy or FM Telephony at 900 Megacycles

D-C Plate Voltage .....	6500 volts
D-C Grid-No. 2 Voltage .....	950 volts
D-C Grid-No. 1 Voltage .....	—150 volts
D-C Plate Current .....	6.0 amperes
D-C Grid-No. 2 Current .....	0.4 ampere
D-C Grid-No. 1 Current .....	0.2 ampere
Driver Power Output .....	800 watts
Useful Power Output .....	12,000 watts

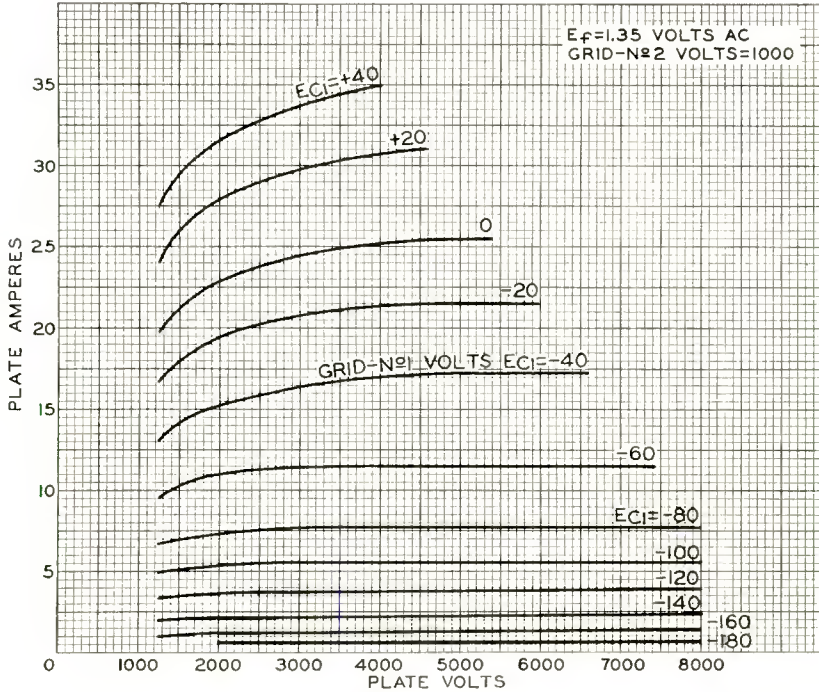


Fig. 10—Average plate characteristics of the 6448.

CIRCUIT DEVELOPMENT

During the tube development work, a circuit development program was also instituted to provide a test station for evaluation of the prototype design and measurement of performance of the 6448. Because it was felt that satisfactory performance would be most difficult to obtain at the highest frequencies, the circuitry and test station were designed for operation at a carrier frequency of 900 megacycles.

The test unit is a "bread-board" arrangement which, for the most part, uses available laboratory-type equipment. The main amplifier is

built into the test cubicle of a universal d-c power supply. The 1-kilowatt driver unit uses a 6181 in its final stage. The three major circuit components which had to be designed were the input cavity, the output cavity, and an r-f load capable of dissipating a power output of 15 to 20 kilowatts.

The 900-megacycle output circuit, shown in Figure 11, consists of two parts: a half-wave resonant portion (below plane AA'), and a means for coupling the 50-ohm transmission-line load or antenna to the open end of the half-wave resonant section. The half-wave resonant portion of the circuit consists of the "dead-head" capacitance at the end of the plate cylinder between the plate and the screen grid, a length of coaxial transmission line inside the tube, a transition in the seal region, and the external low-impedance section outside the tube. The low-impedance section continues in length until the current node is reached. At 900 megacycles the first voltage node occurs in the seal or transition region between the relatively high-impedance line inside the tube and the external low-impedance section. The bandwidth is optimized when the low-impedance section begins at the first voltage node and extends in length to the current node.<sup>6</sup> The impedance of the line on either side of the low-impedance section should be as high as practicable.

In this type of output circuit, very little energy is stored in the external circuit, and the bandwidth approaches that of a simple quarter-wavelength cavity. The principal advantages of this circuit are that it provides:

- (1) a means for coupling the load symmetrically to the cavity and tube.
- (2) a means for tuning the cavity to resonance without changing the cavity loading.
- (3) a means for changing cavity loading without affecting tuning.
- (4) a logical location for the plate-blocking capacitor out of the high-circulating-current, resonant-cavity region.

The low-impedance line section is provided by a water-cooled copper slug placed as an annular ring in the main coaxial transmission-line cavity. The slug is spaced and insulated from the inner and outer

---

<sup>6</sup> A. Van Weel, "A Comparison of the Bandwidths of Resonant Transmission Lines and Lumped LC Circuits," *Philips Research Report*, Vol. 5, p. 241, August, 1950.

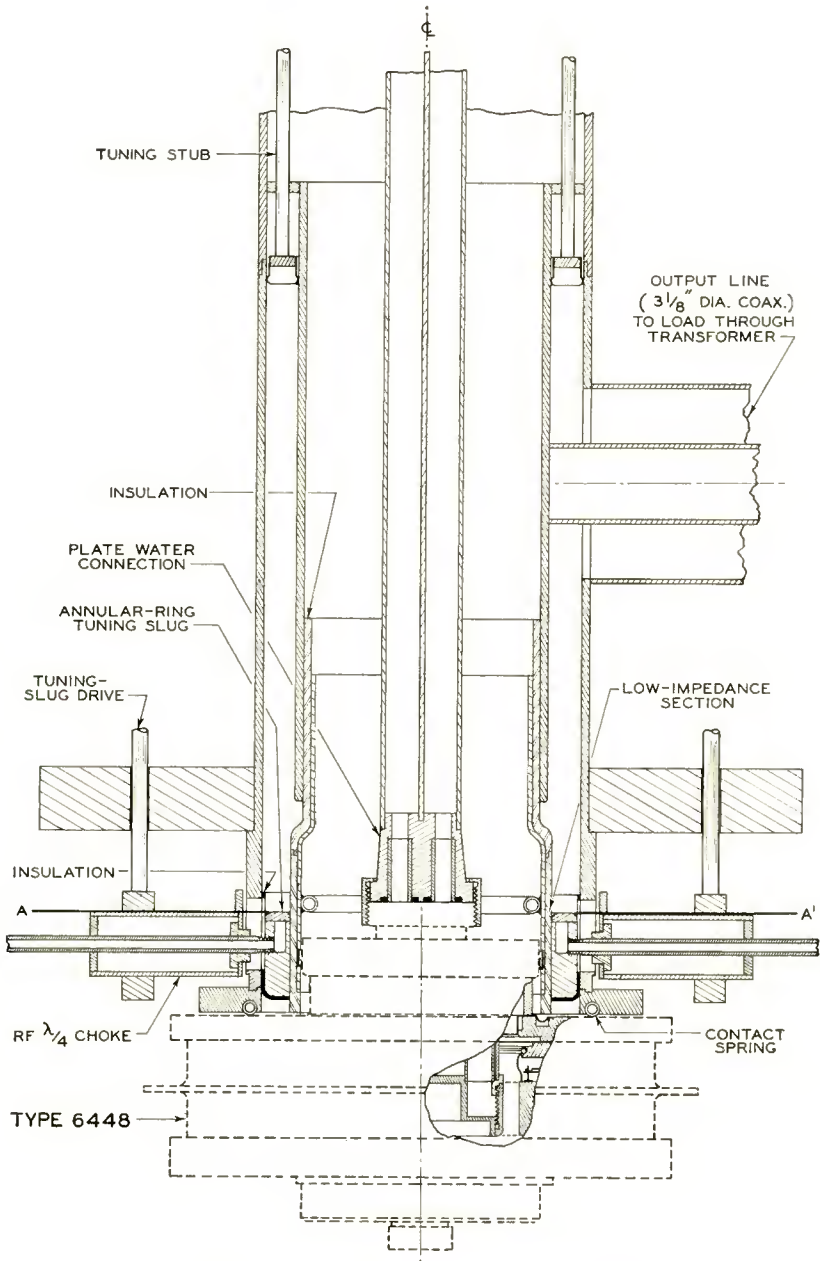


Fig. 11—900-megacycle output circuit.

conductors by Teflon\* insulation. The circuit is tuned by movement of the slug up or down in the line. Metal tubes which are mounted on quarter-wave chokes and pass through slots in the wall of the outer conductor provide a means for the circulation of cooling water through the slug and for movement of the slug for tuning.

The portion of the circuit above plane AA' in Figure 11 transforms the impedance of the 50-ohm load so that the proper load resistance is presented across the coaxial line at the active electrode region. This impedance-transformation section of the circuit stores very little energy, supports only moderate standing-wave ratios during operation, and carries only relatively low circulating currents.

Because the plate blocking capacitor is in the load portion of the circuit, it need not support excessive r-f currents and can easily be made to withstand the required d-c voltages. There are no sliding contacts in the resonant, or high-current, portion of the cavity. Tuning is accomplished by means of a slug sliding on Teflon. Loading of the cavity, and thus bandwidth, is changed by adjustment of the setting of a transformer in the 50-ohm line section between the load and the cavity.

The input cavity, shown in Figure 12, was not designed particularly for bandwidth, although a broadband circuit can be made by use of the techniques described above for the output circuit. The input circuit is a simple, constant-impedance, three-quarter-wavelength, shorted coaxial cavity. The short-circuit tuner uses conventional sliding contact fingers.

The only unusual feature of the input circuit is the manner in which the drive line is connected to the cavity. The feed line is brought through the inner conductor of the main cavity, and is connected to the main cavity by means of a short radial transmission line whose outer edge interrupts the continuity of the inner conductor. The point along the length of the cavity at which the interruption is made is chosen so that, under operating conditions, the feed line is essentially terminated and has a standing-wave ratio of almost unity. It is interesting to note that almost all the driving power required for operation of this system at 900 megacycles appears as  $I^2R$  circuit losses in the external cavity.

In all the 900-megacycle tests, a simple 6-foot-long water load such as that shown in cross-section in Figure 13 was used. A continuous power as high as 18 kilowatts has been safely dissipated by this load. At this frequency, the voltage standing-wave ratio of the water load is less than 1.3.

---

\* Registered trade mark of the E. I. DuPont Co.

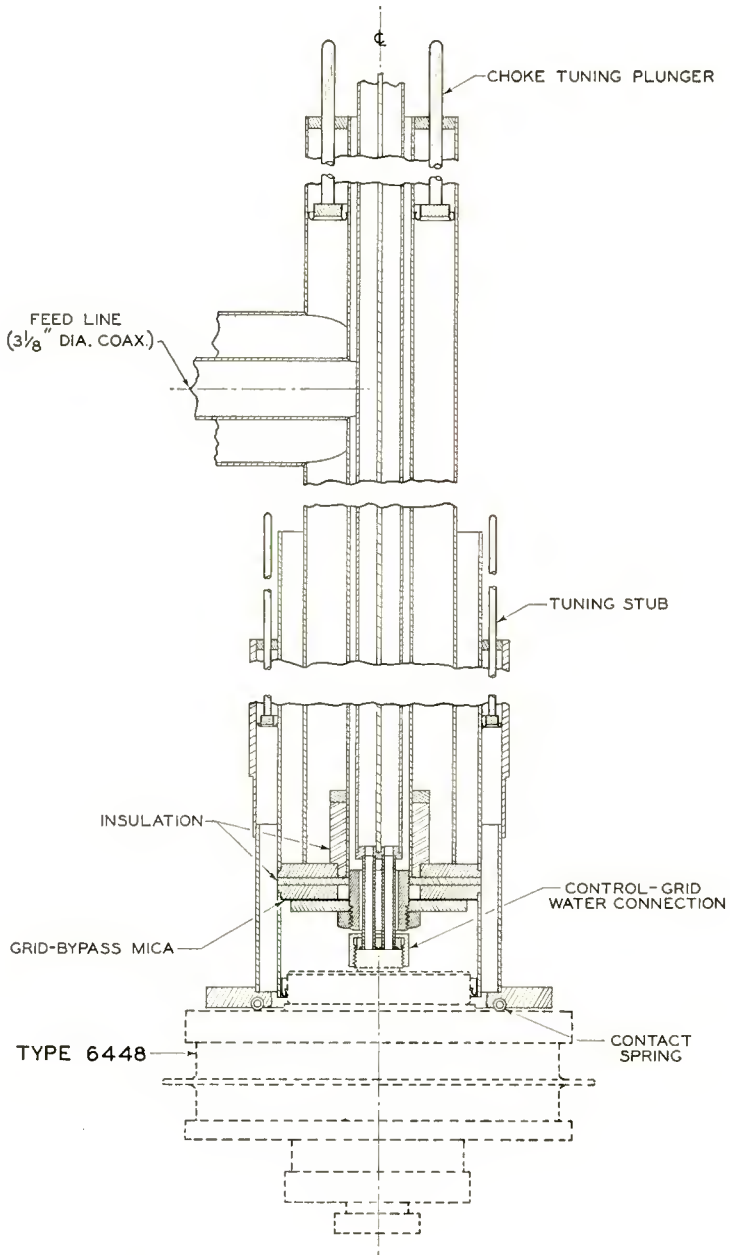


Fig. 12—900-megacycle input circuit.

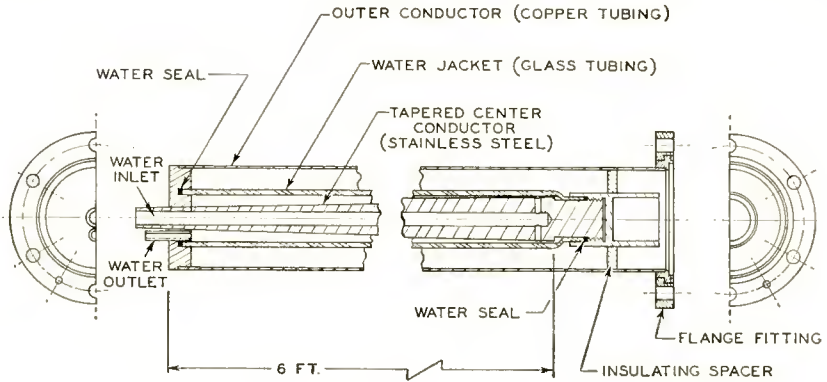


Fig. 13—Water load.

#### ACKNOWLEDGMENT

The author wishes to thank the numerous people of the Tube Division, Lancaster, Pa. who contributed to the success of this development program.

# SIMPLIFIED DESIGN PROCEDURES FOR TUNED TRANSISTOR AMPLIFIERS\*

BY

C. C. CHENG

Tube Division, Radio Corporation of America,  
Harrison, N. J.

*Summary*—This paper describes a systematic and simplified method for the design of tuned amplifier systems using transistors. The method consists of three steps: (1) determination of the requirements of the amplifier system, (2) selection of transistor amplifiers, and (3) selection of coupling networks. Design procedures for various types of coupling networks are presented in tabular form for easy reference.

## INTRODUCTION

THIS paper describes a method which facilitates the design of tuned narrow-band amplifiers using short-circuit stable transistors and employing various single parallel resonant circuits as coupling networks. This method can also be applied to the design of tuned wide-band amplifier systems composed of cascaded narrow-band amplifiers. In addition, it can be used in the design of antenna couplers and common-grid vacuum-tube amplifiers.

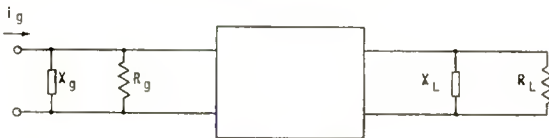


Fig. 1—Schematic diagram of typical narrow-band amplifying system.

## SPECIFICATIONS OF AMPLIFYING SYSTEM

The following information is usually included in the specifications for a narrow-band amplifying system such as that shown in Figure 1:

1. The generator impedance, represented by  $R_g$  and  $X_g$  in parallel;
2. The load impedance, represented by  $R_L$  and  $X_L$  in parallel;
3. The total gain of the system at its center frequency (Total voltage gain,  $K_{vs}$ , is usually specified for amplifier systems having very high input impedances, such as common-cathode vacuum-

\* Decimal classification: R363.11.

- tube amplifiers. Total power gain,  $K_{ps}$ , is usually given for systems having relatively low input impedances, such as common-grid vacuum-tube amplifiers and transistor amplifiers.);
4. The frequency response, including the center frequency ( $f_o$ ), the total bandwidth (usually given as 3-decibel-down bandwidth  $\Delta f_s$ ), and the system  $Q$  ( $Q_s = f_o/\Delta f_s$ ;  $Q_s \gg 10$  for a narrow-band system);
  5. The useful sensitivity, given as the signal input,  $V_g$ , in microvolts for specified signal-to-noise ratio at the output.

#### SELECTION OF AMPLIFIERS

When the specifications for the amplifying system have been obtained, the type of amplifiers to be used and the number of stages required can be determined. For a comparison of different kinds of transistor amplifiers, the important properties (including matched power gain,  $K_p$ , and matched input and output impedances,  $Z_i$  and  $Z_o$ ) at the specified frequency can be obtained (1) from calculations based on measured open-circuit impedance parameters, short-circuit admittance parameters, or hybrid parameters;<sup>1,2</sup> (2) by computation from a specified equivalent circuit; or (3) by direct power-gain measurement.<sup>3</sup> The typical curve<sup>3</sup> of power gain versus frequency for one type of high-frequency junction transistor in Figure 2 shows that the use of the common-emitter circuit provides higher power gain than the use of the common-base circuit. Therefore, the common-emitter circuit is generally used when maximum power gain is the primary consideration.

The number of amplifier stages required can be obtained after both the power gain of the system,  $K_{ps}$ , and the power gain of a single stage,  $K_p$ , at the center frequency are known. If it is assumed that all the stages are synchronously tuned, then the number of stages of amplifiers,  $M$ , is the smallest integer equal to or larger than the ratio of  $K_{ps}$  to  $K_p$ :

$$M = \text{smallest integer} \geq \frac{K_{ps}}{K_p} \quad (1)$$

<sup>1</sup> L. J. Giacoletto, "Terminology and Equations for Linear Active Four-Terminal Networks Including Transistors," *RCA Review*, Vol. XIV, p. 28, March, 1953.

<sup>2</sup> C. C. Cheng, "Transistor Equations Using H-Parameters," *Electronics*, Vol. 27, pp. 191-194, April, 1954.

<sup>3</sup> G. W. Mueller and J. I. Pankove, "A P-N-P Triode Alloy Junction Transistor for Radio Frequency Amplification," *Proc. I.R.E.*, Vol. 42, pp. 386-391, February, 1954.

and the number of coupling networks,  $U$ , is given by

$$U = M + 1. \tag{2}$$

The bandwidth,  $\Delta f$ , of each single-tuned circuit can be determined from the total bandwidth of the system,  $\Delta f_s$ , and the number of single-tuned circuits,  $U$ , by the simple relation shown in Table I.

Table I

$U$ Number of Single-Tuned Circuits	$\eta = \frac{\Delta f_s}{\Delta f} \cong \frac{1}{\sqrt{2^{1/U} - 1}}$ Ratio of total bandwidth to the bandwidth of each single-tuned circuit
1	1
2	1.55
3	1.98
4	2.3
5	2.58
6	2.85

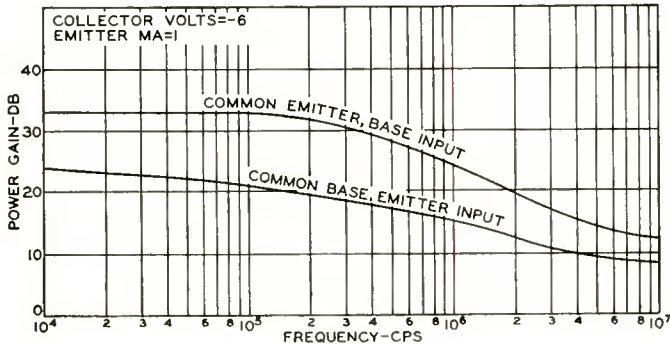


Fig. 2—Power gain as a function of frequency for a typical high-frequency junction transistor.

The sensitivity of the amplifying system is determined by the following method. A curve of noise versus frequency for a typical high-frequency junction transistor is shown in Figure 3. The noise factor of the amplifying system,  $NF_s$ , is defined as

$$NF_s = \frac{\frac{S_t}{N_t}}{\frac{S_o}{N_o}} \tag{3}$$

where  $S_o/N_o$  is the specified signal-to-noise power ratio at the output. The input noise power,  $N_i$ , in watts is determined by the thermal noise of the generator impedance:

$$N_i = KTB$$

where  $K$  = Boltzmann's constant,  
 $T$  = temperature in degrees Kelvin,  
 $B$  = effective noise bandwidth in cycles per second.

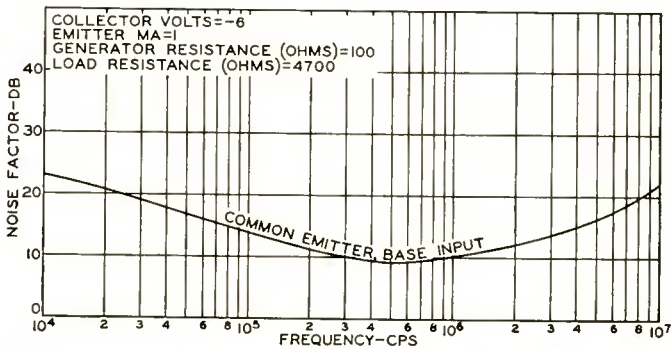


Fig. 3—Noise as a function of frequency for a typical high-frequency junction transistor.

The input signal power,  $S_i$ , in watts is obtained from the required sensitivity,  $V_g$ , in volts as follows:

$$S_i = \frac{V_g^2}{4R_g}$$

where  $R_g$  is the generator resistance in ohms. When the values for  $N_i$  and  $S_i$  are substituted in Equation (3), therefore, the noise factor of the system,  $NF_s$ , for the required sensitivity at the specified signal-to-noise ratio at the output,  $S_o/N_o$ , is given by

$$NF_s = \frac{\frac{V_g^2}{4KTB R_g}}{\frac{S_o}{N_o}} \tag{3a}$$

The actual noise factor of the system  $NF_a$  can be determined from the equation<sup>4</sup>

$$NF_a = NF_1 + \frac{NF_2 - 1}{K_1} + \frac{NF_3 - 1}{K_1 K_2} \quad (4)$$

where  $NF_1$ ,  $NF_2$ , and  $NF_3$  are the noise factors of the first, second, and third stages, respectively, and  $K_1$  and  $K_2$  represent the available power gain of the first and second stages, respectively.

The value of  $NF_a$  can readily be computed from Equation (4) by substitution of data obtained from Figures 2 and 3. This value of  $NF_a$  should be less than the calculated value of  $NF_s$  to satisfy the sensitivity requirement.

#### DETERMINATION OF COUPLING NETWORKS

As stated previously, the amplifying system is composed of  $M$  stages of amplifiers and  $(M+1)$  coupling networks, namely one input, one output, and  $(M-1)$  interstage coupling networks. The main difference between the interstage and the input and output coupling networks lies in the terminations, as shown in Figure 4. The design methods are identical, therefore, and discussion of one type is sufficient to illustrate the process involved; the interstage coupling network will be used as the example.

The matched input and output impedances of the transistor amplifier can be represented by the parallel combination of  $R_i$ ,  $C_i$  and  $R_o$ ,  $C_o$  shown in Figure 5a. If it is assumed that the internal capacitances,  $C_i$  and  $C_o$  of the transistor can be grouped into the coupling network, as shown in Figure 5b, the coupling network to be designed must have a center frequency  $f_o$  and a bandwidth  $\Delta f$ , and must satisfy the matching condition. Various kinds of coupling networks having these features can be derived from two basic networks.

#### SIMPLE PARALLEL L-C CIRCUIT WITH IDEAL TRANSFORMER

The first basic coupling network is a parallel tuned L-C circuit with an ideal transformer, such as that shown in Figure 6a. If the coil loss is neglected, the necessary relationship for the matched condition is given by

$$R_o = a^2 R_i \quad (5)$$

<sup>4</sup> H. T. Friis, "Noise Figure of Receivers," *Proc. I.R.E.*, Vol. 32, p. 419, July, 1944.

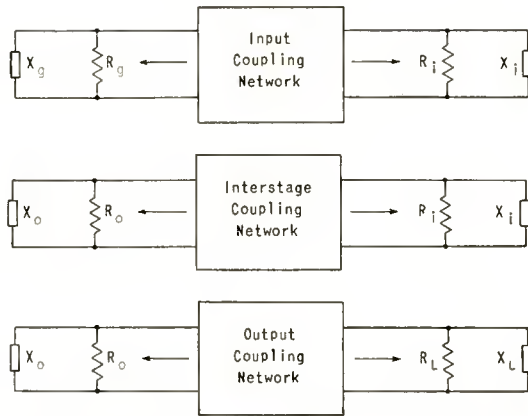


Fig. 4—Schematic diagrams showing difference in terminations for input (top), interstage (middle), and output (bottom) coupling networks.

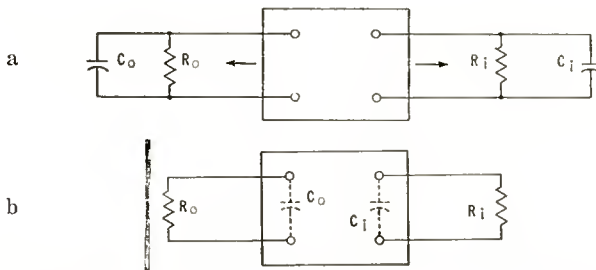


Fig. 5—Schematic diagrams of transistor amplifier having matched input and output impedances. In 5b, internal capacitances  $C_i$  and  $C_o$  are grouped into the interstage coupling network.

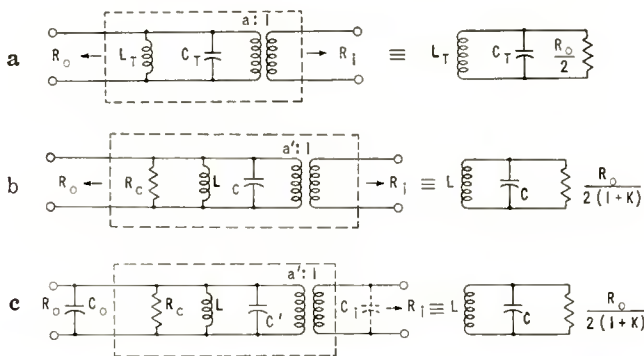


Fig. 6—Schematic diagrams showing (a) basic coupling network containing parallel tuned L-C circuit with ideal transformer, (b) modified circuit including coil loss, and (c) modified circuit in which  $C_i$  and  $C_o$  are grouped into the amplifier.

$$a = \sqrt{\frac{R_o}{R_i}} \quad (6)$$

The bandwidth is given by

$$\Delta f = \frac{1}{\pi R_o C_T} \quad (7)$$

$$C_T = \frac{1}{\pi R_o \Delta f} \quad (8)$$

$$L_T C_T = \frac{1}{4\pi^2 f_o^2} \quad (9)$$

The factors  $a$  and  $C_T$  used in these equations are two of the three derived constants ( $a$ ,  $C_T$ ,  $C_m$ ) which are introduced in this paper to simplify the computations. The constant  $a$  represents the turns ratio of an ideal transformer for matching  $R_o$  and  $R_i$ . The constant  $C_T$  represents the capacitance connected in parallel with  $R_o/2$  required to provide the specified bandwidth.

If the coil loss is included, the value of the total resistance  $R_o'$  is given by

$$\frac{1}{R_o'} = \frac{1}{R_o} + \frac{1}{R_c} = \frac{1+k}{R_o}$$

where  $R_c = \omega_o L_T Q$  is the effective coil resistance,  $k = R_o/R_c$  is the ratio of the output resistance to the effective coil resistance, and  $Q$  is the  $Q$  of the coil.

For the circuit shown in Figure 6b, therefore,

$$R_o' = \frac{R_o}{1+k} \quad (10)$$

and the relationship for the matched condition is given by

$$R_o' = a'^2 R_i \quad (5a)$$

where  $a' = \sqrt{R_o'/R_i} = a/\sqrt{1+k}$  is the turns ratio of the transformer used in the modified circuit of Figure 6b. The bandwidth is given by

$$\Delta f = \frac{1}{\pi C_T R_o} = \frac{1+k}{\pi C R_o}$$

where  $C$  is the actual capacitance used in the circuit of Figure 6b. Therefore,  $C = (1+k) C_T$ ,  $L = L_T/(1+k)$ .

If the effective input and output capacitances,  $C_i$  and  $C_o$  of the transistor are grouped into the amplifier, as shown in Figure 6c, the actual capacitance,  $C'$ , used in the interstage coupling network is given by

$$C' = (1+k) C_T - C_o - \frac{C_i}{a'^2}. \quad (11)$$

The coil loss,  $P_c$ , is given by

$$P_c = 10 \log_{10} \left( 1 + \frac{R_o}{R_c} \right) = 10 \log_{10} (1+k) \text{ decibels.}$$

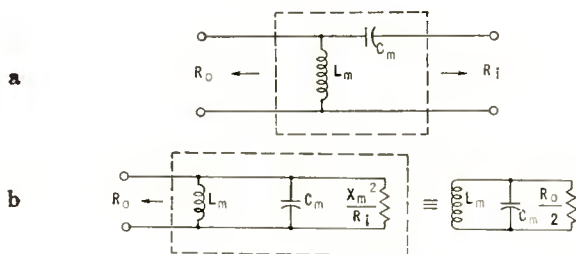


Fig. 7—Schematic diagrams showing (a) basic coupling network using equivalent series-parallel impedance transformation, and (b) modified circuit in which series network  $C_m$ ,  $R_i$  is transformed into a parallel circuit.

#### SIMPLE SERIES-PARALLEL IMPEDANCE TRANSFORMING NETWORK

The second basic interstage coupling network uses the property of equivalent series-parallel impedance transformation at a single frequency, as shown in Figure 7a. In this type of circuit, the series network ( $C_m$ ,  $R_i$ ) can be transformed into a parallel circuit ( $C_m$ ,  $X_m^2/R_i$ ), as shown in Figure 7b where  $X_m = 1/(2\pi f_o C_m)$  is the reactance of the capacitance  $C_m$  at the center frequency,  $f_o$ . It is assumed that  $X_m/R_i \gg 1$ . If the coil loss is neglected, the relationships at the matched condition are given by

$$\frac{X_m^2}{R_i} = R_o, \quad C_m = \frac{1}{\omega_o \sqrt{R_o R_i}}, \quad \omega_o = 2\pi f_o \quad (12)$$

$C_m$ , the third of the derived constants mentioned previously, is defined as the capacitance required to satisfy the matching requirement by series-parallel impedance transformation between  $R_i$  and  $R_o$ . This cir-

cuit, however, does not satisfy the bandwidth requirement except when  $C_m = C_T$ , i.e., when

$$\frac{1}{\omega_o \sqrt{R_o R_i}} = \frac{1}{\pi R_o C_T} \quad (13)$$

which is a special condition. Equations (6), (8), and (12) explain the origin of the three derived constants introduced to simplify the computations in this paper

Various types of coupling networks can be analyzed in a similar manner; results for several types are summarized in the Appendix. In the table, all the equations are represented in a normalized simplified form, containing ratios of  $C/C_T$ ,  $C_m/C_T$ , and so forth. When the three derived constants have been determined, all the other circuit elements for various types of networks can be calculated easily. The method used in the preparation of the Appendix is best illustrated by a detailed analysis of one coupling circuit. An example of the design of an amplifying system will also be given to show the convenience of the application of the simplified design procedure introduced in this paper.

#### ANALYSIS OF SAMPLE COUPLING CIRCUIT

The coupling network shown as circuit (3) in the Appendix is drawn as shown in Figure 8. The necessary relationship for matching is given by

$$\frac{1}{R_o N^2} + \frac{1}{R_o} = \frac{1}{R_o} \left( \frac{1}{N^2} + k \right) = \frac{C_1^2}{R_i (C_1 + C_2)^2} \quad (14)$$

where  $N$  is the turns ratio of the coil  $L$ . The bandwidth is given by

$$\begin{aligned} \Delta f &= \frac{1}{\pi C_T R_o} = \frac{C_1^2}{\pi C R_i (C_1 + C_2)^2} \\ &= \frac{C}{\pi C_2^2 R_i} \end{aligned} \quad (15)$$

where  $C = \frac{C_1 C_2}{C_1 + C_2}$  (16)

From Equation (15),

$$C_2^2 = \frac{R_o}{R_i} CC_T$$

i.e.,  $C_2 = a \sqrt{CC_T}$ . (17)

Combining Equations (14) and (15) gives

$$N = \frac{1}{\sqrt{\frac{C}{C_T} - k}} \tag{18}$$

Equation (16) may be substituted in Equation (17), and the result solved for  $C_1$ , as follows:

$$C_1 = \frac{C}{1 - \frac{1}{a} \sqrt{\frac{C}{C_T}}} \tag{19}$$

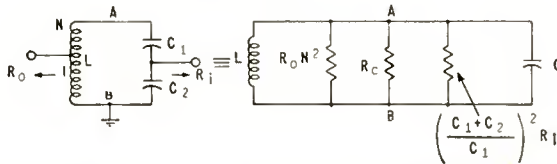


Fig. 8—Schematic diagram of sample coupling network (also shown as circuit 3 in the Appendix).

The coil loss,  $P_c$ , is then given by

$$P_c = 10 \log_{10} \left[ 1 + \frac{N^2 R_o}{R_c} \right] = 10 \log_{10} [1 + k N^2]. \tag{20}$$

If the effects of the output and input capacitance,  $C_o$  and  $C_i$  of the transistor amplifier are considered, Equations (19) and (17) become

$$C_1' = \frac{C - C_o/N^2}{1 - (1/a) \sqrt{(C - C_o/N^2)/C_T}} \tag{19a}$$

$$C_2' = a \sqrt{(C - C_o/N^2) C_T} - C_i. \tag{17a}$$

Equations (18), (19), (17), (20), (19a), and (17a) are used in the Appendix as standard design equations.

## DESIGN OF SAMPLE AMPLIFYING SYSTEM

The typical amplifying system to be designed has the following specifications:

Center frequency,  $f_o = 1$  megacycle

Total bandwidth,  $\Delta f_s = 20$  kilocycles

Total power gain,  $K_{ps} = 40$  decibels

Generator impedance,  $R_g = 300$  ohms

Load impedance,  $R_L = 100$  ohms, 20-microvolt sensitivity at 20 decibels,  $S_o/N_o$ .

The value of  $K_p$  is found (from Figure 2) to be 24 decibels for the common-emitter circuit. Therefore,  $M = 2$ ,  $U = 3$ ; i.e., two amplifier stages and three coupling networks are required. For synchronous tuning, the bandwidth of each circuit is given by

$$\Delta f = 1.98 \Delta f_s = 39.6 \text{ kilocycles.}$$

The noise factor of an individual stage at 1 megacycle, obtained from Figure 3, is given by

$$NF_1 = NF_2 = 10 \text{ decibels}$$

and the total noise factor of the two cascaded stages, derived from Equation (4), is

$$NF_a = 10 \text{ decibels.}$$

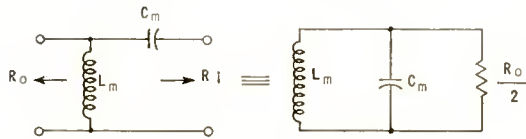
When a value of  $S_o/N_o$  equal to 20 decibels is substituted in Equation (3), the signal-to-noise ratio at the input,  $S_i/N_{i_s}$ , is equal to 30 decibels.

With the specified  $R_g$  of 300 ohms, an effective noise bandwidth of 30 kilocycles, and room temperature, the noise voltage,  $V_n$ , is calculated to be 0.38 microvolt. The signal voltage required, therefore, to provide a 30-decibel signal-to-noise ratio at the input is 12 microvolts. This sensitivity is better than the specified requirement of 15 microvolts.

The following constants were obtained from measurement of the transistor amplifier at 1 megacycle:

$$R_o = 6000 \text{ ohms, } R_i = 300 \text{ ohms, } C_o = 50 \text{ micromicrofarads.}$$

All the required information is available, therefore, for the design of the coupling networks.

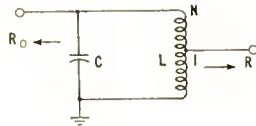


where  $C_m$  is the capacitance required to transform  $R_i$  to  $R_o$  to satisfy matching requirement.

$$k = \frac{R_o}{R_c} = \frac{R_o}{Q \omega_o L}$$

where  $k$  is the ratio of output resistance to effective coil parallel resistance.  $Q$  is the  $Q$  of the coil.

Circuit No. 1.



Neglect coil loss

$$N = a, \quad C = C_T, \quad L = L_T.$$

Include coil loss

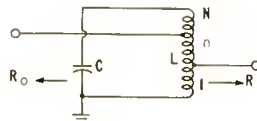
$$N = \frac{a}{\sqrt{1+k}}, \quad C = C_T (1+k), \quad L = \frac{L_T}{1+k}$$

$$P_c = 10 \log_{10} [1+k].$$

Modification for  $C_o, C_i$

$$C' = C_T (1+k) - C_o - \frac{C_i}{N^2}.$$

Circuit No. 2.



Select  $L, Q$ ;  $LC = \frac{1}{\omega_o^2}$ .

Include coil loss

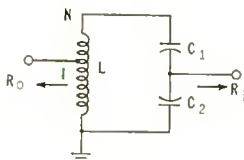
$$N = a \sqrt{\frac{C_T}{C}} = a \sqrt{1 - k \frac{C_T}{C}}$$

$$P_o = 10 \log_{10} \left[ \frac{1 + k \frac{C_T}{C}}{1 - k \frac{C_T}{C}} \right]$$

Modification for  $C_o, C_i$

$$C' = C - C_o \left( \frac{n}{N} \right)^2 - \frac{C_i}{N^2}$$

Circuit No. 3.



Select  $L, Q$ ;  $LC = \frac{1}{\omega_o^2}$ .

Include coil loss

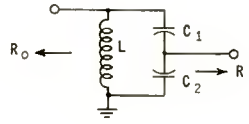
$$N = \frac{1}{\sqrt{\frac{C}{C_T} - k}}, \quad C_1 = \frac{C}{1 - \frac{1}{a} \sqrt{\frac{C}{C_T}}}, \quad C_2 = a \sqrt{CC_T}$$

$$P_o = 10 \log_{10} \left[ 1 + \frac{N^2 R_o}{RC} \right] = 10 \log_{10} [1 + kN^2]$$

Modification for  $C_o, C_i$

$$C'_1 = \frac{C - \frac{C_o}{N^2}}{1 - \frac{1}{a} \sqrt{\frac{1}{C_T} \left( C - \frac{C_o}{N^2} \right)}}, \quad C'_2 = a \sqrt{\left( C - \frac{C_o}{N^2} \right) C_T} - C_i$$

Circuit No. 3a.



Neglect coil loss

$$L = L_T, \quad C_1 = \frac{C_T}{1 - \frac{1}{a}}, \quad C_2 = aC_T.$$

Include coil loss

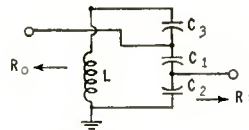
$$L = \frac{L_T}{1 + k}, \quad C_1 = \frac{C_T(1 + k)}{1 - \frac{1}{a}\sqrt{1 + k}}, \quad C_2 = aC_T\sqrt{1 + k}$$

$$P_c = 10 \log_{10} [1 + k].$$

Modification for  $C_o, C_i$

$$C'_1 = \frac{C - C_o}{1 - \frac{1}{a}\sqrt{\frac{C - C_o}{C_T}}}, \quad C'_2 = a\sqrt{C_T(C - C_o)} - C_i.$$

Circuit No. 4.



Select  $L, Q; LC = \frac{1}{\omega_o^2}.$

Include coil loss

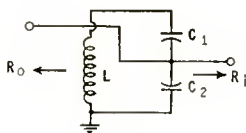
$$C_3 = \frac{C}{1 - \sqrt{\frac{C}{C_T} - k}}, \quad C_1 = \frac{C}{\sqrt{\frac{C}{C_T} - k} - \frac{1}{a\sqrt{CC_T}}}, \quad C_2 = a\sqrt{CC_T}$$

$$P_c = 10 \log_{10} \left[ 1 + \frac{k}{\frac{C}{C_T} - k} \right]$$

Modification for  $C_o, C_i$

$$C'_1 = C_1 - \left(1 + \frac{C_1}{C_2}\right) C_o, \quad C'_2 = C_2 - \left(1 + \frac{C_2}{C_1}\right) C_o - C_i.$$

Circuit No. 5.



Special Requirement  $R_o \doteq R_i$ .

Select  $L, Q$ ;  $LC = \frac{1}{\omega_o^2}$ .

Include coil loss

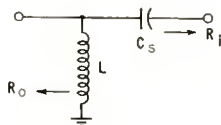
$$C_1 = \frac{C}{1 - \sqrt{\frac{C}{C_T}}}, \quad C_2 = \sqrt{C C_T}, \quad P_o = \log_{10} \left(1 + k \frac{C_T}{C}\right)$$

Modification for  $C_o, C_i$

$$C'_2 = C_2 - C_o - C_i.$$

Circuit No. 6.

$$\left(\frac{f_o}{\Delta f} = \frac{a}{2}\right)$$



Neglect coil loss

$$C_s = C_m, \quad L = L_m.$$

Include coil loss

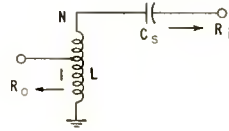
$$C_s = C_m \sqrt{1 + k}, \quad L = \frac{L_m}{\sqrt{1 + k}}.$$

Modification for  $C_o$

$$L' = \frac{L}{1 + \frac{C_o}{C_m \sqrt{1 + k}}}.$$

Circuit No. 6a.

$$\left( \frac{f_o}{\Delta f} > \frac{a}{2} \right)$$



Neglect coil loss

$$C_s = \frac{C_m^2}{C_T}, \quad L = \frac{L_m^2}{L_T}, \quad N = \frac{C_T}{C_m}.$$

Include coil loss

$$C_s = \frac{C_m^2}{C_T}, \quad L = \frac{L_m^2}{L_T}, \quad N = \frac{1}{\sqrt{\left(\frac{C_m}{C_T}\right)^2 - k}}$$

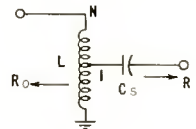
$$P_c = 10 \log_{10} (1 + kN^2).$$

Modification for  $C_o$ 

$$L' = \frac{L}{1 + \frac{C_o}{N^2 C_s}}.$$

Circuit No. 6b.

$$\left( \frac{f_o}{\Delta f} < \frac{a}{2} \right)$$



Neglect coil loss

$$C_s = \frac{C_m^2}{C_T}, \quad L = L_T, \quad N = \frac{C_m}{C_T}.$$

Include coil loss

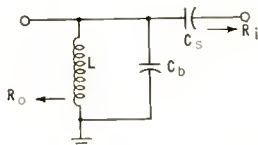
$$C_s = \frac{C_m^2}{C_T}, \quad L = L_T, \quad N = \frac{1}{\sqrt{\left(\frac{C_T}{C_m}\right)^2 - k}}$$

$$P_c = 10 \log_{10} (1 + k).$$

Modification for  $C_o$

$$L' = \frac{L}{1 + \frac{N^2 C_o}{C_s}}$$

Circuit No. 7.



Neglect coil loss

$$C_s = C_m, \quad C_b = C_T - C_m, \quad L = L_T.$$

Include coil loss

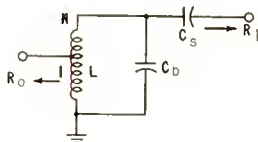
$$C_s = C_m \sqrt{1+k}, \quad L = L_T, \quad C_b = C_T - C_m \sqrt{1+k}$$

$$P_c = 10 \log_{10} (1+k).$$

Modification for  $C_o$

$$C'_b = C_b - C_o.$$

Circuit No. 7a.



Select  $L, Q$ .

$$\text{Calculate } C = \frac{1}{L\omega_o^2}.$$

Include coil loss

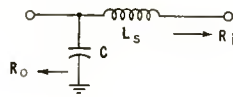
$$C_s = C_m \sqrt{\frac{C}{C_T}}, \quad C_b = C - C_m \sqrt{\frac{C}{C_T}}, \quad N = \sqrt{\frac{1}{\frac{C}{C_T} - k}}$$

$$P_c = 10 \log_{10} (1 + kN^2).$$

Modification for  $C_o$

$$C'_b = C_b - \frac{C_o}{N^2}$$

Circuit No. 8.



Neglect coil loss

$$L_s = L_m, \quad C = C_m$$

Include coil loss

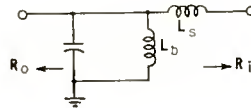
$$L_s = L_m \sqrt{1 + \frac{\alpha^2}{Q^2 k}}, \quad C = \frac{C_m}{\sqrt{1 + \frac{\alpha^2}{Q^2 k}}}$$

$$P_c = 10 \log_{10} \left( 1 + \frac{\alpha^2}{Q^2 k} \right)$$

Modification for  $C_o$

$$C' = C - C_o$$

Circuit No. 9.



Neglect coil loss

$$L_s = L_m, \quad C = C_T, \quad L_b = \frac{L_m L_T}{L_m - L_T}$$

Include coil losses

$Q_b, k_b$  for coil  $L_b$ ,       $Q_s, k_s$  for coil  $L_s$

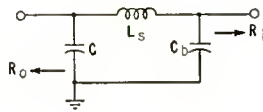
$$L_s = L_m \sqrt{\frac{1 + \frac{\alpha^2}{Q_s^2 k_s}}{1 + k_b}}$$

$$C = C_T (1 + k_b), \quad L_b = \frac{L_T L_s}{L_s (1 + k_b) - L_T}$$

Modification for  $C_c$

$$C' = C - C_o$$

Circuit No. 10.



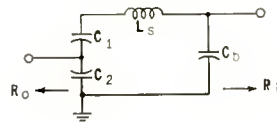
Neglect coil loss

$$L_s = \left( 1 + \frac{1}{a} \right) L_T, \quad C = C_T, \quad C_b = aC_T.$$

Modification for  $C_o, C_i$

$$C' = C - C_o, \quad C'_b = C_b - C_i.$$

Circuit No. 11.



Neglect coil loss, select

$$C_2; L_2 C_2 = \frac{1}{\omega^2_o}, \quad C_1 = \frac{C_2^2}{C_T}$$

$$L_s = \left[ \frac{\frac{C_T}{C_2}}{1 + \frac{1}{a \left( 1 + \frac{C_T}{C_2} \right)}} \right] L_2, \quad C_b = a \frac{C_2}{C_T} (C_2 + C_T).$$

Modification for  $C_o, C_i$

$$C'_2 = C_2 - C_o, \quad C'_b = C_b - C_i.$$

# THE NATURAL EQUIVALENT CIRCUIT OF JUNCTION TRANSISTORS\*

By

J. ZAWELS†

*Summary*—By considering individually and qualitatively each first-order phenomenon in junction transistor action, a circuit is synthesized in which each element represents a particular phenomenon. This approach insures an exact equivalent circuit which is fundamental to all junction transistors (not only to those having a plane parallel geometry) and which may be extended to include point contact transistors and other semiconductor devices.

It is found that the equivalent circuit reduces without loss of accuracy to a passive network in cascade with a frequency-independent amplifier. This configuration has considerable practical advantages particularly in common-base operation. Circuits which are especially useful for common-emitter and common-collector operation, and which employ the same basic passive elements, are also shown.

Finally the  $h$ -parameter expressions for the circuit are examined and a method is shown whereby the magnitude of the elements of the equivalent circuit may be simply computed from low-frequency  $h$ -parameter spot measurements.

## INTRODUCTION

THE method used in the past for obtaining an equivalent circuit for transistors may be stated as follows. First the expressions for four independent parameters, such as the input, output, forward-transfer and reverse-transfer open or short-circuit impedances were obtained, either experimentally<sup>1,2</sup> or theoretically.<sup>3</sup> Next, these parameters were used to determine the elements of the branches of an arbitrary circuit configuration such as a Tee<sup>1</sup> or Pi<sup>2,3</sup> in the hope that the resulting circuit would be the most practical for use in transistor circuit design. Unfortunately, with this approach a great number of

---

\* Decimal Classification: R282.12.

† Formerly with the Radio Corporation of America, RCA Victor Division, Camden, N. J. Now with the S. A. Iron and Steel Industrial Corporation, Pretoria, Union of South Africa.

<sup>1</sup> R. L. Wallace and W. J. Pietenpol, "Some Circuit Properties and Applications of N-P-N Transistors," *Proc. I.R.E.*, Vol. 39, p. 765, July, 1951.

<sup>2</sup> L. J. Giacoletto, "Junction Transistor Equivalent Circuits and Vacuum-Tube Analogy," *Proc. I.R.E.*, Vol. 40, p. 1490, November, 1952.

<sup>3</sup> H. Johnson, "Diffusion Reactances of Junction Transistors," paper presented at *Transistor Research Conference*, State College, Pa., July 6, 1953.

approximations are essential in order to limit the complexity of the circuit. Furthermore, this method hinges either on the fact that the devices which are examined experimentally are fully representative, or that the model which is treated theoretically is not oversimplified.

In this paper a generalized equivalent circuit is synthesized by considering qualitatively each first-order phenomenon on which transistor action is based, and then building up a circuit wherein each element represents a particular phenomenon. One form of this circuit, published earlier,<sup>4</sup> was derived on the basis of the possibility of representing without any approximation the admittance parameters which were derived rigorously for the special case of a plane parallel junction transistor with uniform volume recombination. In the present paper, the synthesis is not restricted to this particular model. Furthermore, the circuit, which may be called the natural equivalent circuit, is examined from the practical engineering point of view as to its utility in the analysis of common-base, common-emitter, and common-collector operation.

#### PHENOMENA IN JUNCTION TRANSISTOR ACTION AND THEIR CIRCUIT REPRESENTATION

##### *Diffusion*

The injected minority carriers propagate in the base of a junction transistor mostly by the process of diffusion. By definition this implies that the rate of propagation at any point is proportional to the density gradient of the carriers at that point. Now, if it is assumed that the general direction of propagation is towards the collector only, then a circuit analogy of the diffusion process is a transmission line having series resistance and parallel capacitance, since in such a line the rate of charge flow down the line, i.e., current, at any point along the line, is proportional to the linear charge density at that point. However, if we consider the flow of charge towards the base lead and the base surface<sup>5</sup> then a three-dimensional array of transmission lines is required to represent this three-dimensional diffusion process.

##### *Hole-Electron Recombination*

If a group of minority carriers propagate by the process of diffusion, and if some of these carriers are annihilated by virtue of hole-electron recombination, then in the transmission line analogy the number of

---

<sup>4</sup>J. Zawels, "Physical Theory for a New Circuit Representation of Junction Transistors," *Jour. Appl. Phys.*, Vol. 25, p. 976, August, 1954.

<sup>5</sup>A. R. Moore and J. I. Pankove, "The Effect of Junction Shape and Surface Recombination on Transistor Current Gain," *Proc. I.R.E.*, Vol. 42, p. 907, June, 1954.

charges injected into the input terminals is clearly more than that flowing out of the output terminals. This situation can be accounted for by permitting leakage along the line in the form of shunting resistance.

Obviously, if the linear rate of annihilation of the minority carriers along their path is uniform then the transmission line will be perfectly uniform. However, should considerable recombination occur near the beginning of the path of the minority carriers, such as occurs near the emitter on the surface of the base wafer in fused alloy transistors,<sup>5</sup> then additional shunting resistance is required near the input of the transmission line.

#### *Potential Barrier*

Figure 1b shows a potential-energy diagram for the minority carriers. It is seen that at each end of the base there is a potential barrier. Assuming no hole-electron recombination in the barrier region, it is clear that a potential barrier does not change the *rate* of charge flow (current) through it, but does change the potential energy of the charged carriers. Thus the circuit analogy of a potential barrier is a device whose input current equals the output current but whose input and output voltages differ. It is seen that such a device has properties similar to a grounded-grid vacuum-tube triode. This device shall be termed a K-amplifier and will be discussed later.

Figure 1c shows an RC transmission line which is terminated at each end by a K-amplifier. This represents the flow of the minority carriers first across the emitter potential barrier, then across the base, and finally across the collector potential barrier. The K-amplifiers may be considered to be independent of frequency since the transit time of the charge carriers across the transition regions, where an electric field is present, is negligible compared to the transit time in the base.

Figure 1a shows the distribution of minority carriers in the base, which is the same as the distribution of charge in a transmission line such as shown in Figure 1c, when a steady direct current is flowing through it. It is seen that the length of the transmission line is taken to be equal to the effective base width,  $W$ . The terminals are labeled  $E$ ,  $C$  and  $B'$  for the emitter, collector, and an internal point in the base, respectively.

#### *Majority Carrier Current*

Consider a p-n-p transistor. Minority carriers, i.e., holes, flow from the emitter into the base, and simultaneously majority carriers, i.e., electrons, flow in the opposite direction by virtue of the voltage across the emitter potential barrier. This implies that some admittance,  $y_n$ , should be placed between  $E$  and  $B'$ , as shown in Figure 2, to represent

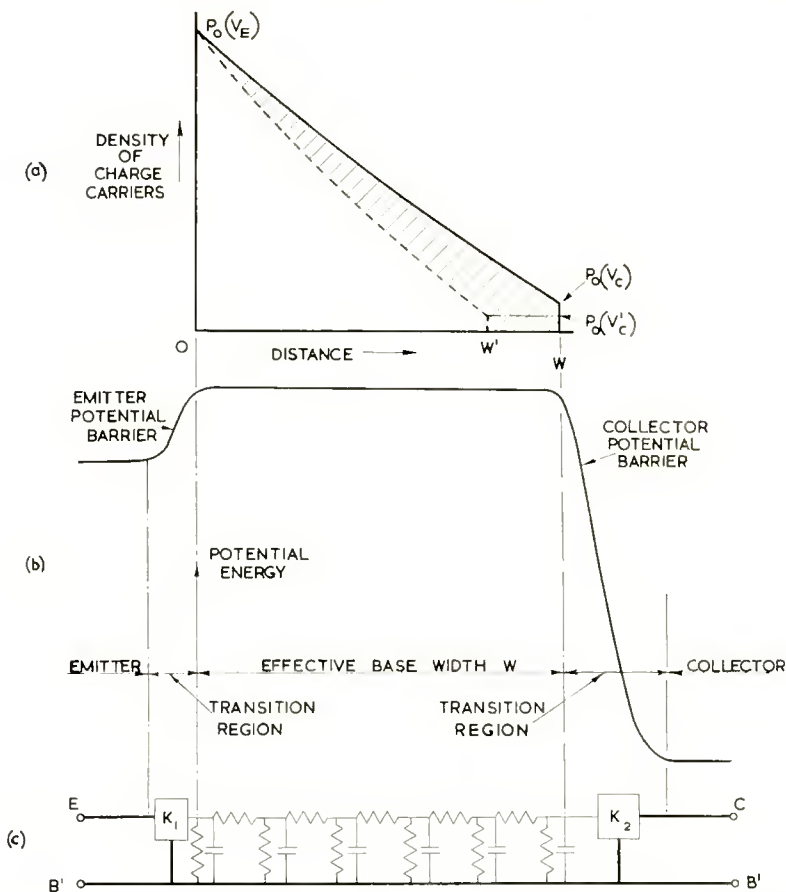


Fig. 1—(a) Distribution of minority charge carriers in base, or distribution of charge in transmission line. (b) Potential energy diagram for minority carriers. (c) Circuit representation of the diffusion of minority carriers in base and their flow across the potential barriers.

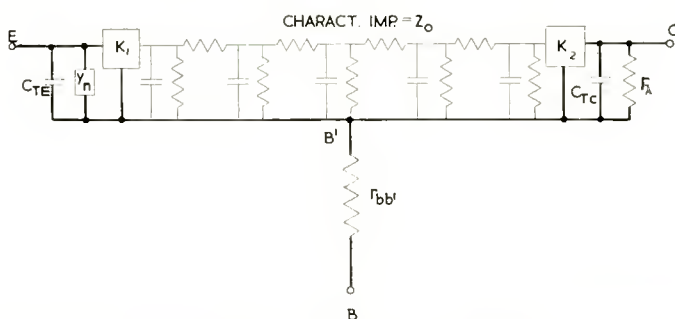


Fig. 2—Circuit representation of major phenomena in junction transistors.

this current path. Now, by a reasoning similar to that used for deriving the transmission line to represent the behaviour of the minority carriers in the base, it is clear that  $y_n$  will also be an RC transmission line for the flow of the electrons in the emitter region. However, for a good transistor the majority carrier current is very small and hence  $y_n$  is small compared to the admittance with which it appears in parallel.

The other elements in Figure 2 have already been discussed in the literature. Thus the barrier capacitances<sup>6</sup>  $C_{TE}$  and  $C_{TC}$  are now connected between  $E$  and  $B'$ , and  $C$  and  $B'$  respectively. Also shown is the base-lead resistance,  $r_{bb'}$ , which is a result of the resistivity of the material constituting the base, and  $r_\lambda$  which is the resistance of the extraneous matter which may be shunting the collector junction (leakage resistance).

Except for  $C_{TE}$ , all the elements of Figure 2 are of first-order importance. Effects which are usually of second-order importance have been neglected. These include the lead resistance of the emitter and collector regions, the majority carrier admittance which can be associated with the collector junction (i.e., analogous to  $y_n$ ), and the interelectrode capacitances, although the interelectrode capacitance between the collector and base may be of some importance at very-high frequencies. Also neglected here is the fact that a portion of  $r_{bb'}$  may be dependent on the voltage across the collector potential barrier, since this voltage determines the effective base width. This can be represented by placing a generator, whose voltage is proportional to the voltage between  $C$  and  $B'$ , in series with  $r_{bb'}$ .<sup>7</sup> Experimentally it is found, however, that for many transistor types this effect is small.

It is interesting to note that the circuit of Figure 2 appears to be symmetrical. This might have been expected since a junction transistor has a physically symmetrical appearance.

#### THE K-AMPLIFIER

As stated in the previous section, a K-amplifier is defined as a four-terminal device where, for all terminations,

$$\frac{\text{output current}}{\text{input current}} = 1, \quad (1a)$$

<sup>6</sup> W. Shockley, "The Theory of P-N Junctions in Semiconductors and P-N Junction Transistors," *Bell Sys. Tech. Jour.*, Vol. 28, p. 435, July, 1949.

<sup>7</sup> J. M. Early, "Effects of Space-Charge Layer Widening in Junction Transistors," *Proc. I.R.E.*, Vol. 40, pp. 1401-1406, November, 1952.

$$\frac{\text{output voltage}}{\text{input voltage}} = K, \quad (1b)$$

where  $K$  is a constant.

The above definition describes the circuit properties of the  $K$ -amplifier completely and requires no further elaboration. However, in order to become familiar with its uses, the implications of the above definition will be examined more closely.

Consider a grounded-grid vacuum-tube triode at low frequency as seen in Figure 3b. Let the amplification factor of the tube be  $\mu$ . It is clear that  $I_{in} = I_{out}$  and  $V_{out}/V_{in} = (\mu + 1)$  for all terminations, provided that the plate resistance of the tube is very low. Comparing this

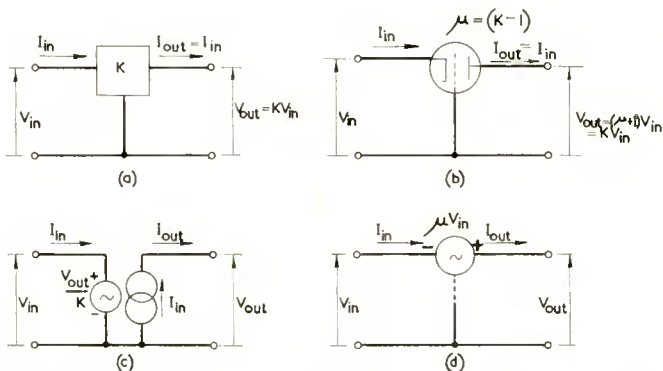


Fig. 3—Four equivalent representations of a  $K$ -amplifier: (a) Block diagram, (b) Grounded-grid vacuum-tube triodes with zero plate resistance, (c) Two-generator representation, (d) Conventional single-generator representation of vacuum tube triode.

statement with Equations (1a) and (1b) it is seen that a  $K$ -amplifier is equivalent to a grounded-grid vacuum-tube triode with low plate resistance, and an amplification factor  $\mu = K - 1$ .

A conventional circuit for representing a vacuum-tube triode consists of a voltage generator,  $\mu V_{in}$ , in series with a resistance representing the plate resistance of the tube. Since for the tube shown in Figure 3b the plate resistance is assumed to be zero, it may be represented by the circuit shown in Figure 3d. Another alternative for representing a  $K$ -amplifier, using one current and one voltage generator, is shown in Figure 3c. However, very often it is simpler to consider the  $K$ -amplifier as a single circuit component, without resorting to generators, as follows.

A  $K$ -amplifier has simple impedance-transforming properties. For

example, if a load  $Z_L$  is connected to the output then, using Equations (1a) and (1b),

$$Z_L = \frac{V_{out}}{I_{out}} = \frac{V_{in} K}{I_{out}} = \frac{V_{in} K}{I_{in}} = Z_{in} K.$$

Hence the input impedance,  $Z_{in} = Z_L/K$ . Alternatively, if an impedance  $Z_o$  is connected to the input, then the output impedance is the product  $Z_o K$ . Thus as far as the impedance transforming properties are concerned, the  $K$ -amplifier acts like an ideal transformer with a turns ratio of  $K^{1/2}$ .

As a result of this impedance transforming property, an impedance which is connected to one side of a  $K$ -amplifier may be transferred to the other side by simply multiplying it by  $K$  (or  $1/K$ ) without changing

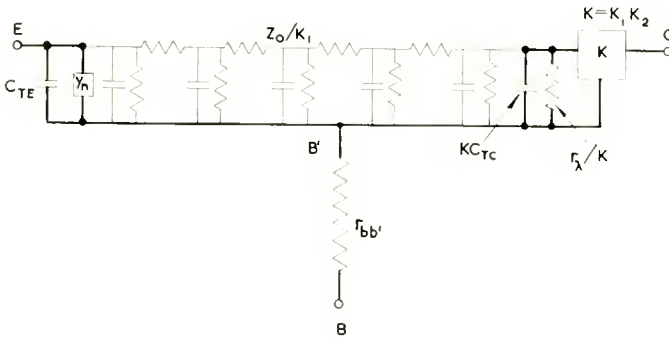


Fig. 4—Simplified (exact) circuit obtained from Figure 2.

the impedance levels as viewed from the terminals. This property can then be used to simplify the circuit shown in Figure 2 without loss of accuracy. Thus all passive elements are transferred to the left, i.e., the two  $K$ -amplifiers are transferred to the right and are combined to yield a single  $K$ -amplifier with  $K = K_1 K_2$ , as shown in Figure 4. The characteristic impedance of the transmission line is now  $Z_o/K_1$ , where  $Z_o$  is the characteristic impedance of the original transmission line. Also, the resistance  $r_{\lambda}$  is divided by  $K$  and the capacitance  $C_{Tc}$  is multiplied by  $K$ , as required by the impedance transforming properties of a  $K$ -amplifier.

### BASE-WIDTH MODULATION

Early<sup>7</sup> has shown that the impedance levels of a transistor are affected to a major extent by the fact that the widths of the transition

regions (where the potential barriers are located) are a function of the voltages across them. These voltages determine the effective base width, since the base is bordered by the two transition regions. Only the effect of the collector transition region will be examined here since it is the more important, being the largest of the two as a result of the higher voltages across it. However, the conclusions which follow can also be interpreted with reference to the emitter transition region.

Consider now, how the circuit of Figure 4 should be modified in order to represent the effect of an a-c voltage across the collector transition region. This voltage will continuously change the base width, which is equivalent to continuously changing the length of the transmission line of Figure 1c or Figure 4. To account for this variation in length as required for a small-signal linear circuit we proceed as follows.

Let the distribution of the minority carriers in the base under steady d-c conditions be as shown by the solid line in Figure 1a. As stated earlier, a similar distribution of charge will also be found in the RC transmission line of Figure 1c when a direct current is flowing in it. A change in the collector voltage from  $V_C$  to  $V'_C$  will now not only change the charge density at point  $x = W$  from  $P_0(V_C)$  to  $P_0(V'_C)$ , but as explained above, it will also change the length of the line from  $W$  to  $W'$  as shown in Figure 1a. The shaded area in Figure 1a now represents the excess charge which will cause an incremental current to flow out of the collector *and which is obviously greater than it would be if the effective base width had remained constant at  $x = W$* . Hence, the ratio of the resultant increment of collector current to the increment of collector voltage is greater, i.e., the impedance is smaller, than if base width modulation were ignored.

To summarize, the net small-signal effect of base width modulation is to decrease the small-signal output impedance of the transistor. To achieve this effect in the circuit of Figure 1c, it is readily seen that we may simply lower the value of  $K_2$  in the collector K-amplifier. This results in a lower value for  $K$  in Figure 4.

Similarly, when considering the *input* impedance of a common-base transistor amplifier for a given load connected to the output, it can be shown that in actual practice it is larger than it would be if the Early effect were absent. Therefore, lowering the value of  $K_2$  in Figure 1c, and hence the value of  $K$  in Figure 4, achieves the desired correction to the equivalent circuit.\*

---

\* Lowering the value of  $K$  implies that the load impedance is divided by a small number, hence the input impedance is higher.

The value of  $K$  for the special case of a plane parallel transistor in terms of physical quantities is given by<sup>4</sup>

$$K = \frac{1}{\frac{1}{\Delta L_p} \cdot \frac{\partial W}{\partial V_C} \operatorname{cosech} \frac{W}{L_p} \frac{\exp.(-\Delta V_C)}{\exp.(\Delta V_E)} + \frac{1}{\Delta L_p} \cdot \frac{\partial W}{\partial V_C} \coth \frac{W}{L_p} + \frac{\exp.(-\Delta V_C)}{\exp.(\Delta V_E)}} \quad (2a)$$

where  $1/\Delta \doteq 25.9$  millivolts at room temperature,

$V_C$  and  $V_E$  = collector and emitter d-c bias voltages respectively,

$L_p$  = diffusion length for minority carriers in base.

The first and second terms in the denominator are the result of the Early effect only, while the third term is the result of the Shockley theory. For the usual collector voltages the first term is the dominating one. Thus, if the width of the collector transition region is given by<sup>6</sup>

$$d = AV^n,$$

where  $A$  is a constant and  $n = 1/2$  for a "step" or Schottky type junction and  $n = 1/3$  for a uniform impurity concentration gradient junction, then for  $W/L_p \ll 1$ , the value for  $K$  reduces to

$$K = \frac{38}{n} \frac{W}{d} V_C. \quad (2b)$$

As an example, for a step junction with a collector voltage of 6 volts, a base width of  $2 \times 10^{-3}$  inch and a collector transition width of  $0.15 \times 10^{-3}$  inch, the value of  $K = 5,000$ .

#### LUMPED-PARAMETER EQUIVALENT CIRCUIT

In practical engineering problems it is desirable to replace the distributed elements of Figure 4 by a lumped network. This circuit is shown in Figure 5. It is obtained by choosing a  $\pi$ -network to replace the transmission line and then simply combining the elements  $C_{TC}$ ,  $C_{TE}$  and  $r_\lambda$  with its parallel branches. The choice of a  $\pi$ -network here has the merit that for a plane parallel transistor with uniform hole-electron recombination, the lumped elements are substantially independent of frequency in the frequency range where a power gain is possible (See Appendix).

In the Appendix it is also shown that the parallel branches of the  $\pi$ -network consist of a conductance,  $g_D$ , in parallel with a capacitance,  $C_D$ , while the series branch consists of a resistance,  $r_d$ , in series with an inductance,  $L_d$ . Also, replacing the admittance  $y_n$ , of Figure 4 with its parallel components, i.e.,  $y_n = g_n + j\omega C_n$ , it follows that the components of the elements of Figure 5 are

$$\begin{aligned} g_e &= g_D + g_n, \\ C_e &= C_D + C_{TE} + C_n, \\ g_{c'} &= g'_D + K/r_\lambda, \\ C_{c'} &= C_D + KC_{TC}. \end{aligned}$$

It should be noted that  $g_D = g'_D$  only if hole-electron recombination is uniform everywhere in the base and if no surface recombination

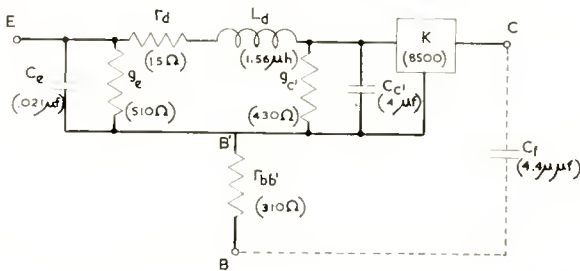


Fig. 5—Lumped parameter approximation of natural equivalent circuit.

occurs. Also, for present-day transistors the dominating components of  $g_e$ ,  $C_e$ , and  $C_{c'}$  are  $g_D$ ,  $C_D$ , and  $KC_{TC}$ , respectively.

The equivalent circuit shown in Figure 5 may be used in circuit design problems at all frequencies where a power gain is possible. The following practical points are noted:

(a) The resistance  $r_d$  has a theoretical value of about 26 ohms at a d-c emitter current of one milliamperere (See Appendix). For currents greater than about 0.2 milliamperere,  $r_d$  is given by

$$r_d = \frac{26}{I_E} \quad (3)$$

where  $I_E$  is emitter current in milliampereres.

(b) As shown later,  $g_e$  is related to  $r_d$  as follows:

$$g_e = \frac{1}{\alpha_{cbo} r_d} \quad (4)$$

where  $\alpha_{cb0}$  is the low-frequency, common-emitter, short-circuit current-amplification factor.

(c) The capacitance  $C_e$  is related to  $g_e$  as follows (see Equation (10)):

$$\omega_{cb} \doteq g_e / C_e \quad (5)$$

where  $\omega_{cb}$  is equal to the angular frequency at which the common-emitter, short-circuit current-amplification factor,  $\alpha_{cb}$ , has decreased by 3 decibels from its low-frequency value. It is sometimes referred to as a cutoff angular frequency.

(d) The inductance  $L_d$  is of importance only at the highest frequencies of the useful frequency range and is responsible for  $\alpha_{cb}$  having a phase shift greater than  $90^\circ$  at these frequencies. In the Appendix it is shown that

$$L_d = \frac{r_d^2 C_e}{n'} \quad (6a)$$

$$= \frac{r_d}{n' \alpha_{cb0} \omega_{cb}} \quad (6b)$$

where, in Equation (6b), use is made of Equations (4) and (5), and where  $n'$  is a number in the order of 3. Thus at an (angular) frequency as high as  $(\alpha_{cb0} \omega_{cb})$  the reactance of  $L_d$  is only  $r_d/n'$  ohms.

The measured values of the elements for a particular alloy transistor (described in Reference (4)) are shown in Figure 5. For this transistor, a collector to base interelectrode capacitance,  $C_f$ , of 4.4 micromicrofarads was also measured. For the transistor of Figure 5, where the transformed collector capacitance is shown as 0.4 microfarad, the actual collector barrier capacitance is approximately  $(0.4 - 0.021) / 8500 = 45$  micromicrofarads.

#### COMMON-EMITTER AND COMMON-COLLECTOR CIRCUITS

The equivalent circuit of Figure 5 is particularly useful in the analysis of common-base circuits since the active and passive parts of the circuit simply appear in cascade. For the common-emitter operation, however, it is convenient to convert the circuit of Figure 5 to that of Figure 6. This circuit uses the same basic elements, with the following modifications:

- (a) The names of nodes  $E$  and  $B'$  are interchanged.
- (b)  $r_{bb'}$  is now connected to the node where  $r_d$  and  $g_e$  join.

- (c) A phase reversing transformer is added in cascade.  
 (d) A current generator is added whose current is equal to the current in the collector lead.

This conversion is based on the premise that  $y_{11} \gg y_{12}$  and  $y_{21} \gg y_{22}$ .\*

An alternative common-emitter circuit is shown in Figure 7b.\*\* This may be obtained from Figure 5 by first shifting the  $K$ -amplifier to the left, as shown in Figure 7a (while noting its impedance transforming properties); next replacing the  $K$ -amplifier by the generator shown in Figure 3d; and finally redrawing the circuit. An advantage which can be claimed for Figure 6 over Figure 7b is that the generator in Figure 6 is dependent on the current at a terminal, namely  $I_c$ , which in practical problems may be known, whereas the generator of Figure 7b is a function of a voltage at an internal point of the circuit,  $V_{b'e}$ , which is quite difficult to determine.

In a manner similar to that used in the derivation of the common-

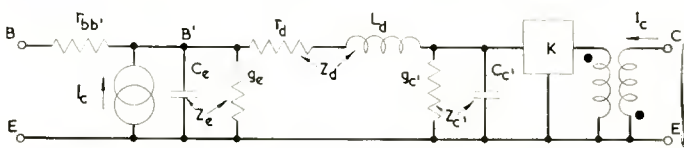


Fig. 6—Equivalent circuit modified for common-emitter operation.

emitter circuit of Figure 7b, a common-collector circuit is derived and is shown in Figure 7c. Note that here the value of the voltage generator is  $(K-1)/KV_{b'e} \doteq V_{b'e}$  since  $K \gg 1$ . Similarly, the value of the generator of Figure 7b is  $(K-1)V_{b'e} \doteq KV_{b'e}$ . These generators are therefore also independent of frequency.

Note also that the passive elements of Figures 6, 7b, and 7c are the same as those of the more basic circuit shown in Figure 5, except for the factor  $K$ . This means that all expressions such as those for power gain etc. are simultaneously applicable to all these circuits, and that they can, furthermore, be easily directly related to the physical properties of the transistor, i.e., resistivities of the material, geometry, etc.

#### RELATION TO EXTERNALLY MEASURED QUANTITIES

Due to the comparatively high output impedance and low input impedance of transistors, it is advantageous to make measurements

\* Equation (12) of Reference (4).

\*\* By replacing the voltage generator in Figure 7b by a current generator, the modified  $\pi$ -circuit is obtained which is discussed by H. Johnson in Reference (3).

which involve a-c short circuits at the output terminals and open-circuits at the input terminals. Examples of such measurements are those for the short-circuit input impedance,  $1/y_{11}$ ; the short-circuit current amplification factor,  $\alpha_{21}$ ; the open-circuit reverse voltage amplification factor,  $\mu_{21}$ ; and the open-circuit output admittance  $1/z_{22}$ . These quantities have been termed the *h*-parameters, i.e.,  $h_{11}$ ,  $h_{21}$ ,  $h_{12}$ , and  $h_{22}$ , respectively.<sup>8</sup>

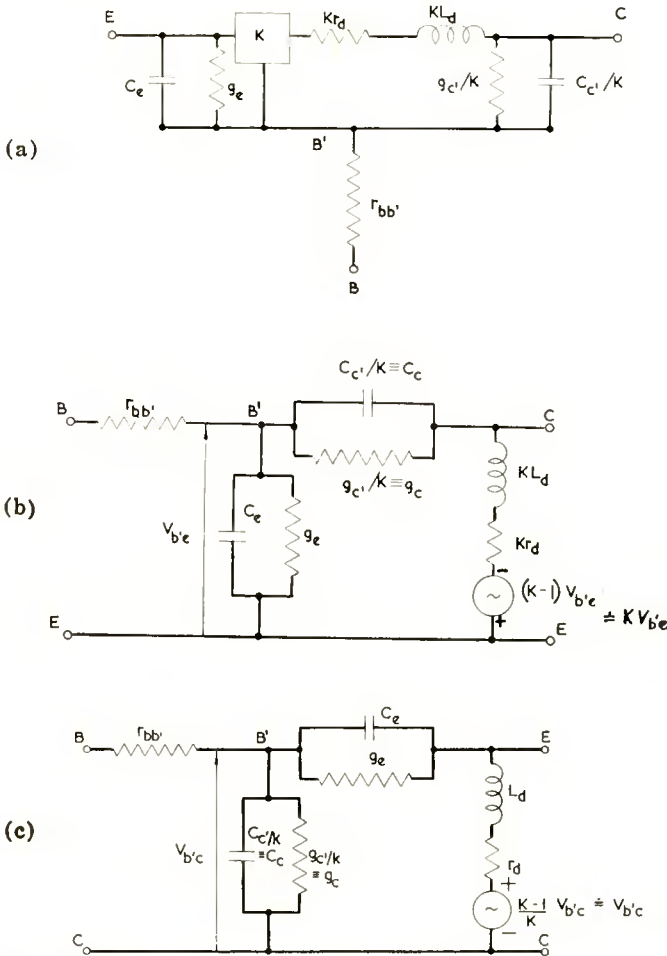


Fig. 7—(a) K-amplifier shifted to left in Figure 5; (b) Figure 7a redrawn with generator replacing K-amplifier to obtain alternative common-emitter circuit; (c) Common-collector equivalent circuit.

<sup>8</sup> E. A. Guillemin, *Communication Networks*, Vol. II, John Wiley & Sons, Inc., New York, N. Y., 1935.

The  $h$ -parameters for the *common-emitter* connection are easily shown to be\* (for  $K \gg 1$ )

$$h_{11} = 1/y_{bb} = r_{bb'} + z_e \quad (7a)$$

$$h_{21} = \alpha_{cb} = \frac{z_e}{z_d} \quad (7b)$$

$$h_{12} = \mu_{bc} = \frac{z_e}{Kz_{c'}} \quad (7c)$$

$$h_{22} = 1/z_{ce} = \left( \frac{1}{z_{c'}} + \frac{1}{z_d} + \frac{z_e}{z_{c'}z_d} \right) \frac{1}{K} \quad (7d)$$

where  $z_e = 1/(g_e + j\omega C_e)$ ,  $z_d = (r_d + j\omega L_d)$ , and  $z_{c'} = 1/(g_{c'} + j\omega C_{c'})$ .

The effect of the interelectrode capacitance,  $C_f$ , has been neglected in the above equations. Experimentally it is found that for most present-day transistors it affects only  $\mu_{bc}$  substantially, particularly at high frequencies. This is seen in Figure 8\*\* which shows the variation with frequency of the phase angle and magnitude of  $\mu_{bc}$  for the particular transistor whose values are indicated in Figure 5. The solid curve is calculated and includes the effect of  $C_f$  while the dotted curve excludes it. Since in the useful frequency range the reactance of  $C_f$  is large compared to  $r_{bb'}$ , its effect on Equation (7c) is merely to add a term  $r_{bb'}/X_f$  to it, where  $X_f = 1/j\omega C_f$ .

Of special interest is the expression for  $\alpha_{cb}$  given by Equation (7b). Substituting the full values for  $z_e$  and  $z_d$  in this equation,  $\alpha_{cb}$  may be written

$$\alpha_{cb} = \frac{1}{(g_e + j\omega C_e)(r_d + j\omega L_d)} \quad (8a)$$

$$\equiv \frac{\alpha_{cb0}}{(1 + j\omega/\omega_c)(1 + j\omega/\omega_d)}, \quad (8b)$$

where

\* It is interesting to note that the  $h$ -parameters for a  $K$ -amplifier are  $h_{11} = 0$ ,  $h_{21} = -1$ ,  $h_{12} = 1/K$  and  $h_{22} = 0$ . The negative sign for  $h_{21}$  is a result of a particular sign convention which states that all currents flowing into a device are positive.

\*\* Figure 8 corresponds to Figure 5d of Reference (4) and is reproduced here for convenience. The small circles indicate experimental measurements.

$$\alpha_{cbo} \equiv 1/r_d g_e, \tag{9a}$$

$$\omega_e \equiv g_e/C_e, \tag{9b}$$

and 
$$\omega_d \equiv r_d/L_d. \tag{9c}$$

From Equations (9a) and (6a) it follows that

$$\omega_d/\omega_e = n' \alpha_{cbo}.$$

Thus for a good transistor where  $\alpha_{cbo}$  is high,  $\omega_d$  is very much larger than  $\omega_e$ , and from Equation (8b) the angular frequency at which  $|\alpha_{cb}|$  has decreased by 3 decibels is, to a good approximation,

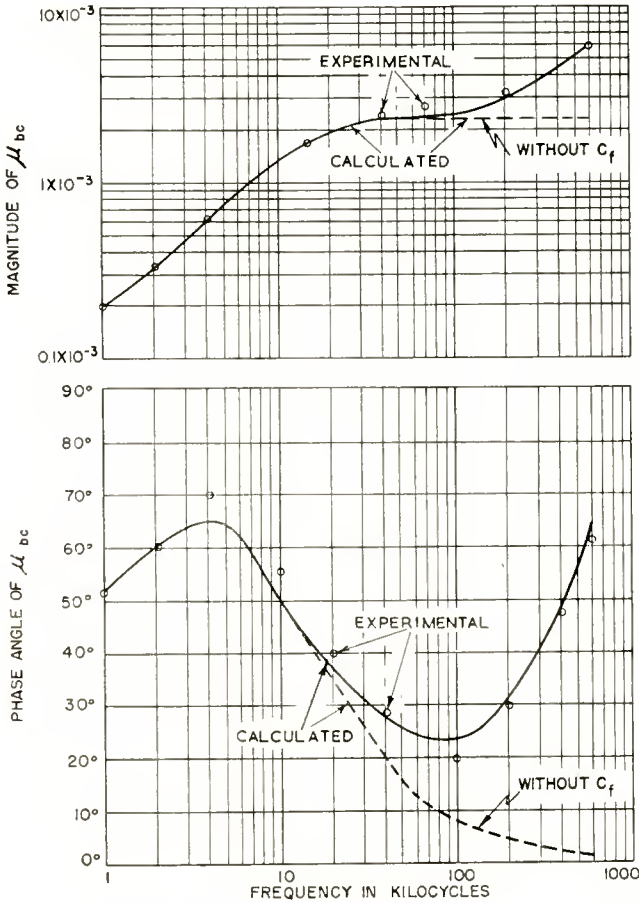


Fig. 8—Frequency dependence of magnitude and phase angle of open-circuit reverse voltage amplification factor  $\mu_{bc}$ .

$$\omega_{cb} \doteq \omega_e = g_e/C_e. \quad (10)$$

Equations (9a) and (10) confirm Equations (4) and (5). Also Equation (8b) may now be written

$$\alpha_{cb} = \frac{\alpha_{cbo}}{(1 + j\omega/\omega_{cb})(1 + j\omega/n'\alpha_{cbo}\omega_{cb})}. \quad (11a)$$

This expression, which has two terms in the denominator, is applicable in the complete frequency range where a power gain is expected. However, if the transmission-line circuit of Figure 4 were used, an infinite number of terms would appear in the denominator. It is also noted that in the medium frequency range, where  $L_d$  is assumed to be zero, we may write, from Equations (8a) and (10),

$$\alpha_{cb} = \frac{\alpha_{cbo}}{(1 + j\omega/\omega_{cb})} \quad (11b)$$

which is the expression used in the earlier literature.<sup>1</sup>

It is seen from the above that the capacitance  $C_c$  is mainly responsible for the  $\alpha_{cb}$  cutoff frequency,  $\omega_{cb}$ . In the same way, the capacitance  $C_{c'}$  is largely responsible for the *rise* with frequency of the magnitude of  $\mu_{bc}$ . This follows from Equation (7c), which may be written

$$\mu_{bc} = \frac{g_{c'} + j\omega C_{c'}}{K(g_e + j\omega C_e)} \quad (12a)$$

$$= \frac{g_{c'}(1 + j\omega/\omega_c)}{Kg_c(1 + j\omega/\omega_{cb})} \quad (12b)$$

where  $\omega_c \equiv g_{c'}/C_{c'}$  and  $\omega_{cb}$  is given by Equation (10). For present-day junction transistors,  $\omega_c \ll \omega_{cb}$  and thus  $\omega_c$  is very nearly equal to the angular frequency at which the magnitude of  $\mu_{bc}$  has increased 3 decibels from its low-frequency value.

To determine experimentally the values of the elements of a circuit, the number of spot measurements required is equal to the number of independent elements which are present. Let the following common-emitter  $h$ -parameter spot measurements be made:

$r_{bc}$  = low-frequency value of  $1/y_{bb}$ ,

$r_{bh}$  = high-frequency value of  $1/y_{bb}$ ,

$\alpha_{cbo}$  = low-frequency value of  $\alpha_{cb}$ ,

$\omega_{cb}$  = angular frequency at which  $|\alpha_{cb}|$  has fallen 3 decibels from its low-frequency value,

$r_{co}$  = low-frequency value of  $z_{co}$ ,

$\mu_o$  = low-frequency value of  $\mu_{bc}$ ,

$\omega_o$  = angular frequency at which  $\mu_{bc}$  has risen 3 decibels from its low-frequency value (it is assumed that  $\omega_o \ll \omega_{cb}$ ).

Thus the elements of the equivalent circuit are, from Equations (7a) to (7d),

$$\begin{aligned} r_{bb'} &= r_{bh} \\ 1/g_e &= r_{bo} - r_{bb'} \\ r_d &= 1/g_e \alpha_{cbo} \\ C_e &= g_e/\omega_{cb} \\ K &= 1/\mu_o \left( \frac{r_d}{\mu_o r_{co}} - 1 \right) \\ g_{e'} &= K \mu_o g_e \\ C_{e'} &= g_{e'}/\omega_o. \end{aligned}$$

As stated earlier, these seven elements are the most important. If still greater accuracy is required,  $L_d$  can be found provided an eighth spot measurement is made.

Note that  $r_{bh}$  is the only measurement which is made here at an angular frequency which exceeds  $\omega_{cb}$ . As an alternative, the magnitude of  $y_{bb}$  may be determined at the angular frequency  $\omega_{cb}$ . Let this measurement be designated  $|y_{b3}|$ . It can now be shown from Equation (7a) that

$$1/g_e = r_{bo} \left( 1 - \sqrt{2/(|y_{b3}| r_{bo})^2 - 1} \right)$$

and

$$r_{bb'} = r_{bo} - \frac{1}{g_e}.$$

The other elements are found as above.

### CONCLUSIONS

An equivalent circuit for a junction transistor has been synthesized from circuit elements representing the individual physical phenomena, and as such it is unique and fundamental. The circuit has been found

to reduce without approximation into an active part and a passive part which are in cascade. It is seen that the short-circuit current amplification factor,  $\alpha_{cb}$ , which has been used in the past, only partly describes the circuit; of equal importance however is the factor  $K$ , which is the amplification factor of the active part. Furthermore, a reduction in base width increases the value of  $\alpha_{cbo}$ , but it also decreases the factor  $K$ , and hence design compromises must be made.

It was found that the exact circuit which contains a transmission line may be quite accurately approximated by a lumped-constant network in the complete frequency range where a power gain is expected, since the line is comparatively short. Modified circuits particularly useful for common-emitter and common-collector operation have also been shown. Furthermore, the cascaded nature of the basic circuit, the relative frequency independence of the active and the passive elements, and the simplicity of the expression for the  $h$ -parameters commend its use in practical circuit applications.

#### ACKNOWLEDGMENT

This work has been discussed and constructively criticized by H. Johnson and L. J. Giacoletto of the RCA Laboratories, Princeton, N. J., and F. D. Waldhauer and C. C. Cheng of the Engineering Products Division of the Radio Corporation of America. The experimental data was taken by R. K. Gerlach of the Engineering Products Division.

#### APPENDIX

The admittances of the parallel branches of a  $\pi$ -network representing a general four-terminal passive network are easily shown to be  $(y_{11} + y_{12})$  and  $(y_{22} + y_{12})$  while the admittance of the series branch is  $-y_{12} = -y_{21}$ , where  $y_{11}$ ,  $y_{12}$ ,  $y_{21}$  and  $y_{22}$  are the general short-circuit admittances.

Consider now the transmission line representation resulting from the flow of minority carriers in the base. For the *special case* of a plane parallel transistor it follows\* that

$$y'_{11} = y'_{22} = G \theta \coth \theta \quad (13)$$

$$\text{and} \quad y'_{12} = y'_{21} = -G \theta \operatorname{cosech} \theta \quad (14)$$

$$\text{where} \quad G \doteq qI_E/kT \quad (15)$$

---

\* From Equations (9a) to (10b) of Reference (4).

and 
$$\theta = \frac{W}{L_p} (1 + j\omega\tau_p)^{1/2}. \quad (16)$$

To represent this transmission line by a  $\pi$ -network having lumped elements, the hyperbolic functions may be expanded neglecting all terms involving powers of  $(W/L_p)$  higher than 2, since for a good transistor  $(W/L_p) \ll 1$ . Thus for all frequencies where a power gain may be expected, the admittances of the parallel branches of the  $\pi$ -network are

$$\begin{aligned} y'_{11} + y'_{12} &\doteq \frac{GW^2}{2L_p^2} + j\omega \frac{GW^2}{2L_p^2} \tau_p \\ &\equiv g_D + j\omega C_D \end{aligned} \quad (17)$$

while the admittance of the series branch is

$$-y'_{12} \doteq \frac{1}{\frac{1}{G} + j\omega \frac{\tau_p W^2}{6L_p^2 G}} \equiv \frac{1}{r_d + j\omega L_d}. \quad (18)$$

From Equations (17) and (18) it follows that

$$L_d = r_d^2 C_D / n' \quad (19)$$

where  $n' \doteq 3$ . This confirms Equation (6a) if  $C_D \doteq C_e$ .

# FREQUENCY CHARACTERISTICS OF LOCAL OSCILLATORS\*

BY

W. Y. PAN

RCA Victor Television Division,  
Camden, N. J.

*Summary*—The frequency characteristics of local oscillators under conditions of heat flow inside and outside the oscillator tubes can be expressed approximately in simple mathematical formulas. With the aid of such an analytical treatment, the various factors affecting the instantaneous oscillator frequency may be evaluated.

This investigation discloses the possibility of more accurate compensations for oscillator frequency deviations, particularly during the warm-up period, by logical approaches, thus eliminating the conventional trial-and-error processes.

## GENERAL DISCUSSION

WITH the advent of color television at very-high frequencies (VHF) and ultra-high frequencies (UHF), the requirement for local oscillator stability is difficult to fulfill with the conventional method of frequency compensation. A study of this problem has been made, based on the local oscillator circuit shown in Figure 1 which is typical for receivers covering frequencies up to 1,000 megacycles.

At low frequencies, the series circuit capacitance  $C_s$  is usually a short circuit, and the parallel circuit capacitance  $C_p$  is of some finite value. Furthermore, the plate and grid lead inductances  $L_p$  and  $L_g$ , respectively, can be neglected; and the interelectrode capacitances  $C_{gp}$ ,  $C_{gk}$ ,  $C_{hk}$ , and  $C_{pk}$  have relatively insignificant effects in the determination of the oscillator frequency. At VHF and UHF, however,  $C_p$  is invariably an open circuit and  $C_s$  is often used; the lead inductances and interelectrode capacitances of the oscillator tube become important factors profoundly affecting the oscillator frequency.

During the warm-up period, heat flows are taking place inside as well as outside the oscillator tube by radiation and conduction from the hot elements — the cathode and plate. Initially the grid intercepts heat from both hot elements, though it may eventually reach a temperature even higher than the plate temperature in certain types of tubes. The flow of heat in various forms and directions unavoidably

---

\* Decimal Classification: R361.102.2.

changes the tube and circuit constants and, consequently, the oscillator frequency.

The problem of oscillator frequency characteristics was approached by investigating the behavior of (1) the oscillator tube, and (2) the associated circuit elements, particularly during the warm-up period. From a knowledge of this behavior it should be possible to provide a more accurate and logical means of frequency stabilization in any receiver and equipment applications.

### BEHAVIOR OF OSCILLATOR TUBES

#### *Heat Flow Among Tube Elements*

The heat flow in an oscillator tube depends upon the instantaneous

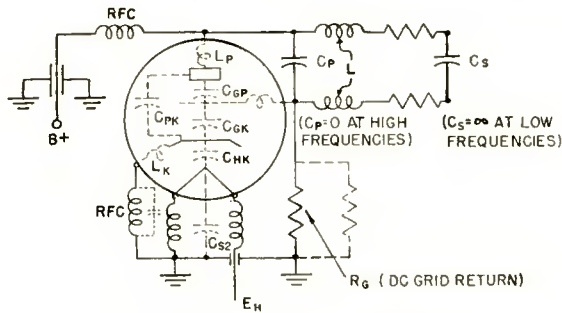


Fig. 1—Local oscillator circuit.

temperature of the hot elements, the geometry of the tube elements, and other factors of a complex nature.<sup>1</sup> In most oscillator tubes of the miniature type such as the 6X8, 6BE6, 6AF4, 6T4, and 6F4, the heat flows of dominant effect on the oscillator frequency are (1) the cathode-to-grid radiation, (2) the cathode-to-plate radiation, and (3) the plate-to-grid or grid-to-plate radiation. Other forms of heat flow by conduction to and away from the grid through the side rods, through the supporting material, and due to electric bombardment are relatively small in magnitude.

According to the Stefan-Boltzmann law, the radiation power is proportional to the fourth power of the absolute temperature of the radiator. The instantaneous cathode-to-grid radiation, for instance, has been found to be

$$Q = \sigma e_k A_k T_k^4 F_a F_s (1 - e^{-bt}) \quad (1)$$

<sup>1</sup>H. C. Hottel, "Radiant Heat Transmission Between Surfaces Separated by Non-Absorbing Media," *Transactions, A.S.M.E.*, 1931.

where

$Q$  = radiation in watts,

$\sigma = 5.67 \times 10^{-12}$  watts/cm<sup>2</sup> °K<sup>4</sup>,

$e_k$  = thermal emissivity (= 0.2 for ordinary cathode surface),

$A_k$  = cathode area, cm<sup>2</sup>,

$T_k$  = cathode temperature, °K, assumed much higher than the grid temperature at all times,

$F_f$  = length (of cathode) to spacing (between cathode and grid) factor,

$F_f$	Length to Spacing Ratio
0.8	10
0.9	25
0.95	50

$F_a$  = grid winding pitch to grid wire diameter factor,

$F_a$	Pitch to Diameter Ratio
0.3	5
0.45	3
0.65	2

$F_e$  = effect of grid emissivity, 0.8 for ordinary grid surface,

$t$  = time in minutes,

$b$  = a time constant, determining the rate of heat flow from the cathode to the grid.

For a given oscillator tube with normal heater and plate powers the cathode-to-grid radiation can be represented by a simpler expression,

$$Q = a (1 - e^{-bt}) \tag{2}$$

where

$$a = \sigma e_k A_k T_k^4 F_f F_a F_e.$$

*Temperature Rise in Tube Elements*

The cathode-to-grid radiation raises the grid temperature,  $T$ . Again, for a given oscillator tube with normal heater and plate powers the temperature rise of the grid also follows the same expression as Equation (2).

$$\Delta T = c (1 - e^{-dt}) \quad (3)$$

where

$\Delta T$  = instantaneous grid-temperature rise due to cathode-to-grid radiation,

$c$  = total grid-temperature rise in  $^{\circ}\text{C}$  due to cathode-to-grid radiation,

$d$  = a time constant determining the rate of grid-temperature rise due to cathode-to-grid radiation.

Similarly, the plate-to-grid radiation (if the plate is hotter than the grid) gives rise to the same effects on the grid temperature, but having different magnitudes in constants  $c$  and  $d$ .

#### *Change of Tube Capacitance*

The resultant temperature rise of the grid transforms the grid configuration and geometry which leads to variances of the grid-to-plate and grid-to-cathode capacitances:

$$\Delta C_{gp} = \delta (1 - e^{-\theta t}) \quad (4)$$

where

$\Delta C_{gp}$  = instantaneous change of grid-to-plate capacitance,

$\delta$  = maximum change of grid-to-plate capacitance,

$\theta$  = a time constant determining the rate of change of grid-to-plate capacitance.

The grid-to-cathode and other interelectrode capacitances are changed due to temperature rises according to similar expressions.

#### *Oscillator Frequency Deviations*

The changes in interelectrode capacitances may substantially deviate the oscillator frequency in a manner similar to that of varying the constants of the associated circuit elements such as  $L$  and  $C_s$  or  $C_p$  of Figure 1.

In analyzing the behavior of the oscillator tube and its effect on the oscillator frequency due to heat flow, the associated circuit elements are assumed to have zero temperature coefficient. Therefore, such constants are not influenced by the heat radiation and conduction to the elements outside the oscillator tube. Under these conditions the oscillator circuit of Figure 1 can be represented by an equivalent

circuit indicated in Figure 2 where  $r$  is the equivalent damping factor which also takes into account the transit time effect of the tube at the oscillator frequency.

The capacitance  $C_t$  is the equivalent tube capacitance other than  $C_{gp}$ , but electrically effective in determining the oscillator frequency. In actual operation  $C_{gp} \gg C_t$  and  $\Delta C_{gp} \gg \Delta C_t$  for most oscillator tube types.

For a small change of the tube capacitance  $C_0$ , where  $C_0 = C_{gp} + C_t$ , the deviation of oscillator frequency  $\Delta F$  is proportional to  $\Delta C_0$ . With the aid of Equation (4), the oscillator frequency characteristics can also be expressed by the general formula

$$\Delta F = \alpha (1 - e^{-\beta t}) \tag{5}$$

where

$\Delta F$  = instantaneous change of oscillator frequency in megacycles,

$\alpha$  = maximum frequency deviation in megacycles,

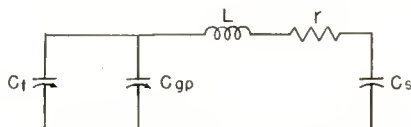


Fig. 2—Equivalent local oscillator circuit.

$\beta$  = a constant determining the rate of change of oscillator frequency with respect to time,  $t$ , in minutes.

The change of oscillator frequency  $\Delta F$  consists of two components,  $\Delta F'$  due to  $\Delta C_{gp}$  and  $\Delta F''$  due to  $\Delta C_t$ , where

$$\Delta F' = \alpha' (1 - e^{-\beta' t}),$$

$$\Delta F'' = \alpha'' (1 - e^{-\beta'' t}).$$

The expression for  $\Delta F$  indicated in Equation (5) is approximately satisfied only if either of the following conditions holds:

$$\alpha' \gg \alpha'' \quad \text{or} \quad \beta' = \beta''.$$

Since  $\Delta C_{gp} \gg \Delta C_t$ ,  $\alpha' \gg \alpha''$ .

To ascertain the validity of Equation (5), the frequency characteristics of a typical UHF television local oscillator, henceforth referred

to as "oscillator X", have been carefully observed. Oscillator X employed a 6AF4A tube and operated at 500 megacycles in a circuit similar to that of Figure 1, except that  $C_p = 0$  and  $C_s = \text{infinity}$ . The circuit inductance,  $L$ , was made of silver-plated invar conductor having a very low coefficient of thermal expansion. The solid curve of Figure 3 is plotted according to Equation (5), while the dots are the observed values. The discrepancy between the dots and the solid curve is a measure of the approximation involved in Equation (5).

The oscillator frequency at exactly 0.5 minute after the oscillator tube had been energized was taken as reference. Any deviation from this reference frequency is defined as frequency drift. The 0.5-minute

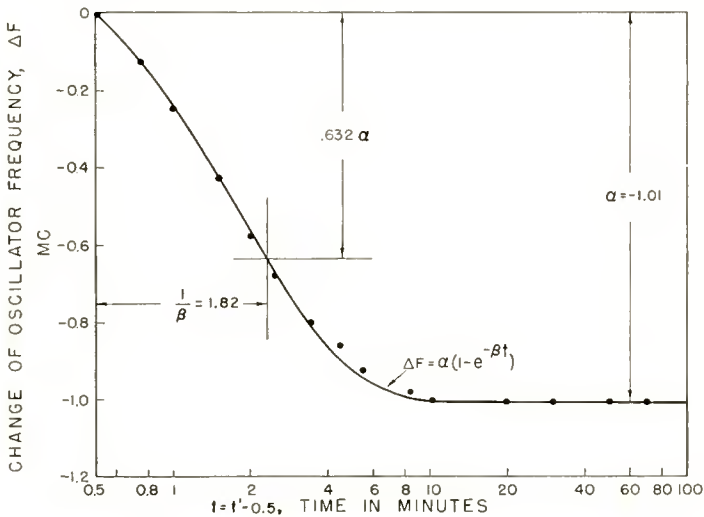


Fig. 3—Frequency characteristics of oscillator X.

delay in establishing the reference oscillator frequency is to enable the receiver to attain operable conditions. For convenience,  $t = t' - 0.5$  minute, or  $t = 0$  when the oscillator tube has been energized exactly 0.5 minute.

The frequency of oscillator X decreased with time, indicating that the tube capacitances exhibited a positive temperature coefficient. The oscillator became substantially stabilized after 20 minutes at which time the frequency deviation was 1.01 megacycles or  $\alpha = -1.01$ . The change of oscillator frequency reached  $0.632\alpha$  in  $t = 1.82$  minutes. Therefore,  $\beta (=1/t) = 0.55$ . According to Equation (5) the constants  $\alpha$  and  $\beta$  can fully describe the frequency characteristics of oscillator X. However, the magnitudes of these constants may vary with local oscillators and different operating conditions.

FACTORS AFFECTING OSCILLATOR FREQUENCY CHARACTERISTICS

The relative magnitudes of constants  $\alpha$  and  $\beta$  primarily depend upon (1) the thermal emissivity of all tube electrodes, (2) the heater and plate powers, (3) the constructions and geometry of the electrodes, and (4) the lead connections and supports. For a given oscillator tube,  $\alpha$  also varies considerably with (1) the oscillator frequency, (2) the oscillator compartment size and configuration, and (3) the associated circuit constants. In pursuit of the determination of the quantitative significance of  $\alpha$  and  $\beta$ , the following factors affecting the oscillator frequency characteristics have been evaluated experimentally.

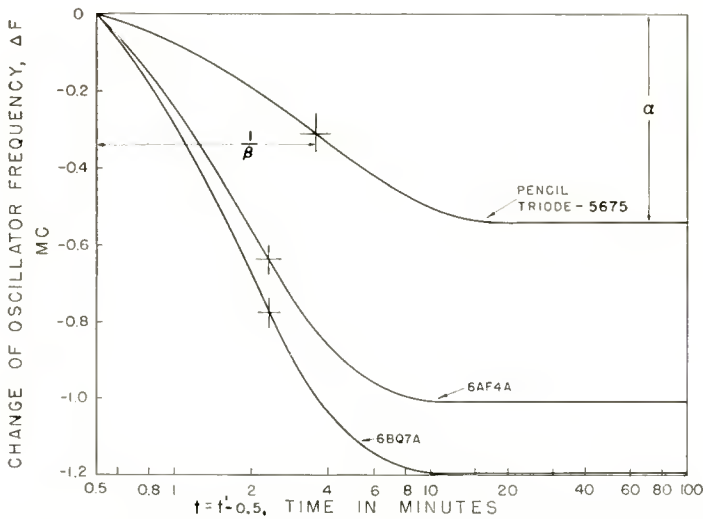


Fig. 4—Oscillator frequency characteristics with different tube types.

Oscillator Tube Types

Three identical oscillator chassis have been constructed, employing a 5675 pencil triode, a 6AF4A, and a 6BQ7A tube. All oscillators were operated at 500 megacycles using the same oscillator circuit elements, and normal heater and plate power. For every tube type an average tube was chosen from a lot of six selected at random. The differences in frequency characteristics of these three types of oscillator tubes are shown in Figure 4. The oscillator frequency of the 5675 pencil triode drifted approximately half as much as the miniature type tubes in an uncompensated oscillator circuit and it took a much longer time to reach the  $0.632\alpha$  point.

Table I—Variations of Constants  $\alpha$  and  $\beta$  With Different Tube Types.

Tube Type	$\alpha$	$\beta$
Pencil triode, 5675	-0.54	0.32
6AF4A	-1.01	0.55
6BQ7A	-1.19	0.56

(a) **Heater Power Variations**—By keeping the plate power constant at 1.0 watt, the oscillator frequency drifted differently with varying amounts of heater power. The 6AF4A tube, for instance, has

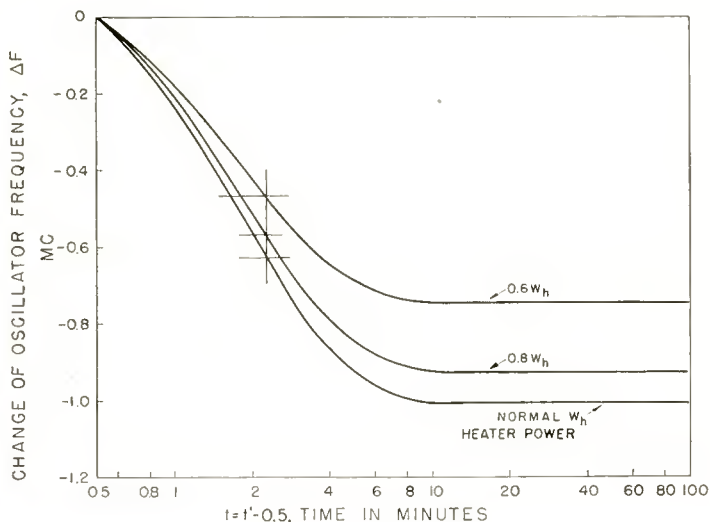


Fig. 5—Frequency characteristics of oscillator X with heater power variations; plate power is kept constant at 1.0 watt.

been designed to withstand a cathode temperature of the order of  $1000^{\circ}\text{K}$  with a normal heater voltage of 6.3 volts or a heater power of 1.42 watts. A reduction of heater power decreased the cathode radiation, thus lowering the ultimate temperatures of the tube electrodes.

Experimental results taken with oscillator X under these conditions are illustrated in Figure 5 using heater powers of 1.42, 0.8, and 0.6 watt.

The constant  $\alpha$  is not a simple function of the corresponding heater powers. However, it is noted that the percentage change of  $\alpha$  is much less than that of the heater power, and  $\beta$  remains practically unchanged.

Table II—Relative Magnitudes of Constants  $\alpha$  and  $\beta$  With Variations of Heater Power, Plate Power = 1.0 Watt

Heater Power	$\alpha$	$\beta$
1.42 watts	-1.01	0.55
0.8	-0.93	0.55
0.6	-0.75	0.55

(b) **Plate Power Variations**—Similarly, by keeping the heater power constant at 1.42 watts, the frequency characteristics of oscillator X are described by the following table for plate powers of 1.5, 1.0, and 0.6 watt.

Table III—Relative Magnitudes of Constants  $\alpha$  and  $\beta$  With Variations of Plate Power, Heater Power = 1.42 Watts

Plate Power	$\alpha$	$\beta$
1.5 watts	-1.18	0.55
1.0	-1.01	0.55
0.6	-0.84	0.55

Again, the percentage change of  $\alpha$  is much less than that of the plate power, and  $\beta$  is substantially of the same magnitude.

#### *Oscillator Compartment*

For a given oscillator tube and associated circuit elements, the frequency characteristics are related to the compartment size and configuration. To determine such relationship, four enclosed chassis were built to house the same 6AF4A tube and using identical circuitry similar to that of oscillator X.

In the case of the completely enclosed chassis, Nos. 2 to 4 inclusive, the highest values of both  $\alpha$  and  $\beta$  occurred with the smallest compartment, but the variation of either constant was by no means proportional to the chassis size. By increasing the heat circulation as in chassis No. 1, both constants were considerably reduced. Generally, the compartment size has only a second-order effect on the oscillator frequency characteristics. For example, chassis No. 4 is more than five times the size of chassis No. 2, yet the change of either constant amounts to less than 20 per cent.

Table IV—Effect of Oscillator Compartment on Constants  $\alpha$  and  $\beta$ 

Chassis No.	Dimensions	Congurations	$\alpha$	$\beta$
1	1½ × 2 × 3"	6 holes, ¼" dia.	—0.84	0.47
2	1½ × 2 × 3"	completely enclosed	—1.01	0.55
3	1½ × 3 × 4½"	completely enclosed	—0.92	0.54
4	2 × 4 × 6"	completely enclosed	—0.82	0.52

*Oscillator Frequency*

To evaluate the effect of oscillator frequency on  $\alpha$  and  $\beta$ , the oscillator chassis No. 2 has been operated at frequencies from 100 to 1000 megacycles in 100-megacycle steps under identical conditions.

Table V—Effect of Oscillator Frequency on Constants  $\alpha$  and  $\beta$ 

Oscillator Frequency	$\alpha$	$\beta$
100 Mc	—0.20	0.55
200	—0.41	0.55
300	—0.63	0.55
400	—0.77	0.55
500	—1.01	0.55
600	—1.22	0.55
700	—1.45	0.55
800	—1.66	0.55
900	—1.82	0.55
1000	—1.98	0.55

The constant  $\beta$  is independent of oscillator frequency, but the constant  $\alpha$  at 1000 megacycles is about twice the corresponding  $\alpha$  at 500 megacycles. Accordingly, for the same circuitry using the same tube and housed in the same compartment, the following approximate relation holds:

$$\frac{\alpha}{\text{oscillator frequency}} = \text{constant.} \quad (6)$$

*Parallel Circuit Capacitance*

In a practical local oscillator, the effect of the tube capacitances on the oscillator frequency due to heat flow inside the tube may be mate-

rially reduced by the presence of a parallel capacitance<sup>2, 3</sup> such as  $C_p$  of Figure 1 having a zero temperature coefficient (NPO). Let  $C_p = nC_0$  where  $C_0$  is the total effective tube capacitance in the determination of the oscillator frequency; then when  $\Delta C_0 \ll C_0$ ,

$$\frac{\alpha \text{ (when } C_p = 0\text{)}}{\alpha \text{ (when } C_p = nC_0\text{)}} = n + 1. \quad (7)$$

The constant  $\beta$  is not significantly affected by  $C_p$  which is normally of the ceramic type having a negligible thermal mass.

#### Series Circuit Capacitance

The presence of an NPO series circuit capacitance such as  $C_s$  of Figure 1 lowers the magnitude of  $\alpha$  in a different manner. Let  $C_s = mC_0$ , then when  $\Delta C_0 \ll C_0$ ,

$$\frac{\alpha \text{ (when } C_s = \text{infinity)}}{\alpha \text{ (when } C_s = mC_0\text{)}} = \frac{m + 1}{m}. \quad (8)$$

Again the constant  $\beta$  is practically independent of  $C_s$ .

#### Ambient Temperature

The frequency characteristics of oscillator X were also observed at ambient temperatures of 25° F and 80° F with practically identical results for all types of miniature tubes tested and with slight discrepancies for the pencil triode tube. The pencil triode differs from the miniature type tubes in the relative amount of heat conducted to the associated circuit elements and radiated to the chassis.

#### Oscillator Circuit Q

By replacing the circuit inductance  $L$  of oscillator X with plain (not silver-plated) brass, bronze, or copper conductor of the same dimensions, both constants  $\alpha$  and  $\beta$  remained approximately unchanged. The use of plain invar conductor weakened the oscillation so much that it was no longer possible to maintain the same power distribution inside the oscillator tube.

<sup>2</sup> H. Sherman, "Temperature Compensation," *Electronics*, Vol. 18, April, 1944.

<sup>3</sup> C. H. Young, "Measuring Inter-Electrode Capacitances," *Bell Laboratories Record*, Vol. 24, pp. 433-438, December, 1946.

## BEHAVIOR OF TEMPERATURE-SENSITIVE CIRCUIT ELEMENTS

The heat transferred to the associated circuit elements of local oscillators using miniature type tubes is predominantly due to conduction from the hot elements inside the tube. In the case of pencil triodes, however, the radiated heat from the plate, cathode, and grid is not negligibly small and must be considered for accurate evaluations. If any of the associated circuit elements were temperature sensitive, its electrical properties would be influenced by the heat in a manner similar to that of Equation (5).

$$\Delta F_1 = \alpha_1 (1 - e^{-\beta_1 t}). \quad (9)$$

The new constants  $\alpha_1$  and  $\beta_1$  and the change of oscillator frequency,  $\Delta F_1$ , are analogous to the corresponding constants and  $\Delta F$  of Equation (5).

Because of the fact that the associated circuit elements are located outside the tube, additional factors affecting the relative magnitudes of these new constants must be taken into consideration.

*Temperature Coefficient of Circuit Capacitance*

Heretofore the circuit capacitance such as  $C_s$  or  $C_p$  of Figure 1 has been assumed to have zero temperature coefficient. The frequency characteristics of local oscillators can be made radically different by the use of a temperature-sensitive circuit capacitance.<sup>4,5</sup> The relative magnitude of  $\alpha_1$  under these conditions is directly proportional to the temperature coefficient and the factor  $(n + 1)$  according to Equation (7) for parallel circuit capacitance or the factor  $(m + 1)/m$  according to Equation (8) for series circuit capacitance. For the same value of  $n$  or  $m$  an N220 capacitor (capacitance decreases 220 parts per million per degree centigrade increase in temperature) deviates the oscillator frequency twice as much as does an N110 capacitor. As a matter of fact, the change of oscillator frequency at any instant with an N220 capacitor is two times that with an N110 capacitor since  $\beta_1$  is independent of  $n$  (or  $m$ ) and the temperature coefficient. It is understood that the capacitor is assumed to be capable of retracing its linear temperature-sensitivity characteristic.

<sup>4</sup>J. A. Connor, "Optimum Thermal Compensation of Capacitance-Tuned L-C Circuits," Naval Research Laboratory, Report No. 3688, June 23, 1950.

<sup>5</sup>Joint Army-Navy Specification, January-C-20A, Temperature Compensating Filled Ceramic Dielectric Capacitors.

*Circuit Inductance*

In VHF and UHF television local oscillators where frequency stability is most critical, the circuit inductance usually consists of a high-conductivity metallic conductor of various dimensions and shapes. It is terminated by a series capacitor which can serve a dual purpose of partial frequency determination and compensation. Therefore, in such oscillators the circuit inductance becomes the medium of heat conduction between the tube and the series circuit capacitance. Evidently, the thermal conductivity, physical length, and cross-sectional area of the conduction medium are all very important factors affecting the oscillator frequency characteristics if a temperature-sensitive series-circuit capacitance is used. In addition, the circuit inductance may influence the oscillator frequency due to thermal expansion even in the absence of the series circuit capacitance.

To assist the study of the circuit inductance behavior in a local oscillator circuit, the relative properties of several commonly used metals are tabulated in Table VI.

Table VI—Properties of Several Commonly Used Metals

Metals	Composition	Relative Resistivity	Relative Thermal Conductivity	Coefficient of Expansion
Copper	99.9 Cu, annealed	1.0	3.88	$17.71 \times 10^{-6}/^{\circ}\text{C}$
Brass	66 Cu, 34 Zn	3.9	1.20	$18.90 \times 10^{-6}/^{\circ}\text{C}$
P. Bronze	4 Sn, .5P, bal. Cu	5.45	0.82	$18.90 \times 10^{-6}/^{\circ}\text{C}$
Silver	—	0.95	4.19	$18.80 \times 10^{-6}/^{\circ}\text{C}$
German Silver	60 Cu, 15 Ni, 25 Zn	16.9	0.32	$18.36 \times 10^{-6}/^{\circ}\text{C}$
Invar	36 Ni, .2C, 63.8 Fe	46.0	0.11	$0.80 \times 10^{-6}/^{\circ}\text{C}$

(a) **Coefficient of Thermal Expansion**—The effect of thermal expansion on the oscillator frequency characteristics depends primarily upon (1) the coefficient of thermal expansion of the inductance material, and (2) the average temperature rise in  $^{\circ}\text{C}$  along the inductance line.

The annealed copper has a coefficient of thermal expansion of  $17.71 \times 10^{-6}/^{\circ}\text{C}$ . If the average temperature rise were  $20^{\circ}\text{C}$ , the inductance line would be stretched 0.354 per cent in length and the same percentage in diameter.

At VHF and UHF the inductance of a straight round conductor

approaches the limiting value<sup>6</sup> of

$$L = 0.00508l (2.303 \log_{10} \frac{4l}{d} - 1) \text{ microhenrys} \quad (10)$$

where  $l$  = wire length and  $d$  = wire diameter, both in inches. As the wire temperature is raised the wire length becomes  $l + \Delta l$  and wire diameter  $d + \Delta d$ .

Since 
$$\frac{\Delta l}{l} = \frac{\Delta d}{d}, \quad \frac{l + \Delta l}{d + \Delta d} = \frac{l}{d}.$$

Consequently, the change of inductance  $\Delta L$  is directly proportional to the average temperature rise and is independent of the conductor diameter at VHF and UHF.

For a small  $\Delta L/L$  ratio, the percentage change of oscillator frequency  $\Delta F/F$  due to thermal expansion of the inductance line is equal to  $-\frac{1}{2}(\Delta L/L)$ . At 500 megacycles the oscillator frequency using a pencil triode would be deviated approximately 88 kilocycles for 20°C rise in the annealed copper inductance line; the average temperature rise along the inductance line would be considerably lower when used in conjunction with a miniature type oscillator tube. All oscillators under test used silver-plated invar lines, unless otherwise specified, which would cause the 500-megacycle oscillator to deviate by only 4 kilocycles with 20°C rise along the line. In this calculation the circuit inductance  $L$  is assumed to be large compared to the tube lead inductances.

(b) **Thermal Conductivity**—The thermal conductivity,  $K$ , of the inductance line controls the rate of heat transfer,  $q$ , from the tube to the associated circuit elements.

$$q = K \frac{dT}{ds} A, \quad (11)$$

where  $dT/ds$  = temperature gradient and  $A$  = cross-sectional area. The slow rate of heat transfer for a material of poor thermal conductivity such as invar establishes a lower temperature rise at any point along the line owing to convection and radiation from the line.

<sup>6</sup> F. E. Terman, *Radio Engineers' Handbook*. McGraw-Hill Book Co., New York, N. Y., 1943; p. 49.

Therefore, the effectiveness of a temperature-sensitive series circuit capacitance is a function of the thermal conductivity of the inductance line.

The solid curves of Figure 6 illustrate the effect of an N150 ( $m = 1.0$ ) series circuit capacitance on the frequency characteristics of the 500-megacycle pencil triode oscillator with copper and invar inductance materials. The dotted curves show the same characteristics for the 6AF4A oscillator under identical conditions.

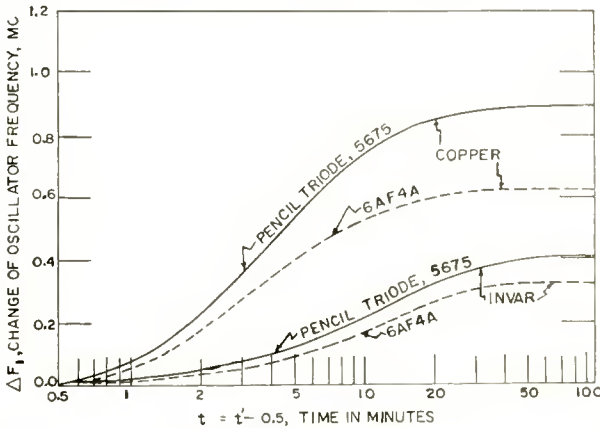


Fig. 6—Effect of series circuit capacitance  $C_s$  on the change of oscillator frequency  $\Delta F_1$  as a function of conductor thermal conductivity.

Table VII—Effect of N150  $C_s$  ( $m = 1.0$ ) on  $\Delta F_1$  as a Function of Thermal Conductivity of  $L$  at 500 Megacycles

$L$ Material	Thermal Conductivity	$\alpha_1$ (Mc)		$\beta_1$	
		Pencil Triode	6AF4A	Pencil Triode	6AF4A
Copper	3.88	0.51	0.31	0.24	0.35
Phosphor Bronze	0.82	0.40	0.26	0.21	0.30
Invar	0.11	0.22	0.18	0.15	0.27

The constant  $\alpha_1$  of the 5675 pencil triode oscillator is greater than that of the miniature type tube, indicating larger temperature gradient according to Equation (11) and higher temperature rise of the series circuit capacitance  $C_s$ . This difference between the pencil triode and the 6AF4A tube is quite understandable because the small wires connecting the plate and grid of the miniature type tubes to the socket pins are the limitations of heat transfer.

(c) **Cross-Sectional Area**—For a given temperature gradient, the effect of conductor cross-sectional area according to Equation (11) is similar to that of the conductor thermal conductivity on the rate of heat transfer. In practice, however, a part of the heat flowing through the conductor is lost to the surrounding air and other heat absorbing objects due to radiation and convection. The amount of heat lost in this manner is a function of the conductor surface area as well as emissivity.

The effect of a temperature sensitive series circuit capacitance on oscillator frequency characteristics as a function of conductor diameter (silver-plated annealed copper) is given in Figure 7. The solid curves are for the 500-megacycle oscillator using a  $1\frac{1}{2} \times 3 \times 4\frac{1}{2}$ -inch chassis and a pencil triode, while the dotted curves are for a same size chassis but using a 6AF4A tube. The constant  $\alpha_1$  for either tube increases gradually with the conductor diameter of slightly over 0.20 inch for

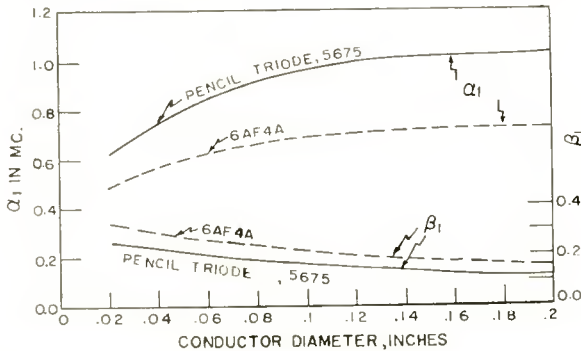


Fig. 7—Effect of  $C_s$  on  $\Delta F_1$  as a function of conductor diameter.

that particular chassis. Because of the increase in loss of heat,  $\beta_1$  decreases somewhat with conductor diameter.

(d) **Physical Length**—By increasing the conductor length, less heat reaches the series circuit capacitance  $C_s$  due to thermal drop along the added conductor length. Accordingly, the constant  $\alpha_1$  is reduced as indicated in Figure 8 for the local oscillator using a  $1\frac{1}{2} \times 3 \times 4\frac{1}{2}$ -inch chassis and a silver-plated annealed copper conductor. The  $\alpha_1$  values were normalized to 500 megacycles. The constant  $\beta_1$  for either tube remains substantially, but not exactly, unchanged.

The above considerations relative to the magnitudes of  $\alpha_1$  and  $\beta_1$  are on the basis of (1) a fixed chassis size, (2) an ambient temperature of 75° F, (3) normal heater power, (4) a plate power of 1.0 watt, (5) a series circuit capacitance  $C_s$  equal to the equivalent tube capacitance  $C_0$ , and (6) the fact that all  $\alpha_1$  and  $\beta_1$  values are normalized to

an oscillator frequency of 500 megacycles. The investigations of some of the factors such as oscillator frequency and  $C_s/C_0$  ratio affecting the  $\alpha$  and  $\beta$  of the oscillator tube also apply to the constants  $\alpha_1$  and  $\beta_1$  of the associated circuit elements. Nevertheless, the effect of chassis size, heater and plate powers on the magnitudes of  $\alpha_1$  and  $\beta_1$  may be somewhat different. Inasmuch as the latter factors are all of secondary importance, further investigations were not carried out.

COMPENSATIONS FOR OSCILLATOR FREQUENCY DEVIATIONS

In the past, a partial compensation of oscillator frequency characteristics has been accomplished by the use of a capacitance or an inductance means having a certain temperature coefficient. With the aid of Equations (5) and (9), the same compensation can now be obtained without the necessity of the trial and error processes;

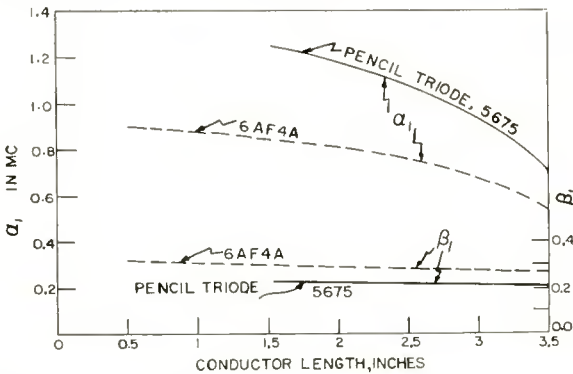


Fig. 8—Effect of  $C_s$  on  $\Delta F_1$  as a function of conductor length.

furthermore, more accurate results are possible by employing composite frequency compensations.

Conventional Compensation Means

To illustrate how Equations (5) and (9) can be used to advantage for compensating the frequency characteristics, a series circuit capacitance  $C_s$  ( $3.0 \mu\mu\text{f}$ , N470) was added to oscillator X. Under these conditions,  $\alpha$  (of oscillator X) =  $-1.01$  and  $\alpha_1$  (of  $C_s$ ) =  $+1.01$ , but  $\beta_1 < \beta$  because  $C_s$  was located outside the oscillator tube. The magnitude of  $\beta_1$  depends upon the size and thermal conductivity of the circuit inductance conductor as previously described. Figure 9 shows the frequency characteristics of  $\Delta F + \Delta F_1$  and  $\Delta F + \Delta F_2$  of oscillator X with  $\beta_1 = 0.25$  and  $0.10$ , respectively. The  $(\Delta F + \Delta F_1)$  curve drifted rather rapidly at first and reached a deviation of  $-0.20$  megacycle at

3 minutes. It gradually drifted positively thereafter and finally back to practically zero after  $t = 20$  minutes. During the period  $1 \leq t \leq 8$  minutes, the oscillator frequency departed beyond the limits for satisfactory reception of television programs. The  $\Delta F + \Delta F_2$  curve exhibits even less desirable characteristics.

A somewhat better compensation of this kind could be obtained by the use of a lower temperature coefficient for  $C_s$  as indicated by the  $\Delta f + \Delta F_3$  curve. It is noted that the oscillator frequency was shifted approximately  $-0.25$  megacycle shortly after oscillation had taken place, but it was stable within  $\pm 0.05$  megacycle for  $t \geq 2.0$  minutes.

To obtain perfect compensation both of the following relations must be satisfied.

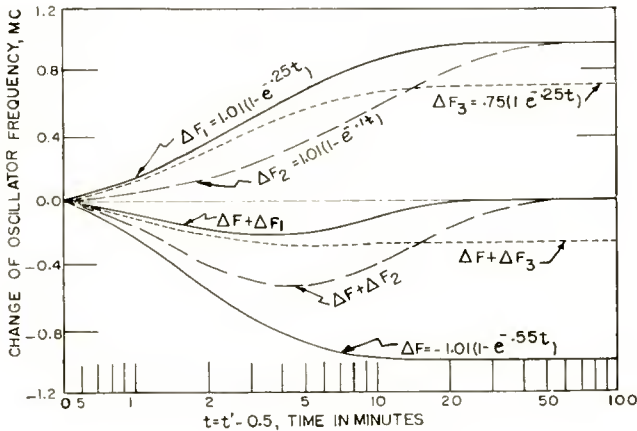


Fig. 9—Simple compensation means.

$$\alpha_1 = \alpha \tag{12}$$

and

$$\beta_1 = \beta. \tag{12a}$$

The fulfillment of Equation (12) is a matter of proper selection of the  $C_s/C_0$  ratio and the temperature coefficient of  $C_s$ . For a given oscillator application with normal heater and plate powers, this relation can be satisfied over a wide frequency range. The limitation of such simple means of compensation, therefore, lies in the  $\beta_1$  constant. Unless a capacitor of certain value and temperature coefficient is built inside the oscillator tube, the conventional simple compensation means can only improve the oscillator frequency characteristic, but it will never completely stabilize the oscillator.

*Composite Frequency Compensation*

Knowing the behavior of the oscillator tube and the associated circuit elements under the complex conditions of heat flow, more accurate and analytic frequency compensations for various local oscillator applications are possible. For example, one of the many potential compensation systems is illustrated in Figure 10 where the circuit inductance is made of low thermal conductivity material such as silver-plated invar conductor to minimize the heat transfer between the oscillator tube and the temperature-sensitive  $C_s$ . Heat is transferred to  $C_s$  through radiation and conduction from its companion resistive component  $R_s$ . Values for the equivalent  $\alpha_1$  and  $\beta_1$  (at normalized values of oscillator frequency, effective tube capacitance, and applied voltage) of the  $C_s$ - $R_s$  unit can be specified by varying (1) the capacitance and the temperature sensitivity of the capacity component,

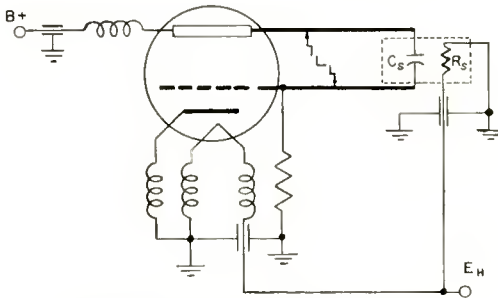


Fig. 10—Composite compensations.

(2) the resistance of the resistor component, and (3) the thermal coupling between the two components.

The study of this problem of oscillator stability thus far has been limited to the frequency characteristics of local oscillators which are governed by the flow of heat with particular emphasis at VHF and UHF. Frequency deviations and irregularities due to line voltage fluctuations and humidity effect would warrant separate investigations.

## ACKNOWLEDGMENT

The author wishes to acknowledge the experimental work done by D. J. Carlson and G. B. Waters in connection with this investigation. The factors  $F_f$ ,  $F_a$ , and  $F_c$  of Equation (1) in conventional receiving tubes were evaluated by O. H. Schade, Jr.

# METHODS FOR REVEALING P-N JUNCTIONS AND INHOMOGENEITIES IN GERMANIUM CRYSTALS\*

BY

JACQUES I. PANKOVE

Research Laboratory, RCA Laboratories,  
Princeton, N. J.

## Abstract

*Summary*—When a p-n junction is biased in the reverse direction under an electrolyte, the junction contour appears as the n-type region etches off, while the p-type region remains relatively undisturbed. The ease of distinguishing the n and p regions can be improved by using a hot germanium-rich electrolyte. A plurality of junctions in the same crystal can be revealed by coating the crystal with a thin layer of electrolyte and passing a current through the crystal. Regions of different impurity concentrations can be shown by etching the crystal through the film of electrolyte with respect to a small negative electrode which scans the crystal.

## INTRODUCTION

IN the fabrication of semiconductor devices, the exposure of p-n junctions and of inhomogeneities in impurity concentration serves the purpose of evaluating materials and of locating the position of junctions. For example, one can find impurity striations in a grown crystal, or measure the width of the base layer in the rate-grown transistor or determine the shape of an alloy junction. Although expediency often dictates the method to be used, it is sometimes important to avoid contaminating the crystal. Several methods of electrolytic etching have been developed which are convenient and noncontaminating.

## IMMERSION ETCH<sup>1</sup>

If a reverse bias is applied across a junction immersed in an electrolyte, the n-type region forms the anode and the p-type region forms the cathode. The n-type region etches off while the p-type region is not affected. This results in a pronounced step down from the p to the n regions and also in a different surface texture for the two regions.

When the sample comprises one p-type region between two n-type

---

\* Decimal Classification: 541.3.

<sup>1</sup> M. Sparks, "Semiconductor Translating Device," U. S. Patent No. 2,656,496. Also E. Billig and J. J. Dowd, "PN Junctions Revealed by Electrolytic Etching," *Nature*, Vol. 172, p. 115, 1953.

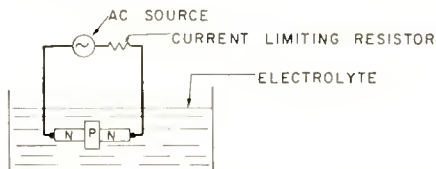


Fig. 1—Immersion etch of crystal having two junctions.

regions, an a-c supply may be used as shown in Figure 1. Then each n region is etched on an alternate half-cycle, and the p region is not etched. On the other hand, when the crystal comprises one n-type region between two p regions, the n region etches at every half cycle while the p regions are etched on alternate half cycles. Hence the surface of the n region is depressed; but since the whole crystal is etched, there is no texture contrast on either side of the junction.

Of course, if a connection is made to the intermediate layer, then it is possible to treat each junction separately.

#### COLOR CONTRAST TECHNIQUE

If the above electrolytic etching technique is allowed to proceed at about 80°C and at a high current density, the p-type region becomes covered with a brown to black film and the p-n junction shows up in color contrast (Figure 2).

Although the nature of the film and the mechanism of its formation are not definitely known, it is suspected that the film consists of either germanium monoxide or amorphous germanium. It is found that the dark film forms on a platinum cathode when germanium is used as an anode in the etching cell. With a platinum anode, a fresh electrolyte gives no visible film, but an electrolyte which has already been used

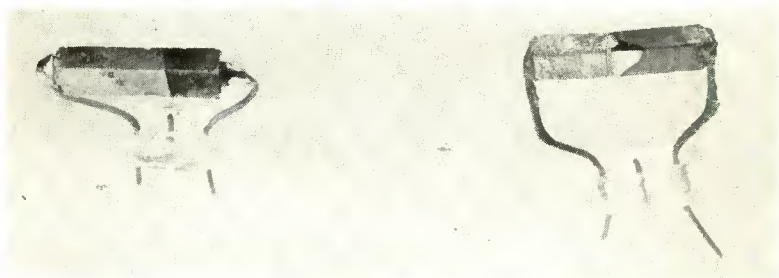


Fig. 2—Color contrasted p-n junctions. The dark non-shiny surface indicates the p-type region, the shiny pitted surface marks the n-type region. The left unit shows a flat junction. The right unit comprises three different regions: The very pitted n-type region, a central smooth region also n-type but of much higher resistivity, and a p-type region forming a strongly curved p-n junction.

to etch germanium produces the dark film. Hence, the dark film must be due to plated germanium which would either oxidize or remain in the amorphous form. One per cent aqueous solutions of NaOH, KOH, and HCl produce the dark film. None was obtained with NaCl.

#### CASE OF MULTIPLE JUNCTIONS

When it is inconvenient to make an individual connection to each region in a crystal having many junctions, it is still possible to reveal each junction. For example, one might wish to expose all the junctions along the longitudinal section of a rate-grown crystal. The surface to be examined is given a dull polish and coated with a layer of electrolyte; then a bias is applied across the crystal to produce a current transverse to all the junctions (Figure 3). All the junctions biased in the reverse direction form an etching cell, the n region being the anode, the p region the cathode. Because of the high lateral resistance of the electrolyte, the etching action is strongest at the junction and decreases farther away from it. By reversing the polarity of the bias, the other

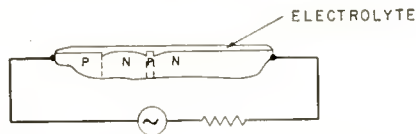


Fig. 3—Method of etching a plurality of junctions.

set of junctions is brought out. An a-c bias will also expose all the junctions. The p-type regions are distinguished by their dull finish, whereas the n-type regions are bounded by lightly pitted zones which are dark or shiny depending on the illumination (Figure 4).

If this process is carried out at about 80°C, a black film appears on the p region, this process being similar to that described above as a color contrast technique.

#### EXPOSURE OF INHOMOGENEITIES

The technique to be presently described is more sensitive than those discussed above, and in fact is so sensitive in showing up inhomogeneities in impurity concentration that one cannot distinguish between a p-n junction and a change in concentration. However, once the p-n junctions have been located by one of the above techniques it is possible to recognize them among the newly formed patterns. This technique is useful for revealing resistivity striations and for studying the shape of the liquid solid interface in rate-grown crystals (see Figure 5).

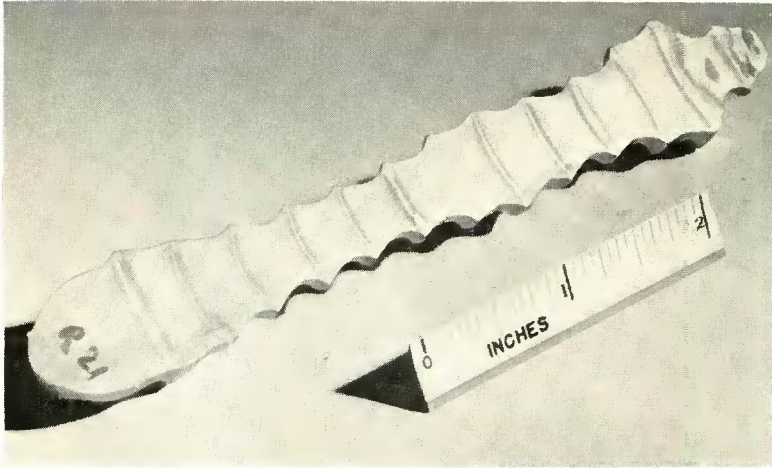


Fig. 4—A rate-grown crystal with the p-type layers made visible.

After the surface of the crystal has been carefully polished, a longitudinal current is passed through the crystal as in the technique described above for revealing multiple junctions. A film of electrolyte wets the polished surface. The crystal is made positive with respect to a mobile cathode which spans the width of the crystal and which is located very close to the polished surface (Figure 6). A mechanical arrangement causes the cathode to slowly scan the crystal while it is etched. When the cathode is over a region of low resistivity, i.e., high impurity concentration, the etching current increases and leaves a more profoundly disturbed surface (for example the etch pits become coarser). The longitudinal field sets up potential gradients along the crystal depending on the nature of the inhomogeneity (p-n junction,  $p^+p$  or  $nn^+$  transitions) so that the more positive region tends to etch faster. The longitudinal field must be reversed in a second scan in

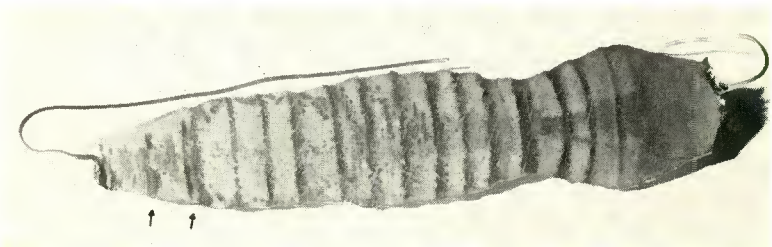


Fig. 5—Rate-grown crystal which comprises only two p-type layers near the seed end of the crystal (arrows). The dark bands are the highly doped regions which have etched more than the rest of the crystal.

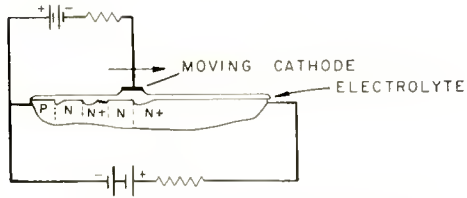


Fig. 6—Electrolytic method for exposing inhomogeneities.

order to set up a potential gradient at the rectifying transitions that were biased in the forward direction during the first scan.

It may be concluded that the electrolytic etching of crystals coated with a thin layer of electrolyte offers simplicity, clarity, and good resolution.

# STABILIZATION OF PULSE DURATION IN MONOSTABLE MULTIVIBRATORS\*

BY

ARCH C. LUTHER, JR.

Engineering Products Division, Radio Corporation of America,  
Camden, N. J.

## INTRODUCTION

*Summary*—The elementary principles of multivibrator operation are reviewed to develop the circuit properties which affect the duration of the timing interval. Stabilization of the duration by means of a particular circuit containing d-c feedback is described. Theory for this circuit is developed to the extent that the effects of tolerances are explained. Further improvement is demonstrated for constant-frequency applications by the insertion of average operating point feedback. Practical circuits are described for frequency division and pulse generation in broadcast television equipment.

A GREAT number of electronic systems require devices which will accurately define a particular time interval. One of the more widely used circuits for this purpose is the multivibrator. This device in its simplest form consists of a two-stage amplifying circuit provided with a regenerative connection which gives it essentially binary or two-position characteristics. By virtue of the regeneration, it is capable of extremely rapid transitions between its two states. In addition, the characteristics of the amplifying stages and the inter-stage coupling may be adjusted to control the length of time during which the circuit will remain in either of its two possible states. This timing property is the subject of this paper.

Timing multivibrators take two forms, depending on whether the circuit contains a timing function for one or both of its states. These are called "monostable" and "astable," respectively. A monostable multivibrator changes state immediately after a trigger pulse, and after a predetermined length of time it returns automatically to its original state, remaining there until the next trigger pulse. Thus, this circuit can produce pulses of controlled width in response to a triggering wave. It represents the simplest case of a timing multivibrator and the discussion will be restricted to this type.

Astable multivibrators, on the other hand, are free-running, and operate without triggers. They are used principally for generation of

---

\* Decimal Classification: R146.2.

a particular frequency rather than a pulse width. The timing principles presented here for monostable circuits are also readily applied to most astable circuits.

Bistable multivibrators, which produce only one transition in response to each trigger pulse, are also useful; but since they contain no timing property, they are not affected by many of the considerations discussed here.

#### GENERAL PROPERTIES OF MONOSTABLE MULTIVIBRATORS

The distinction between astable and monostable multivibrators occurs principally in the manner of biasing the amplifying stages. For a monostable circuit, biasing of the two stages will be such that the condition of conduction in one tube and cutoff in the other tube can be maintained for an indefinite length of time. However, a multivibrator biased for astable operation may be used as a monostable circuit if it is triggered at a rate high compared to its natural frequency. This characteristic is utilized in some of the stabilized circuits to be discussed here.

A monostable multivibrator cycle may be divided into three separate intervals. Interval I, which begins upon application of the trigger pulse, includes the mechanics of triggering and the setting up of initial conditions in the timing circuit. When interval I is completed, the conducting condition in the multivibrator tubes will have reversed from the resting state prior to the trigger. The second interval is the actual timing period of the multivibrator. During this interval, the timing circuit discharges from its initial condition set up by interval I. Interval II is terminated by rapid regenerative action when the discharge of the timing circuit reaches a predetermined level. Interval III then follows, and it includes the recharge cycle of the timing network necessary to return to the resting state. Thus, interval I may be thought of as the triggering delay time, interval II is the actual timed pulse period, and interval III is the recovery time, which must pass before the circuit can be re-triggered to produce another accurate pulse.

This paper is concerned chiefly with the factors which determine the duration of interval II. These may be listed in general terms as follows:

1. The initial condition of the timing circuit set up in interval I.
2. The rate of discharge of the timing circuit during interval II.
3. The predetermined charge level in the timing circuit which determines the start of interval III.

These factors are of approximately equal importance in the performance of most multivibrators. In order to understand their significance more fully, consider the simple monostable multivibrator of Figure 1 (a), with its waveforms shown by Figure 1 (b).

Bias  $E_R$  applied through  $R$  causes V2 to be normally conducting, to the extent that the drop across the V2 load resistor  $R_1$  will hold V1 beyond cutoff. Application of a negative trigger pulse to the indicated terminal will momentarily drive V2 to cutoff, thus making V1 conduct.

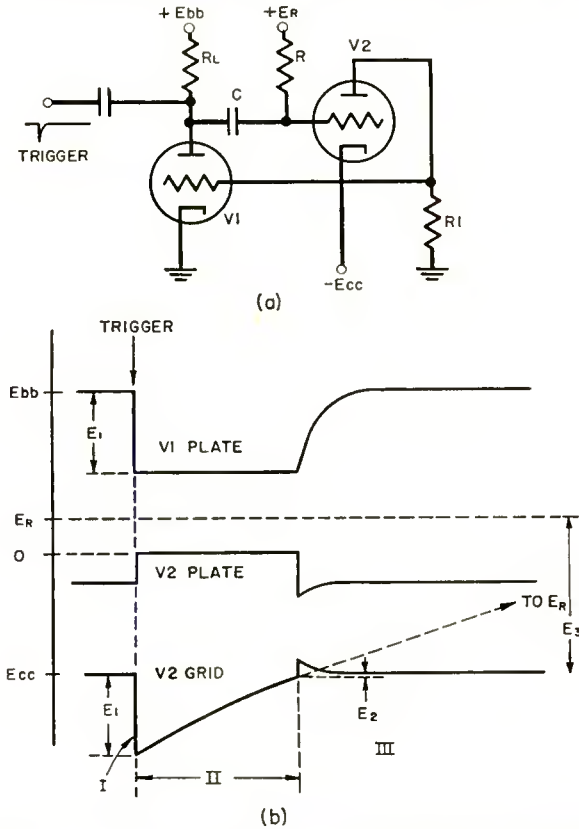


Fig. 1—Typical monostable multivibrator (a) with its waveforms (b).

This will cause a large drop of V1 plate voltage; which, when coupled through  $C$  will cause a similar drop  $E_1$  of V2 grid-to-cathode voltage, driving V2 far beyond cutoff.  $E_1$ , therefore, is the initial voltage developed on the timing circuit. Then the current flowing down through  $R$  and from right to left through  $C$  will cause the right-hand end of  $C$  to charge in a positive direction. This is the action of interval II; the grid voltage of V2 charges exponentially toward  $E_R$ .

Eventually, the rising grid voltage of V2 will cross the cutoff voltage  $E_2$  of V2, bringing this tube back into conduction, and causing a regenerative return to the resting state with V2 conducting and V1 cut off. This marks the start of interval III, where  $C$  is recharged through  $R_L$  and the grid-cathode diode of V2. With the completion of this recharging, the circuit is ready for another trigger.

#### THE TIMING EQUATION

The significant property, then, is that a pulse has been generated, having a duration defined by interval II of the timing cycle. This pulse duration  $t_1$  may be computed from the grid-cathode voltage of V2 during the interval II. Using the notation of Figure 1(b),

$$e_{gk} = -(E_1 + E_3) e^{-\frac{t}{(R+R_L)C}} + E_3.$$

This must be equal to  $-E_2$  at  $t_1$ .

Solving for  $t_1$ ,

$$t_1 = (R + R_L) C \ln \frac{E_1 + E_3}{E_2 + E_3}; \quad (1)$$

thus we find that the pulse duration is a function of the voltage  $E_1$  set up during interval I; the circuit time constant  $(R + R_L) C$ , and the voltage  $E_3$  to which the exponential of interval II is headed; and the voltage  $E_2$  which is the predetermined point for the start of interval III.

#### EFFECT OF TUBE AND CIRCUIT TOLERANCES

Therefore, let us consider how these factors are determined in the circuit.  $E_1$ , the initial voltage, is the voltage drop produced across  $R_L$  by switching V1 from cutoff to zero bias. This voltage may be found from the characteristic curves of V1 as shown by Figure 2, and may be substantially affected by tube change or aging. Figure 2 is drawn to show a typical spread in initial characteristics for a triode as well as an assumed end-life characteristic denoted "half-current" because it is found by dividing the zero-bias plate current for each value of plate voltage in half. Practical experience has shown that such an assumed end-life characteristic is quite realistic for commercial tubes and that further allowance for aging is probably unnecessary because by the time a tube has aged to more than half its nominal plate current it has become highly sensitive to heater voltage and the operation

is generally unreliable. Therefore, the design methods used here allow for aging to half-current on all tube characteristics.

$E_3$  is the voltage drop across the grid resistor  $R$  of V2 when the circuit is in the resting state. This voltage will be slightly affected by the grid current characteristics of V2 although this is usually a small factor. The major variable in  $E_3$  is the reference supply voltage  $E_R$ .

$E_2$  is the cutoff voltage of V2. This may vary from tube to tube by as much as  $\pm 40$  per cent of nominal. In addition, there will be some aging effects, although probably not as large as the initial tolerance effect.

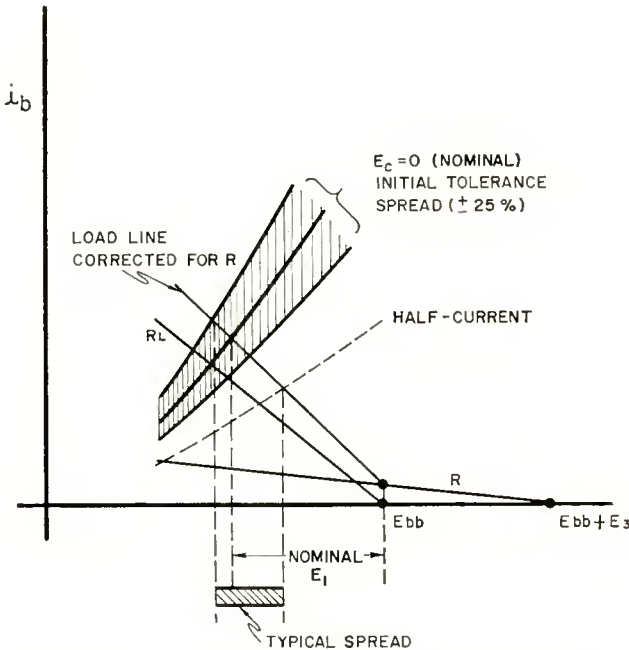


Fig. 2—Determination of operating point of V1. Shaded areas show the effect of tube tolerance and aging.

From the standpoint of providing means for regulating these voltages, it should be noted that various devices have been applied to control of  $E_1$ , such as the use of catching diodes or clippers. Variations in  $E_3$  due to grid current characteristics may be swamped out by making the absolute value of  $E_3$  large. If multiple power supplies are used, it may be necessary to connect  $R$  to the proper voltage to cause all the factors in Equation (1) to be proportional to the same supply voltage. This is a particularly serious problem when catchers are used to stabilize  $E_1$ , for it becomes a necessity that all supply voltages track.  $E_2$ , on the

other hand, is very difficult to control since it is a fundamental characteristic of one of the tubes. It must, therefore, be swamped out of Equation (1) by making  $E_3$  sufficiently large. In addition,  $E_2$  should be held to as small a value as possible by using high- $\mu$  tubes and a low value of plate voltage ( $E_{cc}$ ) on V2.

STABILIZED MONOSTABLE MULTIVIBRATOR

Figure 3 shows a circuit configuration which not only provides the proper connections for obtaining power supply voltage immunity but contains unique feedback means for regulating  $E_1$ .

This circuit is seen to be similar to the circuit of Figure 1(a) except that the grid resistor  $R$  of V2 has been returned to ground

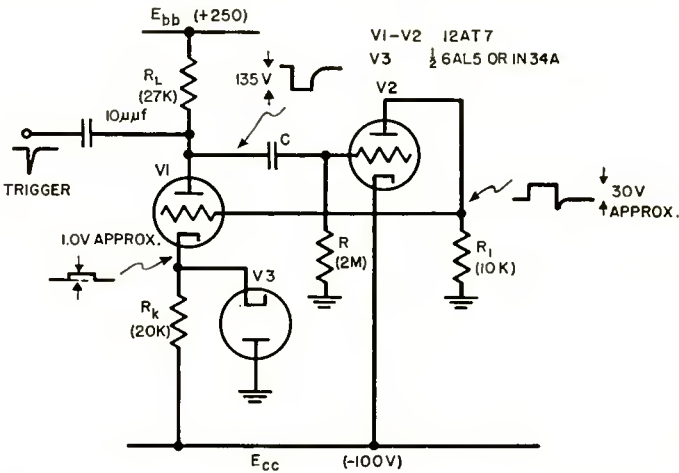


Fig. 3—Monostable multivibrator incorporating direct-current stabilization.

making  $E_3 = E_{cc}$ . In addition, the cathode of V1 now contains a current-stabilization resistor  $R_K$  and a diode V3.

The operation of the circuit is essentially the same as that of Figure 1 except that the cathode resistor  $R_K$  prevents V1 from going to zero bias. During interval II of the multivibrator cycle, when V1 is made conducting, its grid voltage with respect to ground will be exactly zero, since V2 is cut off and there is no current through  $R_1$ . If the operating point of V1 has been properly chosen by choice of  $R_L$  and  $R_K$ , the cathode of V1 will run slightly positive due to cathode follower action, causing a net negative grid-to-cathode bias. This will, of course, cause diode V3 to be cut off, so that all of the current in V1 must flow through  $R_K$  to the negative supply voltage. Thus the current which flows in the plate circuit of V1 may be determined by measuring

the voltage across  $R_K$  when the tube is conducting. If the slight positive voltage at the cathode (with respect to ground) is termed  $e_c$ , the current in V1 will be

$$\hat{i} = \frac{e_c + E_{cc}}{R_K}. \quad (2)$$

$E_1$ , then, will be given by this current flowing through  $R_L$  (if  $R \gg R_L$ ),

$$E_1 = (e_c + E_{cc}) \frac{R_L}{R_K}. \quad (3)$$

Now it should be noted that  $e_c$ , the bias on V1, is the only factor in Equation (3) which is a function of the tube characteristics. Consequently,  $E_1$  may be made insensitive to tube characteristics simply by making  $E_{cc} \gg e_c$ , or at least much greater than the range of variation in  $e_c$  which might be expected from tube change or aging. With a high- $\mu$  tube for V1, it is readily possible to stabilize  $E_1$  to well within 1 per cent for a wide range of tube characteristics and aging to half-current. This may be accomplished with  $E_{cc}$  less than 100 volts.

Figure 4 shows the determination of operating point for V1. Here line "A" has been drawn for Equation (2). The operating point is found at the intersection of line A and the conventional plate load line for  $R_L$ . Ideal stabilization would have line "A" horizontal; however, it always has a slight positive slope, indicating that the operating point will be at a current value just slightly greater than  $E_{cc}/R_K$ . This is very useful for rough calculation. Figure 4b shows a construction which makes use of such an approximation. If  $e_c/R_K$  is added to the value of  $i_b$  found from Figure 4b, the results are satisfactory for most purposes. It should be noted that this method of plate-current stabilization is only suitable with triodes, since it is necessary for the plate and cathode currents to be exactly the same.

When the multivibrator of Figure 3 is in its resting state, V2 conducts to hold V1 beyond cutoff. The diode V3 is necessary to make this possible, and it will conduct to hold the cathode of V1 at ground so that a small drop across  $R_1$  is sufficient to cut off V1.

#### TOLERANCE ANALYSIS

The properties of the circuit of Figure 3 may be further studied by rewriting Equation (1) for this circuit. To do this, it is necessary to make use of Equation (3), and to define

$$E_2 = \frac{E_{cc}}{\mu_2}$$

where  $\mu_2$  is determined for the cutoff point of V2. It must also be recognized that  $E_3 = E_{cc}$ . Then

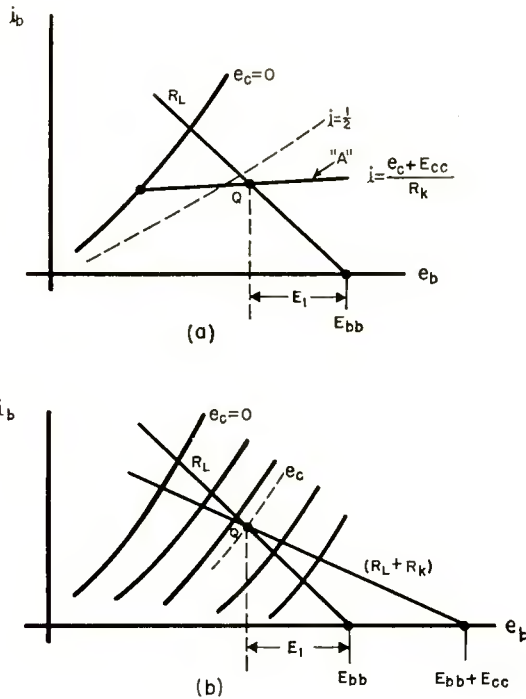


Fig. 4—Characteristics of V1 in Figure 3, showing exact method for location of the operating point (a), and an approximate method (b).

$$t_1 = RC \ln \frac{(e_c + E_{cc}) \frac{R_L}{R_K} + E_{cc}}{\frac{E_{cc}}{\mu_2} + E_{cc}}$$

Rewriting in terms of the following parameters,

$$r = \frac{R_L}{R_K}, \quad e = \frac{e_c}{E_{cc}}, \quad h = \frac{1}{\mu_2},$$

$$t_1 = RC \ln \frac{(1 + e) r + 1}{h + 1}. \quad (4)$$

Here  $h$  and  $e$  are functions of the tubes V1 and V2, and they both may be made small compared to unity. Thus, the immunity to tube parameters is evident. The factor  $e$  further contains the only dependence on power supply voltages. Consequently, keeping  $e$  small also provides supply voltage immunity.

To obtain qualitative results for the sensitivity to these different factors, Equation (4) may be differentiated with respect to  $E_1$ ,  $E_{cc}$ ,  $E_{bb}$ , and  $E_2$ . To do this, one must recognize that

$$e_c = \frac{E_{bb}}{\mu_1} - \text{constant}$$

and define

$$\alpha = \frac{E_{bb}}{E_{cc}}.$$

The results below further assume that  $\mu_1$  and  $\mu_2$  are approximately the same (indicating identical tubes) and that  $e$  and  $h$  are much less than unity.

$$S_{E_1} = \frac{dt_1/t_1}{dE_1/E_1} = \frac{r}{(r + 1) \ln (r + 1)}, \quad (5)$$

$$S_{E_{cc}} = \frac{dt_1/t_1}{dE_{cc}/E_{cc}} = \frac{-r e}{(r + 1) \ln (r + 1)} = -e S_{E_1}, \quad (6)$$

$$S_{E_{bb}} = \frac{dt_1/t_1}{dE_{bb}/E_{bb}} = \frac{\alpha h r}{(r + 1) \ln (r + 1)} = \alpha h S_{E_1}, \quad (7)$$

$$S_{E_2} = \frac{dt_1/t_1}{dE_2/E_2} = \frac{-h}{\ln (r + 1)}. \quad (8)$$

Equations (5), (6), and (7) may be evaluated by use of the curve of Figure 5(a), which is a plot of  $S_{E_1}$  versus  $r$ . Figure 5(b) is a curve for  $1/\ln (r + 1)$  which is useful in determining values for Equation (8).

Evaluation of Equations (5), (6), (7), and (8) for the constants of Figure (3) gives the sensitivities listed in Table I. It must be further stated that aging V1 to 1/2 current causes a 1 per cent change

in  $E_1$ , and  $E_1$  is directly sensitive to  $R_L$  and  $R_K$ . The pulse width is also directly proportional to  $R$  and  $C$  as noted in Equation (4). Thus, Table I indicates, for the rare case of complete build-up of tolerances, a total shift of just over 5 per cent.

In extremely fast multivibrators, or when a wide range of adjustment of  $R$  is necessary, the approximation  $R \gg R_L$  will not be valid. Correction for small values of  $R$  may be made by noting that the current through  $R$  subtracts from Equation (2). Thus

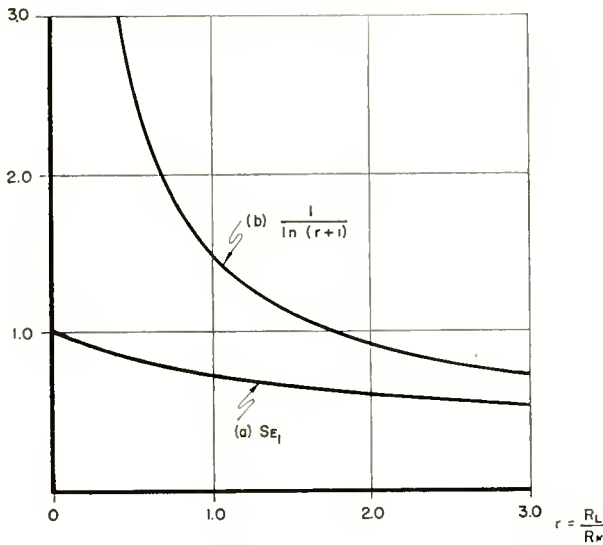


Fig. 5—(a) A curve of the sensitivity to  $E_1$ , versus  $r$ , which may also be used to find the sensitivity to  $E_{bb}$  and  $E_{cc}$ . (b) A curve of  $1/\ln(r+1)$  versus  $r$ , which is useful in calculating the sensitivity to  $E_2$ .

Table I—Tolerance Breakdown for Circuit of Figure 3  
 $r = 1.35$ ;  $e = 0.01$ ;  $h = 0.025$ ;  $\alpha = 2.50$

Age V1 to $\frac{1}{2}$ current	—0.7%
$\pm 5\%$ $E_{cc}$	$\pm 0.04\%$
$\pm 5\%$ $E_{bb}$	$\pm 0.2\%$
$\pm 1\%$ $R$ and $C$	$\pm 2.0\%$
$\pm 1\%$ $R_L$ and $R_K$	$\pm 1.4\%$
$\pm 40\%$ $E_2$	$\pm 1.2\%$
Age V2 to $\frac{1}{2}$ current	no effect
Total:	—5.5 + 4.8%

$$E_1 = \left( \frac{e_c + E_{cc}}{R_K} - \frac{E_1 + E_{cc}}{R} \right) R_L.$$

Solving for  $E_1$  and using the notation of Equation (4), with  $a = R_L/R$ ,

$$E_1 = E_{cc} \frac{r(1+e) - a}{1+a}$$

the exact form of Equation (4) then becomes

$$t_1 = (1+a) RC \ln \frac{r(1+e) + 1}{(1+h)(1+a)}. \quad (4a)$$

Fortunately, the derivatives of Equations (5), (6), (7), and (8) are not affected by this correction, since  $a$  is constant for that differentiation.

#### MONOSTABLE MULTIVIBRATOR COUNTER

The multivibrator of Figure 3 may be operated as a frequency divider in the manner indicated in Figure 6. Here the multivibrator, upon triggering from a particular input pulse, is adjusted to run for a period greater than  $n-1$  trigger periods, but less than  $n$  trigger periods. Then the multivibrator will recover after the  $(n-1)^{\text{th}}$  trigger and return to its stable state, whereupon it will be retriggered by the  $n^{\text{th}}$  trigger. This is possible because the multivibrator is unaffected by trigger pulses occurring during its timing interval. Consequently, the multivibrator divides the trigger frequency by  $n$ .

Figure 6, which is drawn for a count of 5:1, shows that the recovery time of the multivibrator limits how close the end of the timing interval may come to the  $n^{\text{th}}$  trigger before an improper count will occur. Also, it is seen that  $t_1$  may end slightly before the  $(n-1)^{\text{th}}$  trigger, and the recovery process will prevent triggering by that trigger. These two effects are approximately the same, so that the tolerance allowable on  $t_1$  is still equal to the value figured without regard to recovery time, which is

$$\text{tolerance on } t_1 \text{ for } n:1 \text{ counter: } \pm \frac{100}{2n-1} \text{ per cent.} \quad (9)$$

This tolerance interval is shown by the shaded area in Figure 6. Thus, the multivibrator may be designed by use of Equation (1) so that for nominal conditions  $t_1$  is slightly less than  $(n-1/2)$  times the trigger

pulse period; the amount less being a function of the recovery time.

For the 5-counter of Figure 6, Equation (9) comes to  $\pm 11$  per cent. Therefore, according to Table I, the circuit of Figure 3 is amply stable to use for a frequency division of 5:1 with fixed 1 per cent tolerance components. In a case where the triggering frequency of the counter remains constant, all of the tolerance allowed by Equation (9) could be delegated to  $t_1$ . Thus, the performance data of Table I allows a no-adjustment maximum count ratio of 10:1, and even higher if closer tolerance components are available, since the tube tolerances in Table I add up to only  $\pm 1.55$  per cent.

However, in many applications the tolerance on the trigger frequency will be considerable. Under these conditions, the trigger frequency tolerance plus the tolerance on  $t_1$  must not exceed the value

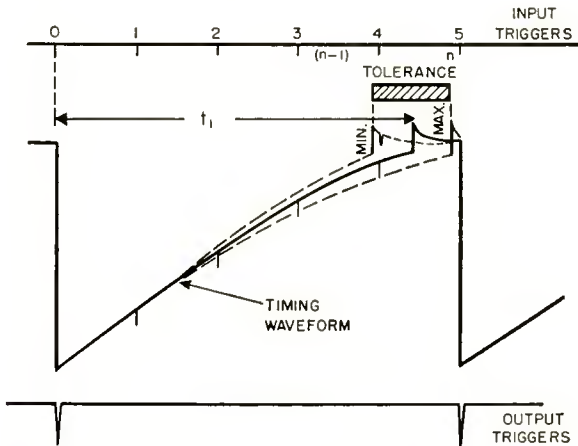


Fig. 6—Operation of a 5:1 monostable multivibrator frequency divider.

given by Equation (9), since from the standpoint of tolerances, it does not matter whether the trigger frequency remains fixed and  $t_1$  varies, or whether  $t_1$  is constant and the trigger pulse period changes.

Production experience with television sync generators, using a circuit similar to Figure 3, has shown that 5:1 dividers which are capable of handling a  $\pm 5$  per cent trigger frequency tolerance may be consistently mass-produced with 1 per cent components. This is rather satisfactory verification of the theory developed here.

Another interesting feature which has been used in sync generators is the fact that the frequency tolerance of a multivibrator divider may be used as a means of measuring the operating margin of a particular counter chain. For the 5:1 dividers just described, the frequency will never change by as much as 5 per cent in normal operation. However,

a control is provided in the equipment which can change the frequency by  $\pm 5$  per cent. If all the tubes and components are within tolerance, proper counting is possible over the entire range of this control. Thus, the frequency control provides a quick over-all reliability test on the entire divider chain.

#### USE OF AVERAGE OPERATING POINT FEEDBACK

The circuit of Figure 3 shows good immunity to power-supply variations and to the characteristics of V1, but the performance is limited by nearly direct dependence on four components and by variations in  $E_c$ . For certain applications, some improvement is possible by replacing V3 with a capacitor. This is possible only for applications where the multivibrator is triggered at a constant frequency. Since this circuit would be astable in the absence of trigger pulses, it relies on the maintenance of certain average operating conditions.

Let us define

$$\delta = \text{duty ratio} = \frac{t_1}{T},$$

where  $T$  is the period of the incoming triggers and  $t_1$  is the length of the multivibrator timing cycle. If the cathode of V1 is bypassed by a capacitor large enough to prevent any appreciable change in voltage during one period, then the current stabilization action will regulate the average plate current:

$$\bar{i} = \frac{e_c + E_{cc}}{R_K}.$$

$E_1$ , however, is determined by the peak current.

$$E_1 = \bar{i} R_L = \frac{\bar{i}}{\delta} R_L = (e_c + E_{cc}) \frac{R_L}{\delta R_K}. \quad (10)$$

The value of  $e_c$  in Equation (10) is determined for the peak current and voltage conditions on V1, the same as shown by Figure 2. The only difference in the averaging cathode circuit is that  $R_K$  is made  $1/\delta$  times larger than when the diode is used. This is apparent when Equation (10) is compared to Equation (3). However, a very important difference shows up when the effects of tolerances are considered. It is rather difficult to present an exact solution for  $t_1$  for this circuit be-

cause the problem is severely complicated by the presence of  $\delta$  (which is a function of  $t_1$ ) in the relation for  $E_1$ . However, Equation (10) in combination with Equation (1) is usually sufficient for design purposes. The effect on tolerances may be inferred by considering what would happen if a change in the circuit occurred in such a direction as to decrease  $t_1$ . This normally would be caused by aging of V1, increase of  $E_2$ , decrease of  $R_1$ ,  $C$ , or  $R$ , or an increase of  $R_K$ . If  $t_1$  decreases,  $\delta$  will be decreased also. However, Equation (9) indicates that a decrease in  $\delta$  will cause an increase in  $E_1$ . But an increase in  $E_1$  causes an increase in  $t_1$ , thus counteracting the original change. Consequently, we have a negative-feedback loop tending to regulate the duty cycle by adjustment of  $E_1$ .

The effectiveness of this feedback may be evaluated by calculating the feedback loop gain. An open-loop circuit for this calculation may be made as shown by Figure 7. Here we have taken the circuit of Figure 3 and added an additional stabilized amplifier which will generate the same  $E_1$  as the multivibrator itself. Now if we consider some change in the circuit of Figure 3 which would cause a change in  $t_1$  to

$$t_1' = t_1 (1 + X),$$

then

$$\delta' = \frac{t_1 (1 + X)}{T} = \delta (1 + X),$$

$$E_1' = (e_c + E_{cc}) \frac{R_L}{R_K \delta (1 + X)} = \frac{E_1}{1 + X} \approx E_1 (1 + X).$$

Thus, a  $100X$  per cent increase in  $t_1$  causes a  $100X$  per cent decrease in  $E_1$  at the plate of V4. Taking  $S_{E_1}$  from Equation (5) for an equivalent diode multivibrator, then the  $100X$  per cent decrease in  $E_1$  would cause a  $100X S_{E_1}$  per cent decrease of  $t_1$ .  $S_{E_1}$ , then, is the loop gain of the feedback system. Therefore, any change in the width of the circuit of Figure 3 will be reduced by

$$\frac{1}{1 + K\beta} = \frac{1}{1 + S_{E_1}} \quad (11)$$

in the circuit where V3 has been replaced by a capacitor. For the numerical values given in Figure 3, and the tolerances listed in Table I, this factor is 0.59. Thus, the  $-5.5 + 4.8$  per cent tolerance of Table I can be reduced to  $-3.2 + 2.8$  per cent for constant-frequency applica-

tions. It should be noted that the cathode capacitor in some cases may be rather large. It is necessary that the time constant  $C_K R_K$  be 50-100 times the period of the trigger to the multivibrator. Therefore, for low frequencies (60 cycles or lower), the cathode capacitor may be so large that a diode would be considerably less expensive.

Unfortunately, this method of tolerance reduction is not applicable to high-ratio frequency dividers. This is because the duty cycle of a counter is not a unique function of the count ratio, and averaging feedback thus introduces hysteresis into the counter. (The feedback is just as effective in regulating the counter in the wrong count as the correct one since the duty cycle may be the same for both conditions.)

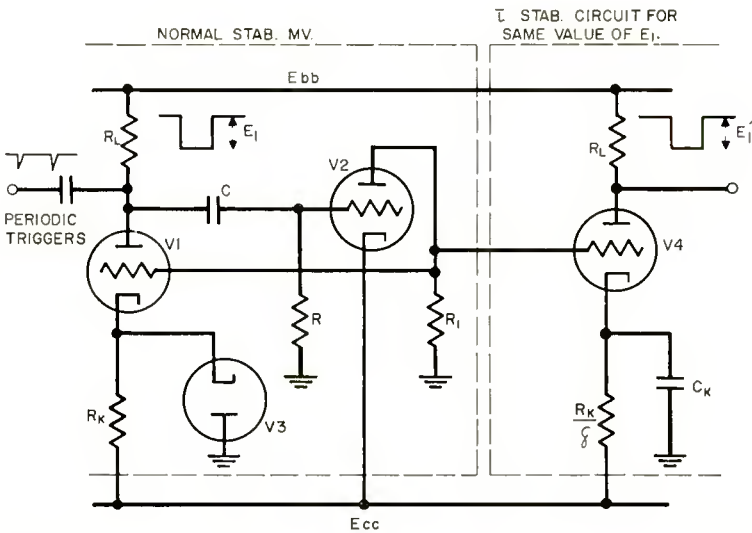


Fig. 7—Circuit for determination of loop gain of averaging feedback current stabilization.

An interesting version of the average current stabilization circuit is shown in Figure 8, where the connections have been arranged for a single power supply. Here, the grid voltage of V1 when V2 cuts off during the pulse is set by the divider  $R_1 - R_2$ . Since the cathode voltage of V1 is only  $e_c$  higher than this level, the cathode voltage may be used as the return point for R. This connection causes the multivibrator to become completely independent of V1, since  $e_c$  appears as a part of  $E_1$  and  $E_3$  both and will practically cancel out of Equation (1). Also, the resistance values of  $R_1$  and  $R_2$  are noncritical since they appear in the timing equation in the same way that  $E_{cc}$  and  $E_{bb}$  appear in Equation (4).

## CATHODE-COUPLED MULTIVIBRATOR

Cathode-coupled multivibrators are extremely useful for many applications because they provide input and output electrodes which are isolated from the multivibrator action. The averaging feedback is applicable to cathode coupling and provides the extremely useful and precise circuit of Figure 9. The values given are for a horizontal pulse generator for a television camera. The circuit is triggered at 15,750 cycles and generates an output pulse 8.5 microseconds wide. Typical performance for tolerances is tabulated in table II.

Stabilization of the cathode-coupled multivibrator is principally accomplished by the use of the  $R_K - C_K$  cathode network on V1 com-

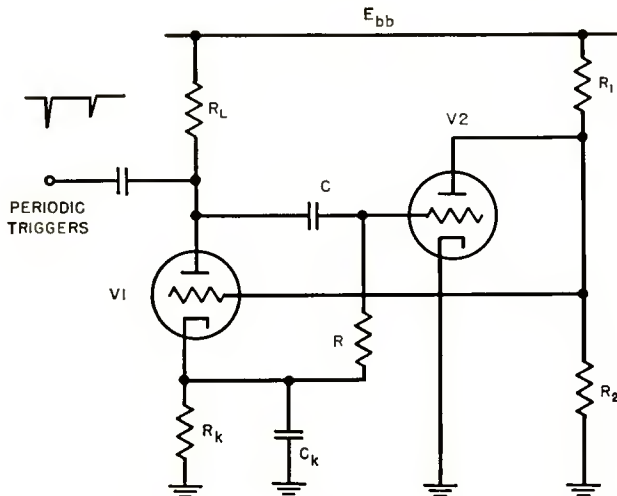


Fig. 8—An average-current stabilized multivibrator for a single power-supply voltage.

binated with positive bias at the grid of V1 derived from the grid return of V2. The action of this circuit may be more clearly seen with the aid of Figure 10, which is a detailed diagram of the V1 cathode waveform.

The average current of V1 is stabilized in the same manner as the average current feedback circuit of Figure 7 operates, except in this case the average current of V1 is controlled by the average voltage  $E_K$  developed across the cathode resistor. Therefore,

$$\bar{i} = \frac{\bar{E}_K}{R_K},$$

$$\bar{E}_K = E_a + e_c + \hat{E}_K (1 - \delta).$$

The peak-to-peak cathode voltage  $\hat{E}_K$  (which is the same on both cathodes since  $C_K$  is a complete bypass for all frequencies of interest) is given by the difference between the two tube currents  $i_1$  and  $i_2$  flowing through  $R_1$  and  $R_K$  in parallel,

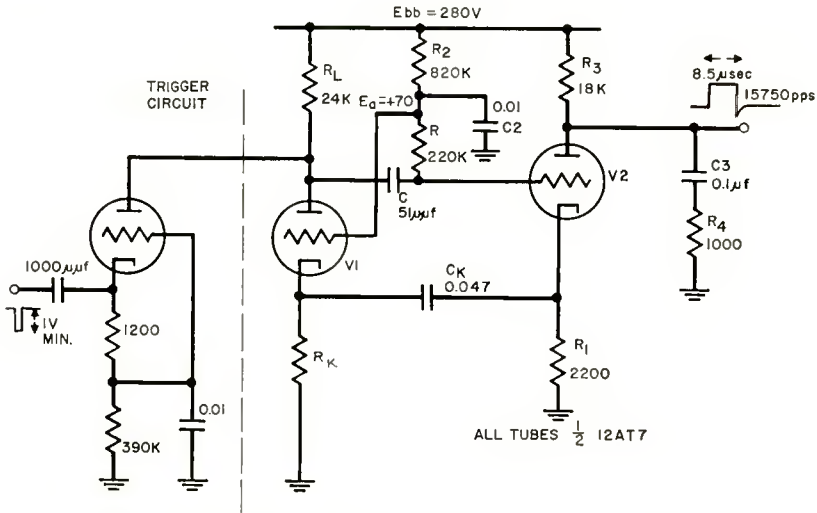


Fig. 9—Stabilized cathode-coupled multivibrator. Values given for 8.5-microsecond 15,750-pulses-per-second operation.

Table II—Tolerance Breakdown for Circuit of Figure 9  
(Experimental Data)

$E_{bb}$		0.003%/Volt from 190 to 490 volts
$\pm 5\%$	$R_1$	$\pm 0.5\%$
$\pm 5\%$	$R_2$	$\pm 0.17\%$
$\pm 10\%$	$R_3$	no change
$\pm 1\%$	$R$	$\pm 0.42\%$
$\pm 1\%$	$C$	$\pm 0.42\%$
$\pm 1\%$	$R_L$	$\pm 0.3\%$
$\pm 1\%$	$R_K$	$\pm 0.5\%$
$\pm 10\%$	$C_K$	$\pm 0.1\%$
Age V2 to $\frac{1}{2}$ current		0.2%
Trigger amplitude from 1.0 to 7.0 volts		0.1%

$$\hat{E}_K = (\hat{i}_2 - \hat{i}_1) \frac{R_1 R_K}{R_1 + R_K},$$

$$\bar{i}_1 = \frac{E_a + e_c + (\hat{i}_2 - \hat{i}_1) (1 - \delta) \frac{R_1 R_K}{R_1 + R_K}}{R_K}.$$

Recognizing that  $\hat{i}_1 = \frac{\bar{i}_1}{\delta}$  and that  $E_1 = \hat{i}_1 R_L$ ,

$$E_1 = \frac{(E_a + e_c) (R_1 + R_K) + (1 - \delta) R_1 R_K \hat{i}_2}{R_1 + \delta R_K} \frac{R_L}{R_K}. \tag{12}$$

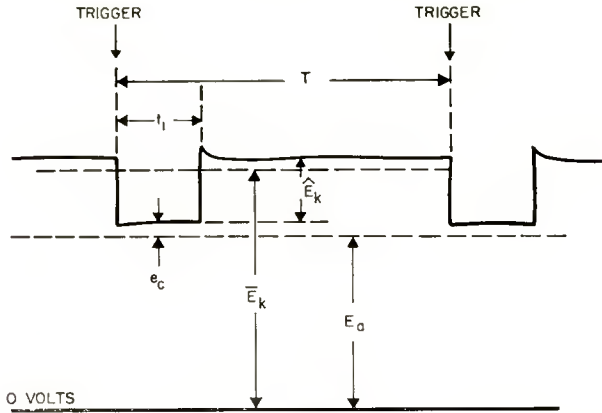


Fig. 10—Voltage diagram for cathode waveform of V1 in Figure 9.

Equation (12) then allows calculation of the initial amplitude of the timing waveform. This expression may be more closely studied if the approximation  $R_K \gg R_1$  is made. This is usually quite valid as can be seen from the constants of Figure 9. Then

$$E_1 \approx [E_a + e_c + \hat{i}_2 R_1 (1 - \delta)] \frac{R_L}{R_1 + \delta R_K}. \tag{13}$$

Now, Equation (13) is in a form which compares to Equation (10), except that it contains parameters relating to both tubes of the multivibrator.  $e_c$  is the same in Equations (10) and (13); it is the operating point bias of V1. The third term of Equation (13),  $\hat{i}_2 R_1 (1 - \delta)$ ,

is a function of the quiescent operation of V2. The current  $\hat{i}_2$  in V2 is not stabilized, since V2 in its conducting state simply operates at zero bias (due to the positive return of  $R$  and  $R_2$ ) with a total load resistance of  $R_1$  and  $R_3$ . Therefore, the current  $\hat{i}_2$  would be subject to considerable variation with change or aging of V2, and the term in Equation (13) containing  $\hat{i}_2$  is not small.

This property, however, is just what is required for stabilization of a cathode-coupled multivibrator against  $\hat{i}_2$ . One of the most serious limitations of conventional cathode-coupled multivibrators is the fact that placing a cathode load  $R_1$  in V2 causes the voltage  $E_2$  in the timing waveform to be increased by the amount of the drop across  $R_1$ . This is explained by Figure 11, which shows waveforms for the grid and cathode of V2. Here it is seen that  $E_2$  for the cathode-coupled multi-

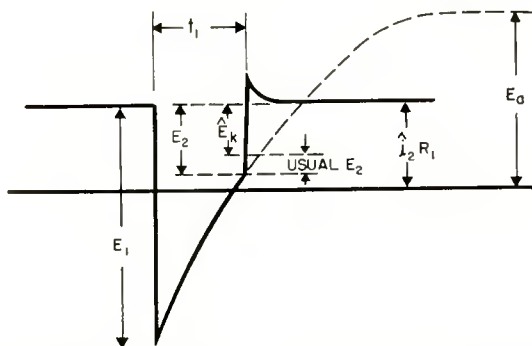


Fig. 11—Timing waveform of a cathode-coupled multivibrator.

vibrator is considerably greater than the usual cutoff voltage of V2, shown by usual  $E_2$ . This increase of  $E_2$  is principally dependent on  $\hat{i}_2 R_1$ , the peak drop across the cathode resistor  $R_1$  of V2.

If  $\hat{i}_2$  were to suddenly increase from its usual value, say by a decrease of the value  $R_3$ , then  $E_2$  would increase slightly. This would tend to reduce  $t$ . However, any increase in  $E_2$  will also appear as an increase in  $\hat{E}_K$ . This dependence of  $\hat{E}_K$  on  $\hat{i}_2$  is what causes the term in  $\hat{i}_2$  to appear in Equation (13). Therefore, the increase of  $\hat{i}_2$  will also cause an increase of  $E_1$ . An increase of  $E_1$  will cause an increase of  $t_1$ , and the dependence of  $t_1$  on  $\hat{i}_2$  may thereby be cancelled out. This is done simply by choosing the proper value of  $E_a$  relative to  $\hat{i}_2 R_1$  in Equation (13). A direct solution for this condition is sufficiently complicated that a trial-and-error process is usually required.

$E_a$  is obtained from a tap on the grid resistor of V2 in order to provide tracking of  $t_1$  against the value of  $E_a$ . Thus it is seen from Table II that the value of  $R_2$ , which determines  $E_a$ , is not very critical.

Of course, the value of  $R_2$  is important in maintaining the compensation against  $\hat{i}_2$  just described.

It will be noted that the circuit of Figure 9 does not use the usually "free" grid of V1 as a trigger input terminal. This is simply because of the rather short pulse width of this circuit. It was not feasible in this application to provide a narrow enough trigger pulse to the grid of V1 to prevent the trigger characteristics from affecting  $t_1$ . Therefore, applying the trigger at the plate of V1 where the circuit is much less sensitive allowed wider tolerances on the trigger shape and amplitude. Figure 9 also shows an a-c loading circuit  $C_3R_4$  across the output of V2. This again is used because of the narrow pulses in order to provide a low impedance load to maintain rise times without seriously disturbing the d-c operating conditions of V2.

#### CONCLUSION

It has often been said that multivibrators are so dependent on tube characteristics that accurate design equations are not very useful. The circuits presented here have largely overcome this problem, and their theory of operation is sufficiently well developed that it is relatively easy to calculate pulse width to within about 1 per cent for circuits operating from seconds to microseconds. The analysis of the diode-stabilized circuit has been presented in essentially complete form, even to the point of calculating the effect of all significant tolerances. Similar calculations for the averaging feedback circuit are considerably more difficult, but sufficient detail has been presented to allow satisfactory design.

#### BIBLIOGRAPHY

Chance, et al., *Waveforms*, McGraw-Hill Book Company, Inc., New York, N. Y., 1949.

M.I.T. Radar School Staff, *Principles of Radar*, 3rd Edition, pp. 92-104, McGraw-Hill Book Company, Inc., New York, N. Y., 1952.

W. A. Edson, *Vacuum-Tube Oscillators*, pp. 281-299, John Wiley and Sons, Inc., New York, N. Y., 1953.

M. V. Kiebert and A. F. Inglis, "Multivibrator Circuits," *Proc. I.R.E.*, Vol. 33, p. 534, August, 1945.

# PERIODIC MAGNETIC FIELD FOCUSING FOR LOW-NOISE TRAVELING-WAVE TUBES\*

BY

KERN K. N. CHANG

Research Laboratory, RCA Laboratories,  
Princeton, N. J.

## Abstract

*Summary*—Beam focusing with a periodic magnetic field for low-noise traveling-wave tubes is discussed. The focusing system consists of a uniform field magnet in the electron gun, a periodic field magnet in the helix region, and a magnetic matching transducer between the two. Measurements show that the gain and the noise figure of a 3000-megacycle traveling-wave tube obtained using the periodic magnetic field is comparable with those obtained with conventional uniform magnetic field systems.

## INTRODUCTION

SINCE the introduction of periodic-field focusing,<sup>1</sup> the use of the periodic magnetic fields for beam focusing in traveling-wave tubes with magnetically shielded cathodes has been quite successful.<sup>2</sup> For those tubes performing best with non-shielded cathodes, such as low-noise traveling-wave tubes, no experimental work on periodic-field focusing has ever been reported. It has been felt by many workers that the presence of the magnetic field at the cathode tends to diverge the electron beam<sup>3</sup> and this divergence might be serious enough to ruin the whole focusing mechanism of the periodic field. This controversy has indeed quite confused and discouraged those who attempted to apply the periodic magnetic field focusing to low-noise tubes, although it was pointed out by the author that it is sound in principle<sup>3</sup> to focus an electron beam which originates from a non-shielded cathode by a periodic field.

The work and the results presented will demonstrate that periodic

---

\* Decimal Classification: R339.2.

<sup>1</sup> J. R. Pierce, "Spatially Alternating Magnetic Fields for Focusing Low-Voltage Electron Beams," *Jour. Appl. Phys.*, Vol. 24, p. 1247, September, 1953.

<sup>2</sup> J. T. Mendel, C. F. Quate, and W. H. Yocom, "Electron Beam Focusing With Periodic Permanent Magnet Fields," *Proc. I.R.E.*, Vol. 42, pp. 800-810, May, 1954.

<sup>3</sup> K. K. N. Chang, "Beam Focusing by Periodic and Complementary Field," *Proc. I.R.E.*, Vol. 43, pp. 62-71, January, 1955.

magnetic field focusing operates as well on traveling-wave tubes with non-shielded cathodes as on those with magnetically shielded cathodes.

### TWO SCHEMES OF PERIODIC FOCUSING

It has been shown<sup>3</sup> that to maintain a confined beam flow at cathode radius, the r-m-s value of the periodic focusing field needed is slightly greater than the field at the cathode. On this basis, two simple periodic focusing schemes for low-noise traveling-wave tubes are proposed. Figure 1 shows a periodic field extending all the way from the cathode to the collector of the tube. The cathode is placed where the periodic magnetic field approximately equals the r-m-s value of the peak field. This model has practical difficulties, for in present low-noise traveling-wave tubes, the field required at the cathode is generally very high.

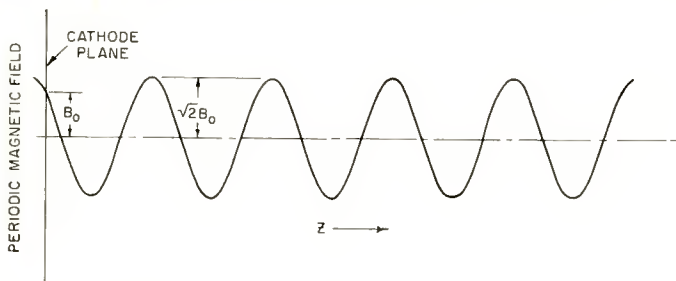


Fig. 1—Focusing system using a periodic magnetic field extending from the cathode to the collector of a low-noise traveling-wave tube.

With permanent magnet materials commercially available, it is very difficult to design a high-field magnet<sup>4</sup> for the gun region of these tubes, which usually has a larger envelope than the helix region. Of course, it may be possible to assemble the magnets inside the tube envelope to produce a higher field. The solution of this practical problem is not, however, included in this discussion.

The other scheme, which has more practical appeal, is shown in Figure 2. Here a uniform field is used in the gun region and a periodic field of about the same r-m-s value in the helix region. To match these two fields, a focusing "transducer" is inserted between them. This transducer (which will be discussed in detail in the next section), in conjunction with the gun magnet, allows adjusting the radius and the radial velocity of the beam to their optimum values required at the beginning of the periodic field.

<sup>4</sup> K. K. N. Chang, "Optimum Design of Periodic Magnet Structures for Electron Beam Focusing," *RCA Review*, Vol. XVI, pp. 65-81, March, 1955.

FOCUSING TRANSDUCER

To describe the principle of the focusing transducer, let us assume a general axially symmetrical magnetic field with axial component  $B_z$  which has the paraxial property

$$B_z = \sum_{n=0}^{\infty} \dot{B}_n \cos \left( \frac{n\pi}{L} z + \alpha_n \right), \quad 0 \leq z \leq L \tag{1}$$

where  $\alpha_n$  is the phase angle of the  $n$ th Fourier component, and  $L$  is the period which is less than the scalloping wavelength of the beam. The well-known beam equations<sup>5</sup> in three coordinates ( $r, \phi, z$ ) are, for axially symmetrical flow,

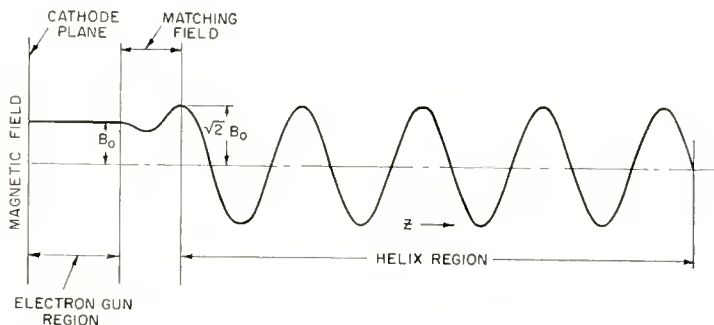


Fig. 2—Focusing system using a periodic magnetic field, a uniform field, and a “matching” magnetic field.

$$\ddot{r} = r\dot{\phi}^2 + \eta \dot{\phi} B_z r + \eta \frac{\partial V}{\partial r}, \tag{2}$$

$$\dot{\phi} = -\frac{\eta}{2} \left[ B_z - \frac{r_c^2}{r^2} B_c \right], \tag{3}$$

$$\ddot{z} = \eta \frac{\partial V}{\partial z} = 0, \tag{4}$$

where  $B_c$  is the magnetic field at the cathode of radius  $r_c$ ,  $V$  is the potential, dots indicate derivatives with respect to time, and  $\eta$  is the ratio of electronic charge to mass. If the angular velocity  $\dot{\phi}$  in Equation

<sup>5</sup> J. R. Pierce, *Theory and Design of Electron Beams*, D. Van Nostrand Co., Inc., New York, N. Y., 1949, p. 76.

(3) is substituted in Equation (2), a beam equation which accounts for all radial forces acting on the beam will be obtained at an equilibrium radius  $r_0$ . After linearizing the equation by considering only small variation of beam radius around  $r_0$ , one finds the paraxial equation

$$r'' + \frac{\eta}{8V} r \left( B_z^2 + 3B_c^2 \frac{r_c^4}{r_o^4} + B_b^2 \frac{r_c^2}{r_o^2} \right) = - \frac{\eta}{8V} r_o \left( B_z^2 - B_c^2 \frac{r_c^4}{r_o^4} - B_b^2 \frac{r_c^2}{r_o^2} \right) \quad (5)$$

where primes denote derivatives with respect to the axial distance  $z$ .  $B_b$  is an equivalent Brillouin field which represents the space charge effect. In rationalized units,

$$B_b^2 = \frac{\sqrt{2} I}{\pi \epsilon_0 \eta^{3/2} V^{1/2} r_c^2} \quad (6)$$

where  $I$  is the beam current. A Hill's equation is obtained if the magnetic field expression (1) is substituted in Equation (5), by writing

$$z_n \text{ for } z + \frac{L}{n\pi} \alpha_n,$$

$$r'' + \frac{\eta}{8V} r \left[ \bar{B}_o^2 + \frac{1}{2} \sum_{n=1}^{\infty} \bar{B}_n^2 + 3B_c^2 \frac{r_c^4}{r_o^4} + B_b^2 \frac{r_c^2}{r_o^2} + \frac{1}{2} \sum_{n=1}^{\infty} \bar{B}_n^2 \cos \frac{2n\pi}{L} z_n + 2 \sum_{n \neq m}^{\infty} \bar{B}_n \bar{B}_m \cos \frac{n\pi}{L} z_n \cos \frac{m\pi}{L} z_m \right] = \quad (7)$$

$$- \frac{\eta}{8V} r_o \left[ \bar{B}_o^2 + \frac{1}{2} \sum_{n=1}^{\infty} \bar{B}_n^2 - B_c^2 \frac{r_c^4}{r_o^4} - B_b^2 \frac{r_c^2}{r_o^2} + \frac{1}{2} \sum_{n=1}^{\infty} \bar{B}_n^2 \cos \frac{2n\pi}{L} z_n + 2 \sum_{n \neq m}^{\infty} \bar{B}_n \bar{B}_m \cos \frac{n\pi}{L} z_n \cos \frac{m\pi}{L} z_m \right]$$

Since Equations (5) and (7) have been linearized by assuming small variations in radius, the self-consistent solution of Equation (7) re-

quires a condition<sup>3</sup> such that the terms independent of  $z$  on the right hand side of the equation should vanish; i.e.

$$\bar{B}_0^2 + \frac{1}{2} \sum_{n=1}^{\infty} \bar{B}_n^2 = B_c^2 \frac{r_c^4}{r_o^4} + B_b^2 \frac{r_c^2}{r_o^2}. \tag{8}^*$$

Equations (7) and (8) will reduce to the uniform-field case or the purely sinusoidal periodic magnetic field case if the corresponding fields are substituted. All these cases are tabulated in Table I. It is common practice to employ a very high cathode field ( $B_c$ ) such that in Equation (8) the last term which represents the space charge effect can be ignored. This is the case of the so-called "confined flow"; i.e.,

Table I—Beam Focusing with Various Types of Magnetic Fields

	UNIFORM MAGNETIC FIELD	MAGNETIC FOCUSING TRANSDUCER	PERIODIC MAGNETIC FIELD
	BEAM EQUATION		
	$r'' + \frac{\eta}{8V} r (B_z^2 + 3B_c^2 \frac{r_c^4}{r_o^4} + B_b^2 \frac{r_c^2}{r_o^2}) = -\frac{\eta}{8V} r_o (B_z^2 - B_c^2 \frac{r_c^4}{r_o^4} - B_b^2 \frac{r_c^2}{r_o^2})$ <p style="text-align: center;"><math>r \ll r_o</math></p>		
$B_z$	$B_o$	$\sum_{n=0}^{\infty} \bar{B}_n \cos(\frac{n\pi}{L} z + \alpha_n)$	$B_1 \cos \frac{2\pi}{L} z$
DIFFERENTIAL EQUATION	TRANSMISSION LINE TYPE	HILL'S TYPE	MATHIEU TYPE
FOCUSING CONDITION	$B_o^2 = B_c^2 \frac{r_c^4}{r_o^4} + B_b^2 \frac{r_c^2}{r_o^2}$	$\bar{B}_0^2 + \frac{1}{2} \sum_{n=1}^{\infty} \bar{B}_n^2 = B_c^2 \frac{r_c^4}{r_o^4} + B_b^2 \frac{r_c^2}{r_o^2}$	$\frac{B_1^2}{2} = B_c^2 \frac{r_c^4}{r_o^4} + B_b^2 \frac{r_c^2}{r_o^2}$

$$\bar{B}_0^2 + \frac{1}{2} \sum_{n=1}^{\infty} \bar{B}_n^2 = B_c^2 \frac{r_c^4}{r_o^4}. \tag{9}$$

Let us consider an example. Suppose we retain only the first three terms of Equation (1) and also choose  $\alpha_0 = \alpha_1 = \alpha_2 = 0$ . Then the requirements (a) that the magnetic field of the transducer match into the uniform field ( $B_o$ ) before the transducer and into the periodic field ( $\sqrt{2} B_o$ ) after the transducer, and (b) that Equation (9) be satisfied, give us only the two possible fields:

\* According to Mendel,<sup>6</sup> J. R. Pierce has proposed a peaked square-wave field. The purpose of peaking is to augment the magnetic field in the field-reversal region so that the mean square field remains at the value prescribed by Equation (8).

<sup>6</sup> J. T. Mendel, "Magnetic Focusing of Electron Beams," *Proc. I.R.E.*, Vol. 43, pp. 327-331, March, 1955.

Case 1:  $B_z = B_0 \left( .976 - .207 \cos \frac{\pi}{L} z + .231 \cos \frac{2\pi}{L} z \right)$ . (10)

Case 2:  $B_z = B_0 \left( -.171 - .207 \cos \frac{\pi}{L} z + 1.378 \cos \frac{2\pi}{L} z \right)$ . (11)

$0 \leq z \leq L$

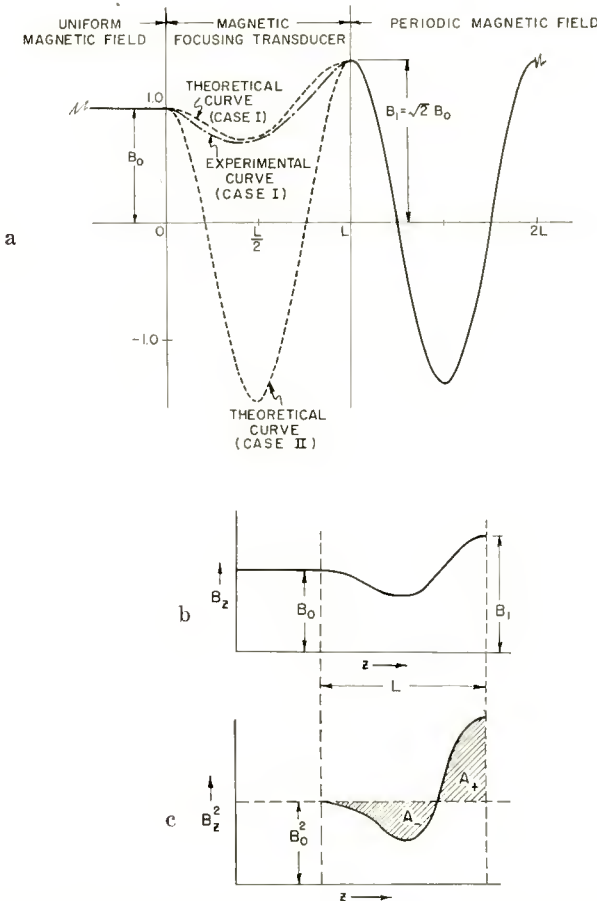


Fig. 3—Magnetic field distribution of a focusing “transducer.”

Attempts were made to approximate Case 1 by introducing a solenoidal field between the periodic field and the uniform field. By careful shaping of this solenoidal field, it was possible to achieve an optimized focusing condition with a measured field distribution which is indicated

in Figure 3a. This measured field agrees very well with the theoretical curve I.

Alternatively, it was pointed out by R. W. Peter that the required field  $B_z$  of the focusing transducer can also be graphically determined in a simple way.

As before, we assume that the length  $L$  of the field disturbance is small; say, less than a quarter of the scalloping-wave-length,  $\lambda_s$ , of the beam in the uniform field  $B_o$ , i.e.,

$$L < \lambda_s/4 \tag{12}$$

where

$$\lambda_s = \frac{2\pi v}{\eta B_o} \left\{ 1 + \frac{1}{\sqrt{1 + \frac{B_c B_o}{B_i^2}}} \right\}^{1/2} \tag{13}$$

$$\cong \frac{2\pi v}{\eta B_o}$$

where  $v$  is the velocity of the electron beam and  $B_c$  is the field threading in the cathode. Under this condition, the resultant radial force exerted on the beam stays constant and the mean square value of the focusing field remains constant, that is

$$\frac{1}{L} \int_0^L B_z^2 dz = B_o^2. \tag{14}$$

Using Equation (14), it is simple to design graphically any matching transducer by plotting  $B_z^2$  versus  $z$  and choosing the field distribution such that the total area is equal to the mean area as shown in the following example.

Suppose the field of a focusing transducer, which matches a uniform field  $B_o$  and a periodic field with a peak value of  $B_1 (= \sqrt{2} B_o)$ , is represented by Figure 3b. The corresponding plot of  $B_z^2$  versus  $z$  is shown by Figure 3c.

According to Equation (14) the area  $A_-$  below the line of mean square value (Figure 3c) should equal to the area  $A_+$  above the line. This criteria, indeed, enables one to design any desired and physically realizable field suitable for the transducer.

It should be noted that the mean square value given by Equation (14) is precisely the quantity on the left-hand side of Equation (8), as it has to be.

## EXPERIMENTAL RESULTS

The 3000-megacycle low-noise tube tested with periodic magnetic field focusing had a cathode diameter of .030 inch, an operating helix voltage of 530 volts, and a beam current of 300 microamperes. The focusing and input coupling assembly is shown in Figure 4. The periodic magnet, made of ferrite rings of Ferroxdure<sup>7</sup> was designed according to previously published curves.<sup>4</sup> All heavy lines shown represent "soft" magnetic material. The uniform-field gun magnet was a solenoid, and the focusing transducer consisted of a 1/8-inch-thick flat coil. All of the focusing magnets are assembled in a precision frame. Waveguide coupling sections are employed for r-f input and output; note that this design produces no gap in the magnetic field

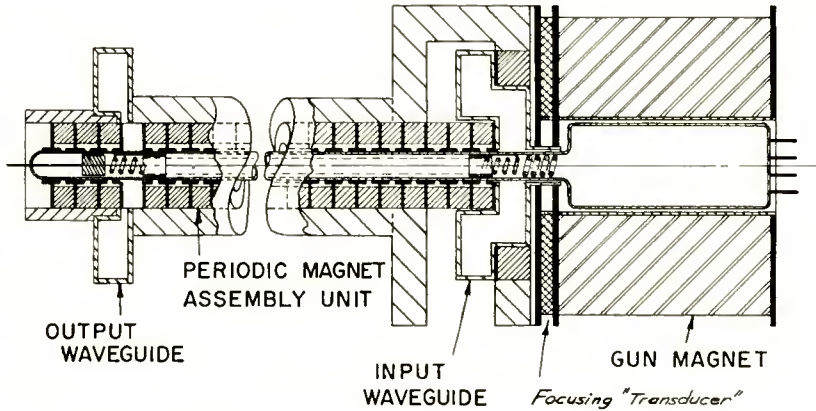


Fig. 4—Periodic magnetic field focusing system for low-noise traveling-wave tubes.

at the input side. This is very important, since good beam focusing is greatly dependent upon proper magnetic fields at the input end. The input coupling is accomplished by introducing a "coaxial" guide section which is coupled to the main guide as shown in Figure 4. At the output side, a gap is left in the periodic magnet for the output waveguide.

The experimental results are listed in Table II. For comparison, results obtained with a conventional uniform field are also given. It is interesting to note that despite the lower (r-m-s) field, and the slightly lower current transmission compared with the uniform field case, the periodic magnetic field focusing yields values of gain and

<sup>7</sup> J. J. Went, G. W. Rathenau, E. W. Gorter, and G. W. Van Oosterhant, "Ferroxdure, a Class of New Permanent Magnet Materials," *Philips Technical Review*, Vol. 13, No. 7, January, 1952.

noise figure comparable to those obtained with the uniform field focusing.

### CONCLUSIONS

The periodic magnetic field used in the experiment was low (320 gauss r-m-s) compared with the 450 gauss which is required at the cathode for uniform field focusing. The use of high peak fields requires the use of small periods as has been discussed in the literature;<sup>2,3</sup> however, with the permanent magnet materials commercially available, this is difficult to achieve. Nevertheless, it is believed that the results obtained can still be improved by redesigning the periodic magnet and increasing the peak field.

Table II—Experimental Results

	UNIFORM MAGNETIC FIELD	PERIODIC MAGNETIC FIELD
d. c. PERFORMANCE		
PERIOD		.500"
RMS FIELD	450 gauss	320 gauss
CATHODE FIELD	450 gauss	320 gauss
COLLECTOR CURRENT	270 $\mu$ a	250 $\mu$ a
% CURRENT TRANSMISSION	99 %	94 %
r. f. PERFORMANCE		
FREQUENCY	2950 m.c.	2950 m.c.
GAIN	25 db	20 db
NOISE FIGURE	9.8 db	10.1 db

TW TUBE DATA:	CATHODE DIAMETER	.030"
	HELIX DIAMETER	.096"
	HELIX LENGTH	10"
	HELIX VOLTAGE	530 volts

To match the periodic magnetic field in the helix region with the uniform magnetic field in the gun region, a focusing transducer is found to be necessary in order to give satisfactory focusing. This transducer is capable of properly guiding the beam in the region of field transition.

Periodic magnetic field focusing for confined electron flow requires an over-all magnet structure of high precision and of perfect axial symmetry. The alignment problem for the periodic field system is more difficult than that for the uniform field; with the periodic field, the alignment problem is even somewhat more severe when cathodes which are not magnetically shielded are used.

It is concluded here that both in principle and in practice, periodic magnetic field focusing can be applied to low-noise traveling-wave tubes just as well as to the conventional uniform field focusing, without degrading the noise factor.

# SYSTEM PARAMETERS USING TROPOSPHERIC SCATTER PROPAGATION\*

BY

H. H. BEVERAGE,<sup>†</sup> E. A. LAPORT,<sup>‡</sup> AND L. C. SIMPSON<sup>#</sup>

*Summary*—Accumulated data from published sources and from unpublished research on tropospheric forward scatter propagation are reviewed and condensed for practical application to FM communication systems. Antennas suitable for use on scatter paths are reviewed and the limitations on usable gains are discussed. General design methods for FM systems are presented and reduced to a design chart that includes the relationship of all parameters in a frequency-division multiplexed FM telephone system. Then follow computed values of transmitter power as functions of distance, frequency and antenna size for a number of systems of practical interest using tropospheric forward scatter.

## I. TROPOSPHERIC FORWARD-SCATTER DATA

WHEN high-power transmitters became available on frequencies above 40 megacycles, it was found that the signal intensities received far beyond the horizon were very much higher than predicted by the existing theories. Booker and Gordon worked out a theory of scattering based on a turbulent medium in the troposphere to account for the observed field strengths far beyond the horizon.<sup>1</sup> Carroll and Ring proposed that the observed propagation can be accounted for by mode theory based on the assumption that the troposphere is idealized to be a linearly tapered layer of dielectric about 9 kilometers thick.<sup>2</sup> Kenneth Bullington published some experimental data which indicated that the median signal levels far beyond the horizon seem to decrease approximately 18 decibels for doubling the distance in addition to the 6 decibels extra free space loss, and that the received power at points far beyond the horizon is relatively

---

\* Decimal Classification: R113.308.

† Research Laboratory, RCA Laboratories, New York, N. Y.

‡ Radio Corporation of America, New York, N. Y.

# RCA International Division, New York, N. Y.

<sup>1</sup> H. G. Booker and W. E. Gordon, "A Theory of Radio Scattering in the Troposphere," *Proc. I.R.E.*, Vol. 38, pp. 401-412, April, 1950.

<sup>2</sup> T. J. Carroll and R. M. Ring, "Normal Tropospheric Propagation of Radio Waves Well Beyond the Horizon," M.I.T. Lincoln Laboratory Technical Report No. 38, February 12, 1954.

independent of frequency, antenna height, and weather effects.<sup>3,4</sup>

In Figure 1, line "A" is based on the median signal levels shown in Bullington's paper for the 40- to 300-megacycle band. Line "B" is likewise based on the median signal levels shown by Bullington for the 300- to 4000-megacycle band. The points plotted on Figure 1 and listed in Table I are taken from various sources not included in Bullington's paper. The median values for WBRE-TV (Wilkes-Barre, Pa.) and WNBC-TV (Binghamton, N. Y.) are taken from unpublished reports. In most cases, the 50 per cent of the time values were obtained from recordings over long periods of time.

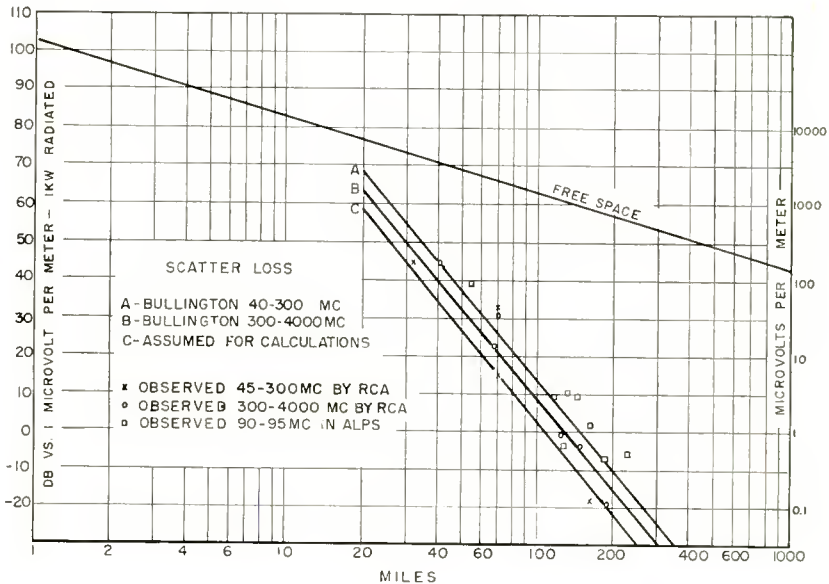


Fig. 1—Median field strength versus distance in the scatter regions.

It will be noted that the observed points are in fair agreement with Bullington's observations. The measurements made in the Alps are included to illustrate the relatively small dependence of the tropospheric scatter propagation fields on obstructions along the path, since several of these paths have mountains between the transmitter and the receiver. It is important, however, that there be no obstructions of consequence within the optical horizon of either the transmitter or receiver.

<sup>3</sup> Kenneth Bullington, "Radio Transmission Beyond the Horizon in the 40-to-4000 Mc Band," *Proc. I.R.E.*, Vol. 41, pp. 132-135, January, 1953.

<sup>4</sup> R. L. Robbins, "Measurement of Path Loss Between Miami and Key West at 3675 Mc," *Transactions of the I.R.E.*, Vol. AP-1, No. 1, July, 1953.

If there is a high obstruction near the middle of the path which is visible from both ends of the circuit, the principal propagation mechanism does not depend on tropospheric scatter but involves the theory of diffraction over a knife edge. The presence of the obstruction may greatly increase the received field intensity above that which would be received if there were no obstruction. Large obstacle gains

Table I—Measurements of Signal Strengths Observed Over Various Paths (decibels referred to 1 microvolt per meter, normalized to 1 kilowatt radiated power)

	Dis- tance Miles	Fre- quency Mc	Min. for 1% of Time	50% of Time	Max for 1% of Time	Free Space Field (dbe)*
Bridgeport to Riverhead, L. I. <sup>5</sup>	33.0	534.75	+38	+45	+61	+73
Alpine to Hauppague, L. I. <sup>6</sup>	40.5	93.1	+35	+45	+58	+71
Alpine to Riverhead <sup>6</sup>	67.2	93.1	+11	+23	+54	+67
Empire State Bldg. to Riverhead <sup>7</sup>	70.1	45.1	+18	+31	+46	+66
Empire State Bldg. to Riverhead <sup>7</sup>	70.1	474.0	+24	+34	+76	+66
Empire State Bldg. to Riverhead <sup>7</sup>	70.1	2800.0	—	+16	+76	+66
WBZ-FM to Riverhead <sup>6</sup>	127.3	92.9	-16	- 1	+37	+61
WBZ-FM to Hauppague <sup>6</sup>	150.4	92.9	-16	- 3	+43	+60
WBRE-TV to Riverhead	165.5	559.75	—	-17	+ 4	+59
WNBF-TV to Riverhead	189.0	209.75	—	-19	+18	+58
Blauen-Berne <sup>8</sup>	55.5	90-95	—	+39	—	+69
Hornisgrinde-Berne	119.0	90-95	—	+10	+26	+62
Waldburg-Mt. Generoso	129.0	90-95	—	- 3	—	+61
Blauen-Mt. Generoso	133.0	90-95	—	+11	+21	+61
Whithon-Mt. Generoso	142.0	90-95	—	+10	+20	+60
Raichberg-Mt. Generoso	162.0	90-95	—	+ 2	—	+59
Hornisgrinde-Mt. Generoso	189.0	90-95	—	- 7	+10	+58
Feldsberg-Berne	229.0	90-95	—	- 5	—	+56

\* 0 db = 1 microvolt per meter.

<sup>5</sup> G. S. Wickizer, "Field Strength of KC2XAK, 534.75 Mc. Recorded at Riverhead, N. Y.," *Proc. I.R.E.*, Vol. 41, pp. 140-142, January, 1953.

<sup>6</sup> G. S. Wickizer and A. M. Braaten, "Field Strengths Recorded on Adjacent FM Channels at 93 Mc Over Distances From 40 to 150 Miles," *Proc. I.R.E.*, Vol. 40, pp. 1694-1699, December, 1952.

<sup>7</sup> G. S. Wickizer and A. M. Braaten, "Propagation Studies on 45.1, 474 and 2800 Megacycles Within and Beyond the Horizon," *Proc. I.R.E.*, Vol. 35, pp. 670-680, July, 1947.

<sup>8</sup> Jean Dufour, "Contribution à L'étude de la Propagation Des Ondes Ultra-Courtes Par-dessus La Barrière Alpine," pp. 124-130, *Technische Mitteilungen PTT*, No. 5, 1953.

are obtained only when the geometry of the path and the frequency used have the proper relationship.<sup>9</sup>

From Figure 1, it was concluded that for the purposes of this paper the best values to use for tropospheric scatter loss calculations should be about 6 decibels greater than the median values shown in Bullington's paper. These values are indicated as curve "C" in Figure 1. The scatter loss alone is shown in Figure 2 for convenience in calculation procedures. The scatter loss is, of course, in addition to the free-space attenuation.

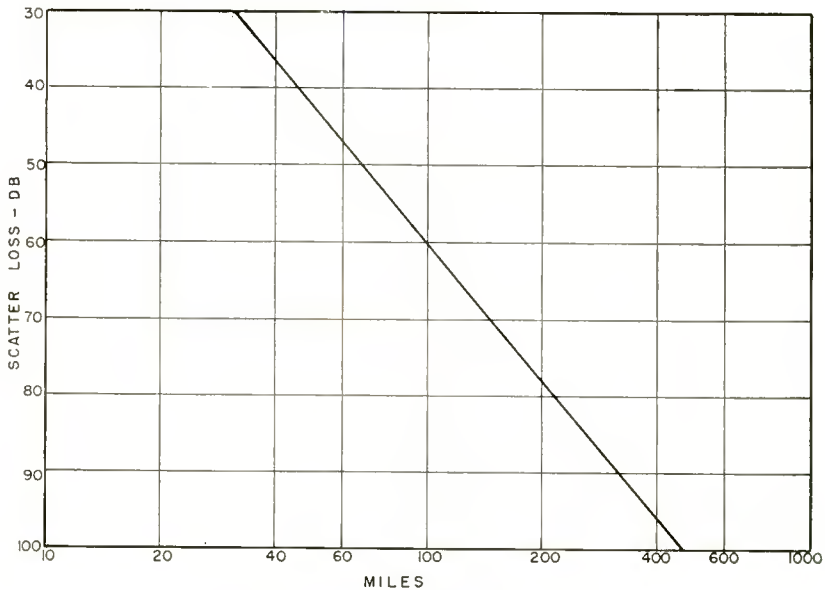


Fig. 2—Scatter loss versus distance.

There are several meanings to the common term "median" as applied to the range of variation of path loss with time. Over a long period, such as a year or more, and including seasonal and diurnal variations, there will be a long-term median value. Then there are a highest monthly median, a highest weekly median, and so on down to highest hourly median value of path loss. The value that the system engineer has to use for design purposes depends upon the nature of the traffic to be carried, and the consequences of circuit failure for even short intervals of time. Most exacting is teleprinter traffic where

<sup>9</sup> Dickson, Egli, Herbstreit, and Wickizer, "Large Reductions of VHF Transmission Loss and Fading by the Presence of a Mountain Obstacle in Beyond-Line-of-Sight Paths," *Proc. I.R.E.*, Vol. 41, pp. 967-969, August, 1953.

momentary drop-outs will mutilate or obliterate messages. Probably the next most exacting service is television video signals, where a drop-out may cause loss of picture synchronization with results immediately apparent and annoying to any viewer. The least exacting choice of median value of path loss would be for a single voice channel for intermittent service, where loss of communication for a certain length of time would not be serious provided acceptable performance is realized for a sufficiently large percentage of the time. The choice of median path loss has a major influence on the cost and complications of a system. Figure 1, curve "C", corresponds to highest monthly median losses.

This is mentioned because measurements from different sources are reported as different kinds of medians in many cases.

Propagation measurements are usually reported directly in field strengths, field strengths in decibels relative to some reference value such as 1 microvolt per meter, or in decibels relative to the free-space loss.

In system engineering it is very convenient to use power levels in dbw (decibels relative to 1 watt). To determine receiver input power from a given field strength, Figure 3 will often be useful. In this chart the relation between receiver input power and field strength is given for a range of frequencies, using for the conversion the effective aperture of a free-space one-half-wavelength electric dipole antenna with no feeder loss. For an antenna having gain with respect to the half-wave dipole, the received power will be increased by the amount of the antenna gain up to a certain limit for scatter propagation of around 40-45 decibels.

It is of interest to observe that an electric half-wave dipole at 100 megacycles has an effective aperture of very nearly 1 square meter, so that this line also gives the value of Poynting's vector in dbw for each field strength.

#### ANTENNAS

The antennas assumed in this paper for computing the power-frequency-distance needs for various systems are paraboloids with ideally true surfaces and illuminated in the optimum way in both planes. Large paraboloids have the advantage of utmost simplicity of the electrical parts, with consequent electrical reliability. The mechanical details may be relatively complicated but once properly done they leave little risk of trouble. A device that must withstand the extremes of temperature and winds from all directions, with and without ice and rime, must be both electrically and mechanically stable

for years after erection. The simplest radiator and feeder systems are most desirable in minimizing noise and maintenance. Mechanical stability of the structure is essential to avoid noise generation in receiving.

Figure 17 is an example of a large paraboloid antenna that was completed at Covey Hill, Quebec, in May 1954. It was designed for scatter-propagation applications. The antenna can be adjusted through an azimuthal range of 30 degrees and a vertical range of 10 degrees. It is presently being used for scatter propagation studies over the 290-mile path to Riverhead, N. Y.

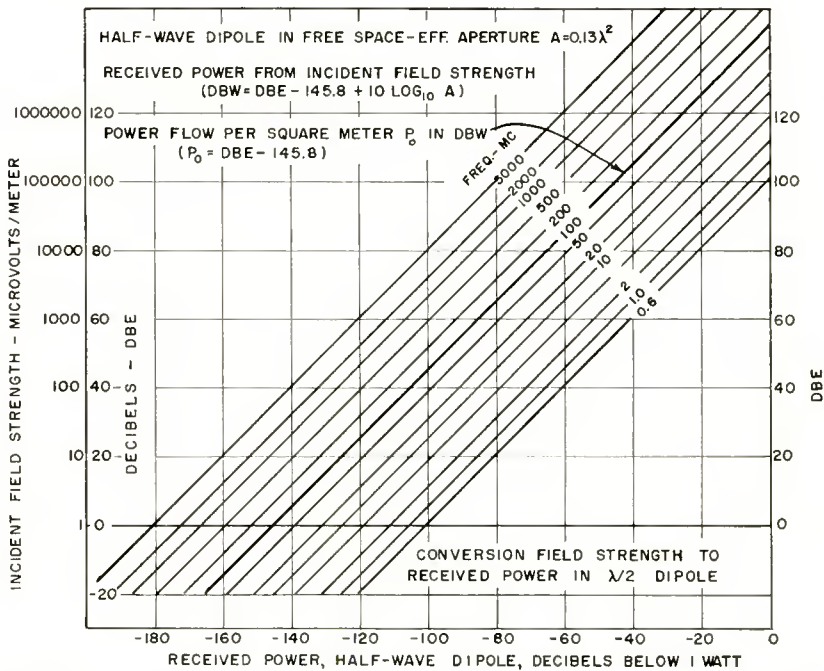


Fig. 3—Relationships between incident field strength and received power for half-wave dipole antennas.

The aperture-gain relations for the assumed paraboloidal antennas are shown in Figure 4. Any other type of antenna having equivalent gain can, of course, be substituted. The gains used herein are with respect to a half-wave electric dipole. The gain as a receiving antenna is that for an ideal plane wave arriving with its equiphase surface parallel to the rim of the paraboloidal reflector.

The effect of aperture-medium coupling losses are discussed later. No allowance for losses of this nature is included in the charts for

the various systems except to exclude cases where the antenna approaches 80 wavelengths diameter, beyond which this effect is known to introduce appreciable losses.

The total system antenna gains are the sum of the transmitting and receiving antenna gains, less any losses in their feeders, and any duplexers that may be used for transmitting and receiving with the same antenna. In the examples to be discussed later, a total loss of 5 decibels for feeders and duplexers is included.

To determine the transmitter power needed to obtain the same performance with antennas of different size, the conversions can be made using Table II. Feeder and duplexer losses for the path are

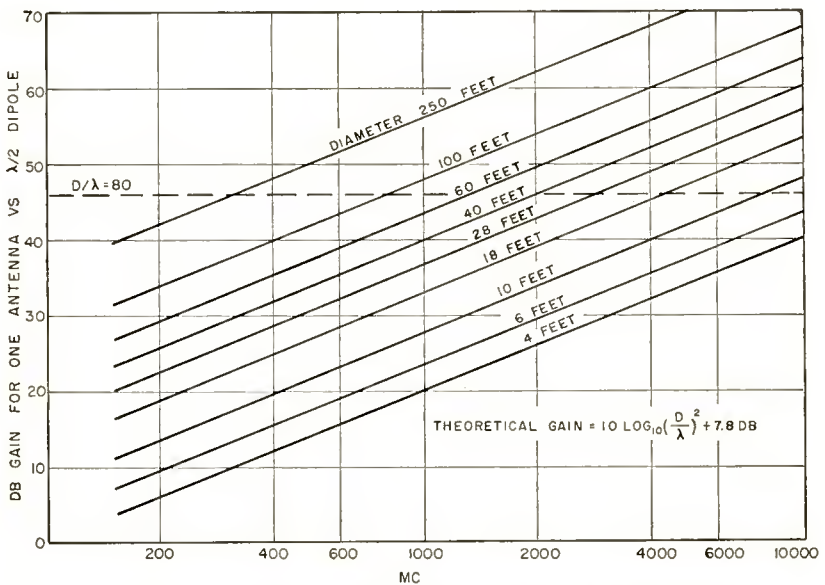


Fig. 4—Gain of paraboloidal antennas versus half-wave dipoles.

assumed to remain the same for all antennas. The relative transmitter power requirements in Table II apply to circuits using identical antennas at each end of the path.

Table II—Power Relations versus Antenna Size

Antenna diameter (feet)	6	10	18	28	40	60	100	250
Relative transmitter power	+26.8	+17.8	+ 7.8	0	- 6.3	-13.3	-22.1	-38.5
Required in decibels	+33.1	+24.1	+14.0	+ 6.3	0	- 7.0	-15.8	-32.2
	+40.0	+31.1	+21.0	+13.3	+ 7.0	0	- 8.8	-25.2
	+48.9	+39.9	+29.8	+22.1	+15.8	+ 8.8	0	-16.4

## SYSTEM SCATTER LOSSES

In Figure 5, the lower line shows the noise at the receiver input in terms of decibels referred to 1 watt (dbw) versus bandwidth for an ideal receiver. The upper lines show the same for practical receivers with excess noise factor as indicated on the curves. By scaling the free-space attenuation from Graph 1 of Figure 8, and adding the tropospheric scatter loss from Figure 2, the total attenuation for the path for 50 per cent of the time is obtained. By adding the antenna gain at each end of the circuit from Figure 4, the effective received power for 50 per cent of the time is obtained in terms of decibels

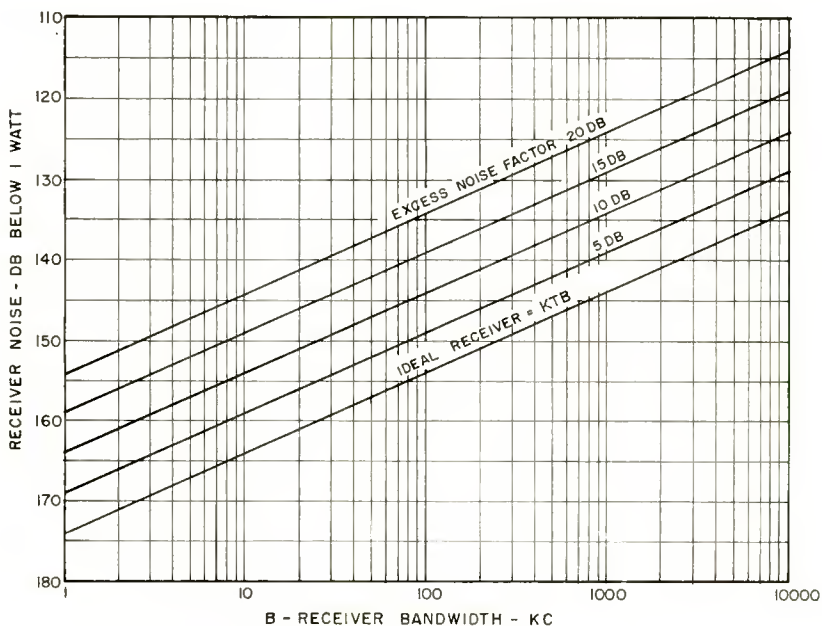


Fig. 5—Equivalent receiver noise power versus bandwidth.

below one watt radiated. The appropriate value of receiver noise from Figure 5 subtracted from the received power is the signal-to-noise ratio in the assumed r-f or i-f bandwidth for 50 per cent of the time for one watt radiated.

To obtain the desired type of service for 99 per cent of the time, it is necessary to increase the power by an amount sufficient to take care of the long-term fading. This increase in power is usually assumed of the order of 15 decibels, although at great distances beyond the horizon where the scatter field predominates, the fading decreases and the difference between the field intensity received 99 per cent of the

time and 50 per cent of the time is generally less than 15 decibels.<sup>10</sup>

On the other hand, there are other losses that should be taken into account under certain conditions. For example, unless there is sufficient margin above the threshold in an FM system, there may be short drop-outs during normal fast fading. The best safeguard against exceptionally deep fades is space diversity reception with antennas spaced 50 or more wavelengths normal to the path. The gain due to space diversity varies over rather wide limits depending upon the type of fading and the signal intensity. On the basis that identical receiving antennas are used, 10 decibels is assumed as the average gain for the power requirement calculations to be discussed.

Another factor which may be of importance when very large antennas are used is loss in gain due to the aperture-medium coupling loss.<sup>11,12</sup>

Figure 6 was calculated on the basis of the information contained in the Booker-deBettencourt paper and indicates the theoretical aperture-medium coupling loss versus distance and antenna size as parameters. A somewhat similar theoretical result is obtained from Gordon's paper. Actually, experience indicates that the gain of a large antenna varies with time. The allowance for the aperture-medium coupling loss must, therefore, be determined statistically on an experimental basis. Booker and deBettencourt indicate that the loss determined by the theory is probably several decibels too high for an antenna diameter of 100 wavelengths. They point out that there is little to be gained in received power by using antennas in excess of 100 wavelengths in diameter. However, they state that there is a theoretical increase in the usable bandwidth for increasing antenna size, and for that reason it may be advisable to use antennas with very large apertures for wide-band services even though the improvement in the received power is minor.

G. S. Wickizer and D. G. Shipley, in an unpublished report, discuss some observations made at Riverhead, L. I. on the regular television transmissions from WNBC-TV, Binghamton, N. Y., on a frequency of 209.75 megacycles. The distance is approximately 189 miles. The

---

<sup>10</sup> P. L. Rice, F. T. Daniel, W. V. Mansfield, and P. J. Short, "Radio Transmission Loss Versus Angular Distance and Antenna Height at 100 Mc," Presented at the NBS Boulder Laboratories Dedication Program, September 8-14, 1954.

<sup>11</sup> H. G. Booker and J. T. deBettencourt, "Theory of Radio Transmission by Tropospheric Scattering Using Very Narrow Beams," *Proc. I.R.E.*, Vol. 43, pp. 281-290, March, 1955.

<sup>12</sup> William E. Gordon, "Radio Scattering in the Troposphere," *Proc. I.R.E.*, Vol. 43, pp. 23-28, January, 1955.

receiving antenna was a double-wire rhombic, 31 wavelengths per leg, 50 feet above the ground. It had a measured gain of 18 to 20 decibels over a half-wave dipole, equivalent to the gain of a paraboloid antenna about 20 feet or 4 wavelengths in diameter. Observations of the multipath delay were made on 17 days spread over a period of several months. The delay varied from zero to a maximum of 1.75 microseconds, averaging about 0.85 microsecond. Generally, the signal was strong during the periods of no delay. These observations point to the desirability of using relatively large antennas, free of side lobes, for wide-band services, as pointed out by Booker and deBettencourt.<sup>11</sup>

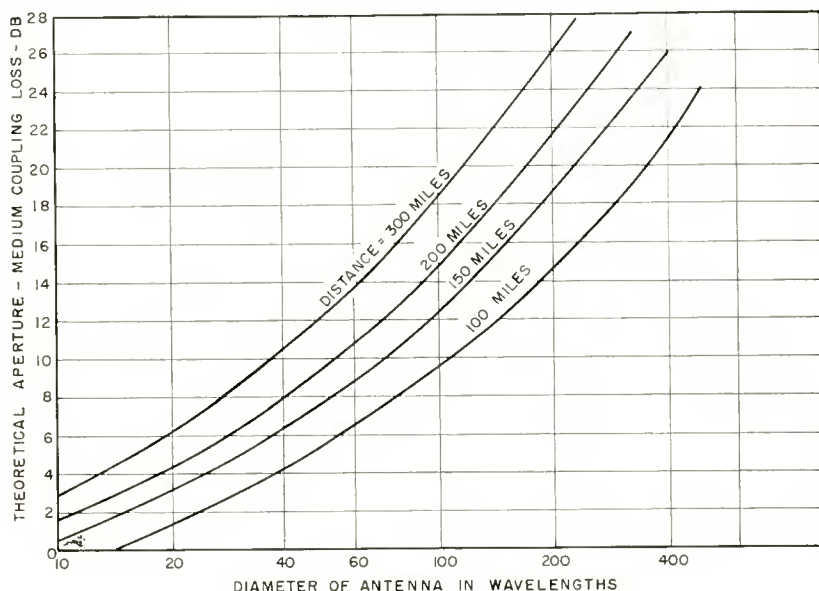


Fig. 6—Theoretical aperture-medium coupling loss.

Their general conclusion was that for their assumed circuit of 300 kilometers with paraboloids of 100 wavelengths diameter at both ends of the circuit (beamwidth 0.73 degree) the bandwidth should be about 6 megacycles and the aperture-medium coupling loss should be on the order of 10 decibels. For beamwidths much larger than 1.5 degrees, the bandwidth should be limited by the medium to about 3 megacycles, with negligible loss.

## II. FM FREQUENCY-DIVISION RADIOTELEPHONE SYSTEMS

Before proceeding with forward-scatter systems it is desirable to review the parameters for frequency-modulation systems from the systems engineer's standpoint.

In the design of a multichannel communication system, one of the main objectives is the assurance of a predetermined value of signal-to-noise ratio. However, the designer may have the possibility of utilizing any one of many combinations of equipment, antenna size and station location which will result in the required signal-to-noise ratio, and the problem becomes one of selecting the best combination from economic or geographic considerations. In order that proper consideration may be given to all aspects of the design, it is advantageous to simplify the purely technical calculations to the point where the performance for any number of system combinations may quickly be evaluated. The FM system parameters are conveniently related by means of a chart.

The system design chart described here was evolved for use in the design of multichannel microwave systems utilizing frequency modulation and frequency division multiplexing to obtain commercial telephone channels of 3 kilocycle bandwidth. Channel signal-to-noise ratio, baseband signal-to-noise ratio, and carrier signal-to-threshold ratio are related to the combined effects (where applicable) of distance, path loss in excess of free space loss, total net antenna gain, transmitter power, effective receiver noise factor, peak frequency deviation, channel position in the baseband, baseband width, and i-f bandwidth.

Several factors that influence the signal-to-noise ratio are not covered by the chart, either because their inclusion would increase the chart to an impractical size, or because simplifying assumptions would be required which it would be dangerous to make without careful consideration in each case. The chart applies to the performance of any single hop of a system. The signal-to-noise ratio for a multi-hop system may be obtained by combining the signal-to-noise ratios of the individual hops, and the effect of fading may be considered by introducing the appropriate variations in the individual path losses. Noise introduced by inter-modulation and by the multiplex equipment is not included.

#### RECEIVED POWER

One of the first essential steps in determining signal-to-noise ratio is the evaluation of the r-f carrier power at the receiver input. The received power depends upon the transmitter power, the total gain of the transmitting and receiving antennas and the path loss.

The path loss between one-half-wave dipole antennas may conveniently be considered as the sum of two parts, (1) the free-space loss and (2) the additional loss in excess of the free-space value. The first and larger of these is determined by distance and frequency.

Accurate determination of the second usually requires detailed consideration of the transmission path and the manner of propagation, utilizing the various procedures described in this paper and in the literature.<sup>3,13</sup> The total path loss may, therefore, be expressed in terms of distance, carrier frequency, and path loss in excess of the free space value.

The received power may then be evaluated as follows:

$$\begin{aligned}
 & - 20 \log_{10} \text{ miles} \\
 & - 20 \log_{10} \text{ megacycles} \\
 & - 32.3 \text{ (Free-space loss at 1 mile with } \lambda/2 \text{ dipole at 1 mega-} \\
 & \quad \text{cycle)} \\
 & - \text{path loss in excess of free space value in decibels} \\
 & + \text{total net antenna gain in decibels} \\
 & + 10 \log_{10} \text{ transmitter watts} \\
 \hline
 & = \text{received power in dbw (0 dbw} = 1 \text{ watt)}
 \end{aligned} \tag{1}$$

### Noise

Although an FM system is usually made insensitive to amplitude variations by means of limiting, the system is not insensitive to noise. When r-f noise components are added to the r-f carrier, the resultant is a wave whose amplitude and phase varies with respect to the phase of the carrier alone. Since the FM receiver is designed to be sensitive to frequency or phase modulation, the output signal-to-noise ratio varies directly with the r-f carrier-to-noise ratio. The principal causes of output noise are (1) thermal r-f noise in the receiver input stages, (2) man-made r-f noise from automobiles and electrical equipment and (3) cosmic r-f noise. It is convenient to refer all r-f noise power to a common point, the receiver input.

The thermal noise power delivered to the receiver input by a matching load resistor is  $KTB$ , where  $K$  is Boltzmann's constant,  $T$  is the absolute temperature, and  $B$  is the bandwidth. The thermal power generated by the receiver itself and the matching load resistor is  $F_r KTB$ , where  $F_r$  is the receiver noise factor as shown in Figure 5.

The man-made noise which will be received from any single source is difficult to predict. However, in such a case it probably will be found possible to so plan the system as to avoid the single noise source entirely. More important in system design is the noise that will be received when a station must be located in an urban or suburban area, and which in the case of VHF can seldom be disregarded. In urban areas there are so many contributing noise sources that the received

<sup>13</sup> Kenneth Bullington, "Radio Propagation at Frequencies Above 30 Megacycles," *Proc. I.R.E.*, Vol. 35, pp. 1122-1136, October, 1947.

noise power has similar characteristics to thermal or random noise, though the crest factor may be somewhat higher.

The prediction of man-made noise must be based upon empirical data rather than theoretical considerations. Admittedly, the correlation of such data is complicated by the effects of antenna directivity, transmission line losses, and variations with time. However, observations made by a number of observers make it possible to establish the general magnitude and frequency distribution of this type of noise.

In system design it is convenient to make use of a "man-made-noise factor,"  $F_m$ , such that the man-made noise power at the output of the receiving antenna equals  $F_m KTB$ . The values of  $F_m$  shown in Figure

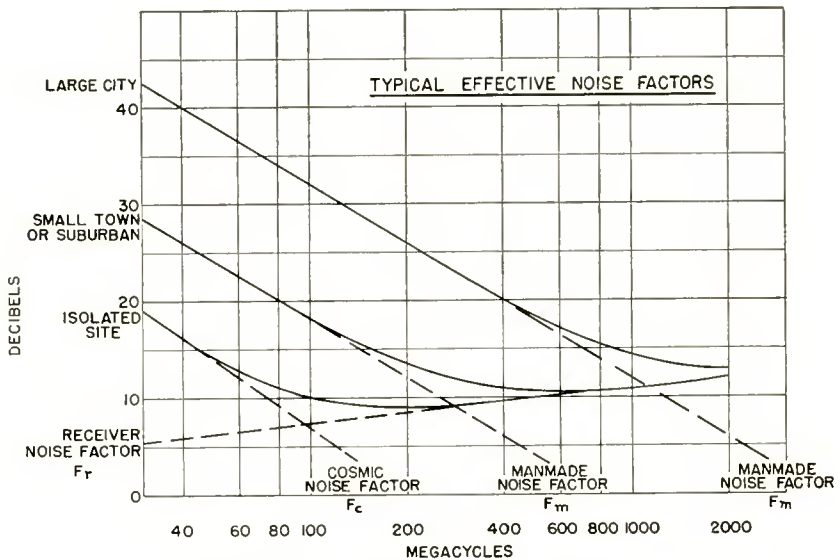


Fig. 7—Typical effective noise factors.

7 are indicative of what may be expected for antennas of medium gain when noise readings are taken in a telephone channel with a telephone noise measuring set such as the W. E. 2B with F1A weighting. Cosmic noise may be received from almost any part of the sky, although the received power is greatest when the antenna is directed toward the galactic plane (Milky Way) or the galactic center (Sagittarius). Since the earth's rotation causes the antenna to continually sweep across some portion of the sky, the received cosmic noise power depends upon the time, antenna azimuth and directivity. Cosmic radiation is of the random type, and may be the predominant source of noise at isolated stations operating in the lower VHF band.

It is convenient to make use of a "cosmic-noise factor,"  $F_c$ . The values shown in Figure 7 are derived from the work of Cottony and Johler,<sup>14</sup> who used a dipole and reflector antenna receiving from a wide area of sky. The curve shows the maximum values for a period of about two hours each day. Higher noise factors, for shorter periods, may be expected from antennas of higher gain and narrower beam-width oriented to intercept a major noise area of the sky.

In Figure 7, the variations of  $F_r$ ,  $F_m$  and  $F_c$  with frequency are shown, and the three factors are combined to produce an over-all of "effective noise factor,"  $F$ . The values shown for  $F_r$  are typical of commercial receivers with average maintenance. In some cases, especially at the higher frequencies where  $F_r$  is the controlling noise factor, it will be preferable to apply the actual noise factor of the receiver used. The total noise power referred to the receiver input equals  $FKTB$ . When the effective noise factor is expressed in decibels,

$$\begin{aligned} & -204 \quad (= 10 \log_{10} KT) \\ & + 10 \log_{10} \text{bandwidth in cycles} \\ & + F \\ & \hline & = \text{received noise power in dbw} \end{aligned} \quad (2)$$

#### Channel Signal-to-Noise Ratio

Phase modulation of the carrier caused by r-f noise components on either side of the carrier frequency produce noise components in the baseband output whose frequency equals the frequency separation between the r-f noise component and the carrier and whose voltage is proportional to its frequency. The baseband noise voltage spectrum is triangular, and the signal-to-noise power ratio for any particular band of output frequencies is as follows:

$$S/N = \frac{3W}{2KTF} \frac{D^2}{(f_2^3 - f_1^3)}, \quad (3)$$

where  $W$  = r-m-s carrier input power in watts,

$K$  = Boltzmann's constant =  $1.38 \times 10^{-23}$ ,

$T$  = absolute temperature = 290 degrees Kelvin,

$F$  = effective noise factor,

$D$  = peak frequency deviation in cycles for the channel,

<sup>14</sup>H. V. Cottony and J. R. Johler, "Cosmic Radio Noise Intensities in the VHF Band," *Proc. I.R.E.*, Vol. 40, pp. 1053-1060, September, 1952.

$f_1$  = lowest output frequency in cycles,

$f_2$  = highest output frequency in cycles.

The noise within a channel varies in accordance with the position of the channel in the baseband, being greater for the higher frequency channels. While the noise spectrum within each channel is not flat, the error resulting from the assumption of a flat channel noise spectrum is less than 0.15 decibel providing  $f_2/f_1$  is less than 2, and this condition is fulfilled by any carrier derived telephone channel. It may then be shown that

$$\frac{S}{N} = \frac{W}{2KTFB} \left( \frac{D}{f_m} \right)^2, \quad (4)$$

where  $B = f_2 - f_1$  = width of channel in cycles,

$f_m = (f_1 + f_2)/2$  = mid-frequency of the channel in cycles.

Expressed in decibels, the channel signal-to-noise is

$$S/N = W_r - F + 20 \log_{10} D - 20 \log_{10} f_m + 204 - 10 \log_{10} 2B, \quad (5)$$

where  $W_r$  = carrier input power in dbw.

To adapt this formula to the system design chart, a few modifications are convenient. (1) The bandwidth  $B$  may be fixed at 3000 cycles. (2) The signal-to-noise ratio may be increased by 3 decibels to cover the effect of the F1A telephone weighting network on the channel noise spectrum. (3) The frequency deviation produced by the signal in an individual channel must be less than the maximum frequency deviation of which the system is capable by a channel loading factor which will be discussed later. It is generally more convenient to enter a chart with the maximum frequency deviation and the loading factor than to compute the actual channel frequency deviation. The weighted channel signal-to-noise ratio in decibels for a 3000-cycle telephone channel is then

$$S/N = W_r - F + 20 \log_{10} D_m - L - 20 \log_{10} f_m + 169, \quad (6)$$

where  $L$  = channel loading factor in decibels.

$D_m$  = maximum peak frequency deviation in cycles.

The final constant in Equation (6) takes into account the channel bandwidth and weighting as mentioned above.

*Baseband Signal-to-Noise Ratio*

For some applications the signal-to-noise ratio for the whole baseband should be known. Designating the top baseband frequency as  $f_t$ , Equation (3) may be used for a band of output frequencies extending from zero to  $f_t$ . The baseband signal-to-noise ratio in decibels is then

$$S/N = W_r - F + 20 \log_{10} D_m - 30 \log_{10} f_t + 206, \quad (7)$$

where  $f_t$  = top baseband frequency in cycles.

*Threshold*

For the condition where the peak carrier voltage equals the peak noise voltage in the i-f band, the peak deviation of the resultant becomes very high, the output noise increases rapidly, and the formulas given previously no longer apply. This condition is commonly called the "improvement threshold." In practice, the ratio of peak carrier to peak noise must be about 3 decibels to obtain the normal output signal-to-noise relationship, and from a design standpoint this latter condition may be regarded as a practical threshold. An essential step in the design is to ensure that the margin between the median carrier power and the threshold value is sufficient to allow for the expected fading of the carrier.

The noise power in the i-f band is given by Equation (2). For random noise having a crest factor of 12 decibels, the ratio of peak carrier power to r-m-s noise power must be 15 decibels at the practical threshold, and the r-m-s to r-m-s ratio must be 12 decibels. The ratio of carrier input to practical threshold input is then

$$W_r = F - 10 \log_{10} I + 204 - 12, \quad (8)$$

where  $I$  = i-f bandwidth in cycles.

*System Design Chart*

Equations (1), (6), (7), and (8) provide the relationships for the ten graphs incorporated in the system design chart shown in Figure 8. The graphs are so arranged that they may be followed through consecutively to the final result.

The weighted signal-to-noise ratio for a telephone channel is obtained by the consecutive use of graphs 1, 2, 3, 4, 5, 6, 7 and 8. Baseband signal-to-noise ratio requires the use of graphs 1, 2, 3, 4, 5, 6, 7 and 7A. The carrier-to-threshold margin is obtained from graphs 1, 2, 3, 4, 5 and 5A.

To illustrate the use of the chart, a tracer line is shown for the following set of conditions:

distance .....	85 miles
frequency .....	250 megacycles
attenuation in excess of free space value ....	56 decibels
total net antenna gain .....	66 decibels
transmitter power .....	50 watts
effective noise factor .....	10 decibels
maximum peak frequency deviation .....	500 kilocycles
channel loading factor (referred to maximum deviation) .....	—16 decibels
channel mid-frequency (position in the baseband) .....	250 kilocycles
top frequency of baseband .....	500 kilocycles
i-f bandwidth .....	2000 kilocycles

The signal-to-noise ratio for the particular telephone channel considered is 57 decibels. The baseband signal-to-noise ratio for the entire 500-kilocycle baseband is 47 decibels. The carrier-to-threshold margin is 27 decibels.

It will be obvious that if the desired signal-to-noise ratio and all other factors are known except one (for example the transmitter power) the chart may be entered from both ends to determine the unknown factor.

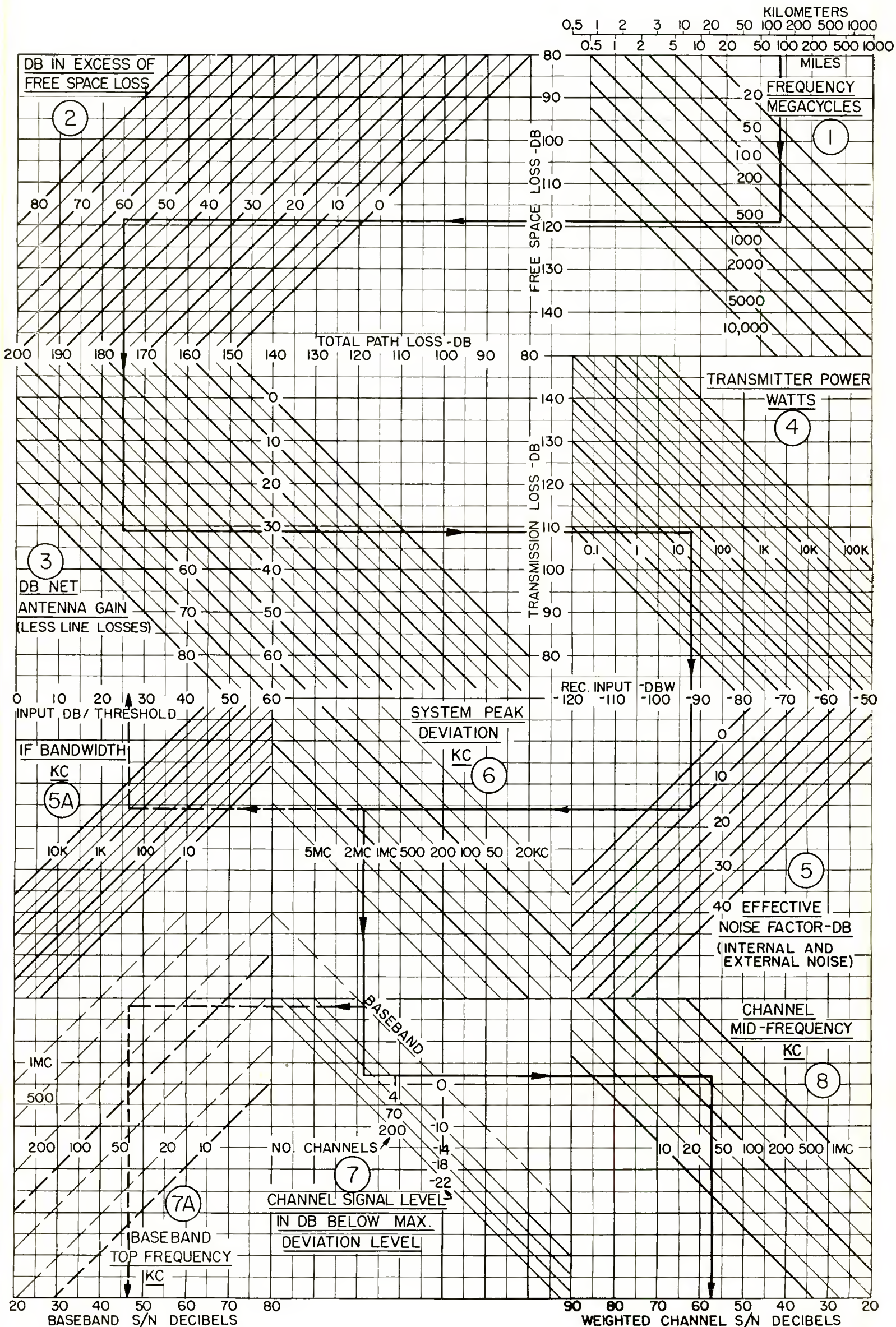
It may be noted also that in the process of following through the graphs certain additional information is obtainable, such as the free-space attenuation between graphs 1 and 2, the total path attenuation between graphs 2 and 3, and the receiver input power between graphs 4 and 5. Should any one of these values be given, the chart may of course be entered directly at that point.

#### *Channel Loading Factor*

To avoid excessive intermodulation, the frequency deviation produced by the signal in any channel must be less than the maximum deviation of which the system is capable by the amount of a suitable loading (or reduction) factor. The factor that is suitable depends upon the distortion characteristics of the equipment and the number of channels. In determining channel signal-to-noise ratio, graph 7 is entered with this factor if it has been established for the particular equipment.

If an appropriate reduction factor has not been established, graph 7 may be entered with the number of channels in the system. The number of channels which are associated with the reduction factors have been taken from Holbrook and Dixon,<sup>15</sup> for channels with peak

<sup>15</sup> B. D. Holbrook and J. T. Dixon, "Load Rating Theory for Multi-Channel Amplifiers," *Bell Sys. Tech. Jour.*, Vol. 18, p. 624, 1939.



A SYSTEM DESIGN CHART FOR FM FREQUENCY DIVISION RADIOTELEPHONE SYSTEMS

GIVES THE WEIGHTED S/N RATIO FOR ANY 3000 CYCLE CHANNEL, THE BASEBAND S/N RATIO, & THE CARRIER-TO-THRESHOLD MARGIN, FOR A SINGLE HOP.

FIG. 8



limiting. It is intended that the channels be so lined up that a 0 dbm\* tone at the hybrid produces the frequency deviation indicated. The signal-to-noise ratio obtained from the chart will be the ratio of this tone to weighted noise. The loading factors are based on the statistical addition of the signals that would be delivered to the channels from a typical telephone switchboard, and the expectancy that excessive intermodulation will not be produced for more than 1 per cent of the time during the busiest hour.

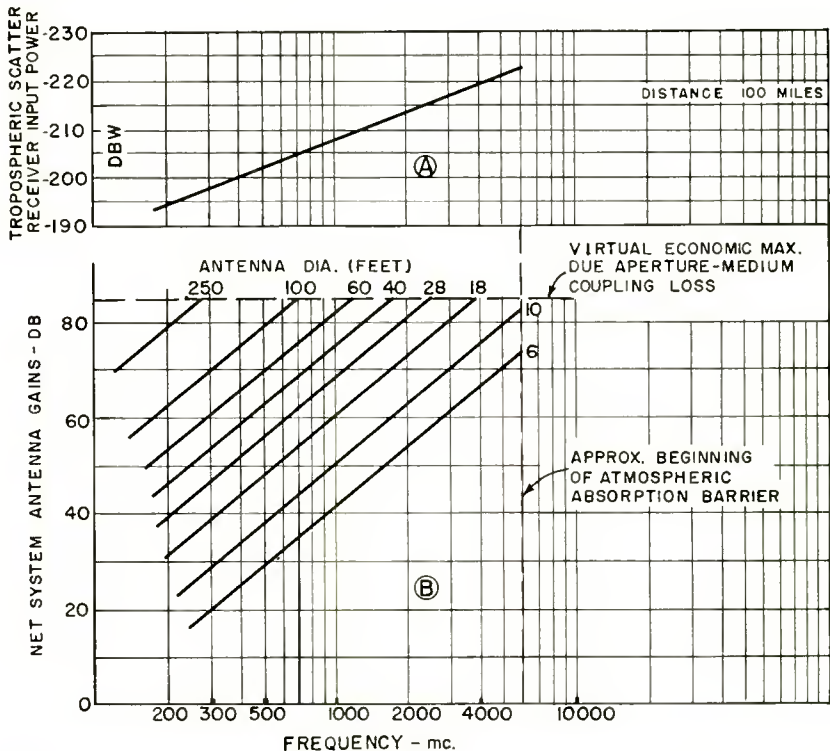


Fig. 9—(A) Receiver input power exceeded 99 per cent of the time at a distance of 100 miles with 1 watt radiated using half-wave dipole antennas. (B) Net system gains between identical ideal paraboloidal antennas including 5-decibel feeder and duplexer loss.

In systems where pre-emphasis is used, the frequency deviation will not be the same for all channels. This can be taken into account in using the chart by introducing the effect of the pre-emphasis characteristic on the channel reduction factor for the particular channel being considered. The baseband signal-to-noise ratio is not directly obtainable in this case.

\* 0 dbm = 1 milliwatt.

### III. TROPOSPHERIC SCATTER PROPAGATION

The system engineer now has four major techniques that he may use for point-to-point microwave systems—radio-optical, quasi-optical, obstacle-gain and tropospheric forward-scatter propagation. The nature, scope, traffic, geography, frequency, economics, and many other factors determine whether any or all of these tools will best fit the needs of any given path.

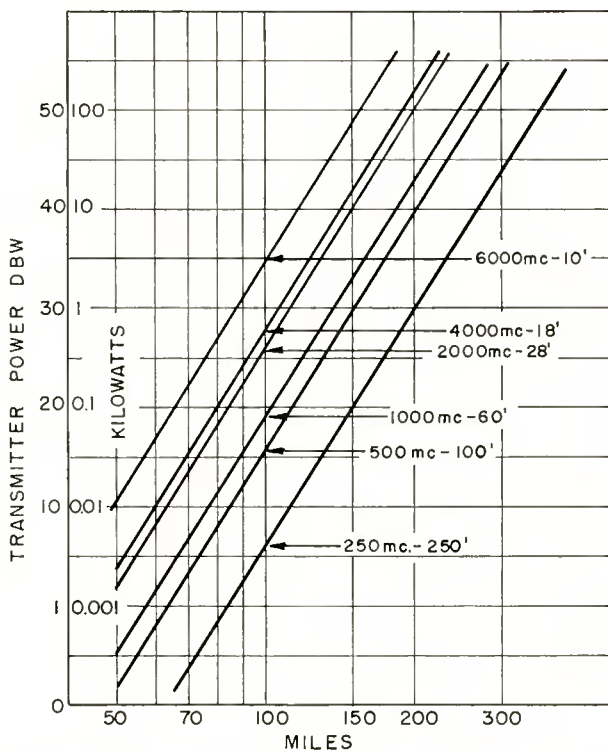


Fig. 10—Transmitter power versus distance and frequency using highest feasible antenna gains for one path of a long-haul 24-channel telephone system using the following parameters: 60 decibels 99 per cent of the time; FM deviation 600 kilocycles; i-f bandwidth 3000 kilocycles; bandwidth 120 kilocycles; noise factor 10 decibels; received power  $-97$  dbw; margin 20 decibels; diversity gain 10 decibels; antenna diameters shown in feet.

The data for forward-scatter propagation can now be combined with the design data for FM systems to predict the major parameters for their practical utilization.

One immediate attraction of scatter propagation is that it appears, up to this time, not to require exacting preliminary path surveying as do the other three techniques. When clear horizons are obtainable

in the direction of the other terminal (and this is essential), the physical profile of the path in the shadowed portion is not important. Stations can usually be located more conveniently for access and power supply because great height is not needed except as a way to get a low radio horizon. What is wanted is transmission and reception at angles as low as possible.

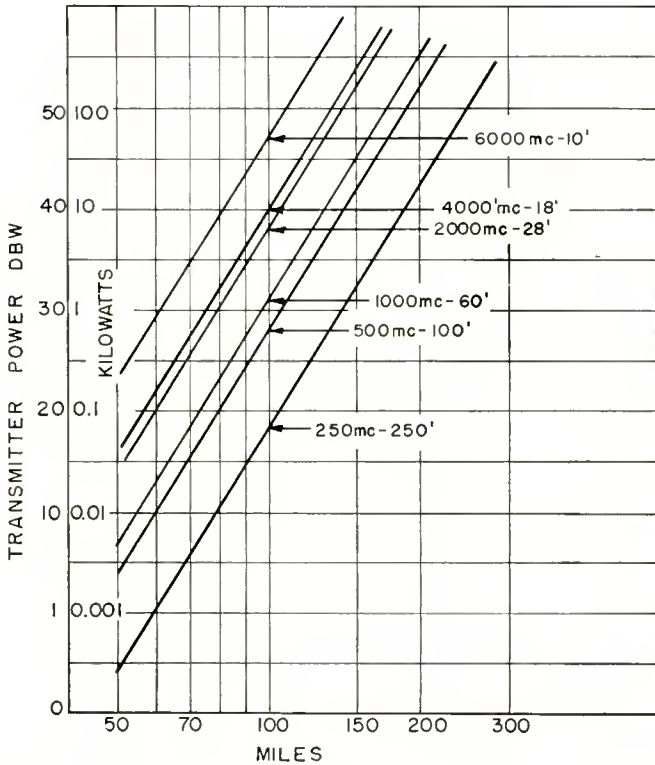


Fig. 11—Transmitter power versus distance and frequency using highest feasible antenna gains for one path of a long-haul 100-channel telephone system using the following parameters: 60 decibels 99 per cent of the time; FM deviation 600 kilocycles; i-f bandwidth 3000 kilocycles; bandwidth 420 kilocycles; noise factor 10 decibels; received power —85 dbw; fading margin 33 decibels; diversity gain 10 decibels.

A system using scatter propagation may be a simple path, or one of several paths in a radio relay system. The design of each path is dependent upon the desired system performance in terms of reliability and signal-to-noise ratio (S/N) for each communication channel. Naturally, the demands on the performance of each path increase as the number of paths in series is increased. The system engineer

encounters such a variety of requirements and conditions that each must make his own allowances for individual path performance in relation to the desired system performance.

*Charts of Power-Distance-Frequency Relations  
For Scatter-Propagation Paths*

As a guide to the utilization of scatter propagation the foregoing general information is now applied to particular systems. Computations of the power needed for various traffic capacities, reliability and quality of service are shown in Figures 10 to 16 inclusive as functions

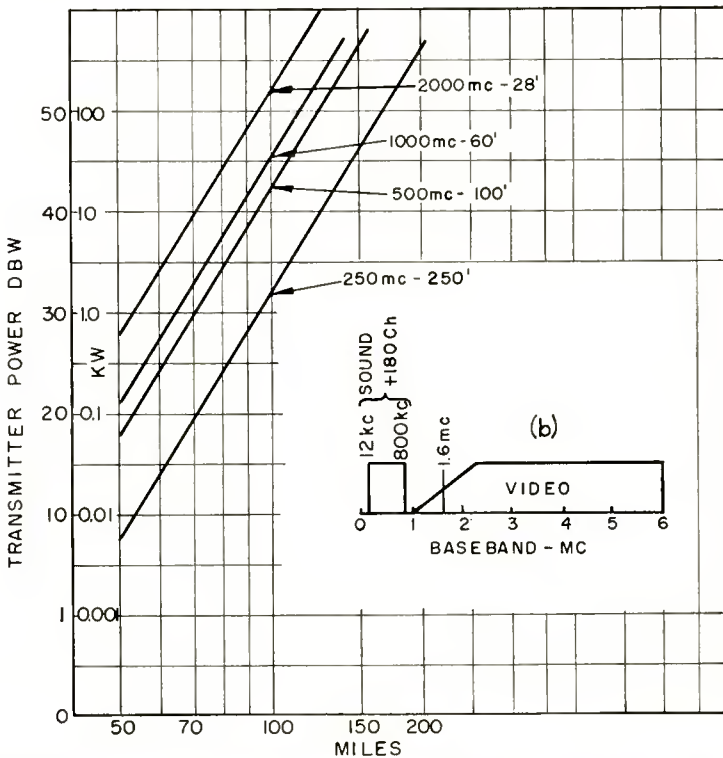


Fig. 12—Transmitter power versus distance and frequency using highest feasible antenna gains for one path of a long-haul system for (a) 400-channel telephone system using the following parameters: 60 decibels 99 per cent of the time; FM deviation 1000 kilocycles; i-f bandwidth 5000 kilocycles; bandwidth 1600 kilocycles; noise factor 10 decibels; margin 46 decibels; received power —71 dbw; diversity gain 10 decibels. The same power requirements apply for (b) television video and sound (AM-double sideband 12-42 kilocycles) plus 180 telephone channels (single sideband 60-780 kilocycles) with the following parameters: video signal-to-noise ratio 45 decibels 99 per cent of the time; telephone and sound channels signal-to-noise ratio greater than 60 decibels; received power —70 dbw; diversity gain 10 decibels; deviation 8 megacycles; i-f bandwidth 20 megacycles; margin 37 decibels.

of frequency and antenna diameter in feet. The system parameters are given with each chart. The computations were based on the conditions stated below.

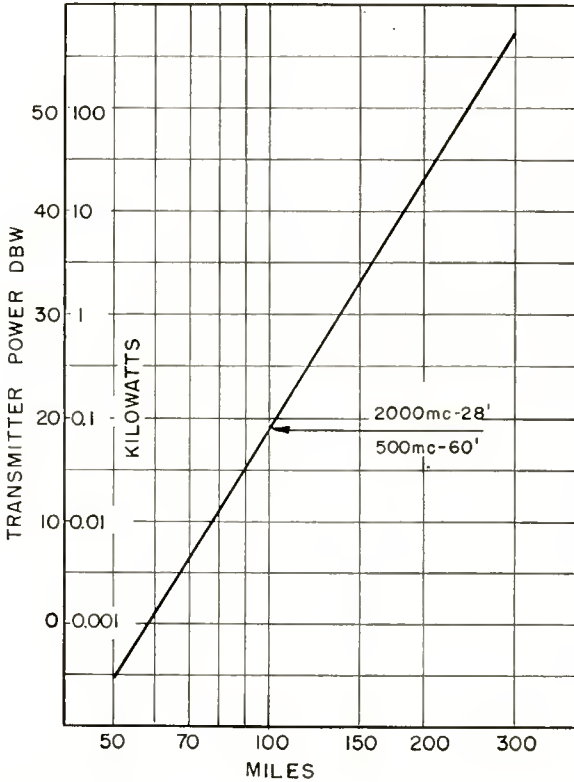


Fig. 13—Transmitter power versus distance for a single-path television video system using highest feasible antenna gains at 500 and 2000 megacycles using the following parameters: signal-to-noise ratio 28 decibels 99 per cent of the time; FM deviation 5 megacycles; i-f bandwidth 12 megacycles; bandwidth 4.5 megacycles; noise factor 10 decibels; received power -104 dbw; diversity gain 10 decibels.

*Path Losses*

The following propagation losses were used:

1) **Scatter loss**

<i>Distance in statute miles</i>	<i>Median scatter loss relative to free space in decibels</i>	(Figure 2)
50	42	
100	60	
200	78	
300	88	

2) **Total path loss** is frequency-dependent. Free-space dipole-to-dipole path loss is read from graph 1 of Figure 8, or computed from Equation (1), page 443.

3) **Downward fading of 15 decibels** was allowed in converting from these median scatter losses to the values for 99 per cent of the time. Reliance is placed on the fading margin of the FM receiver for

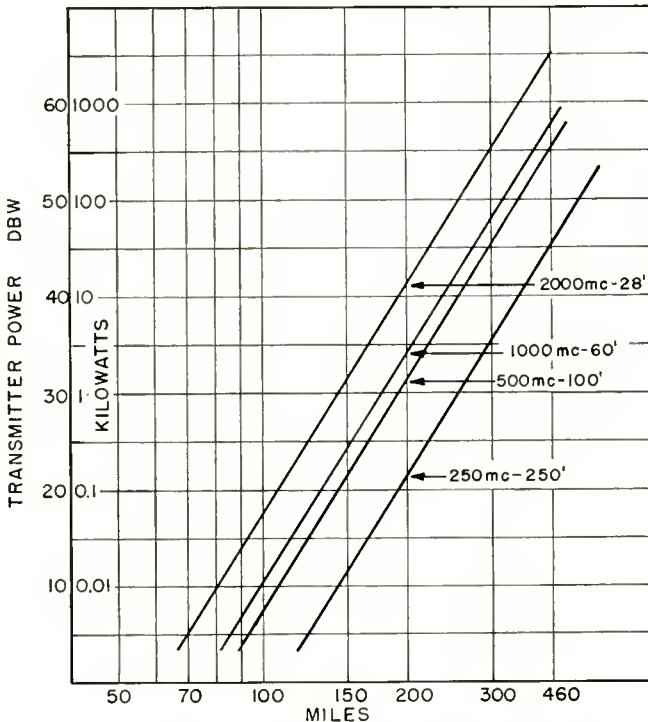


Fig. 14—Transmitter power versus distance and frequency for a one-path link for one high-fidelity (15 kilocycles) broadcast program, using highest feasible antenna gains, using the following parameters: FCC FM broadcast standards; signal-to-noise ratio 60 decibels 99 per cent of the time; received power  $-116$  dbw; noise factor 10 decibels; diversity gain 10 decibels.

1 per cent of the time only during the worst months to obtain reliability for more than 99 per cent of the time. The signal-to-noise ratio falls below the stated value during this 1 per cent of the time, unless space diversity is used.

The total path loss comprising these three factors for a distance of 100 miles is shown as a function of frequency in Figure 9A. The variation of power with distance is 24 decibels per doubling of distance.

In the examples, 5 decibels is also included for the total feeder and duplexer losses.

*Gains*

The net system gains are as follows:

**Antenna gain.** Figure 9B indicates the net system gains between identical paraboloidal antennas including the 5-decibel feeder and

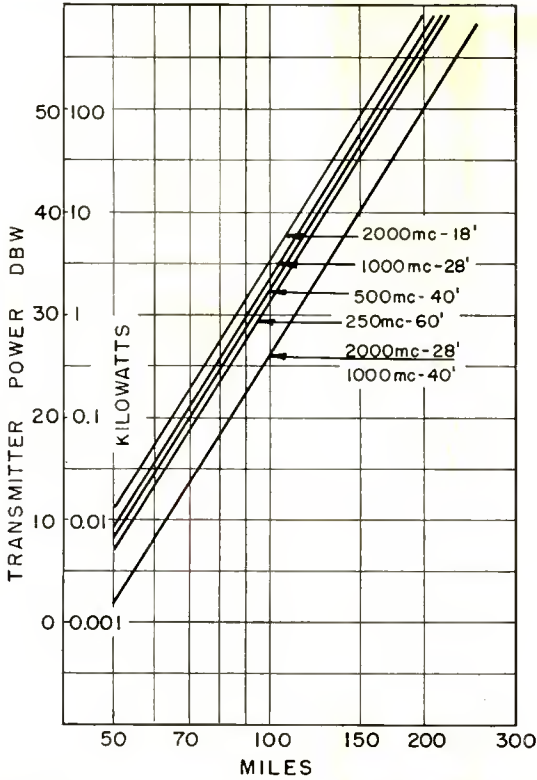


Fig. 15—Transmitter power versus distance and frequency for economical 1-path 12-channel telephone systems without diversity reception, using the following parameters: signal-to-noise ratio 50 decibels 50 per cent of the time; FM deviation 250 kilocycles; i-f bandwidth 750 kilocycles; noise factor 10 decibels; margin 17 decibels; received power  $-107$  dbw; no diversity gain.

duplexer losses. The maximum economic net system gain is limited to about 82 decibels due to the aperture-medium coupling loss. In the examples shown in Figures 10 to 14 inclusive, identical antennas with the highest feasible gains are assumed at each end of the circuit.

**Space diversity**, when used, is assumed to provide an average power gain of 10 decibels.

The value for the signal-to-noise ratio is based on the factors explained in connection with Figure 8, corresponding to established telephone measuring techniques. It is the value for the highest 3-kilocycle channel in a frequency-division single-sideband multiplexed modulating system. For lower channels, the ratio increases 6 decibels per octave. Therefore the lowest frequency channels usually are used for the longest distances, and the higher channels for shorter distance "drop" channels, although on scatter paths this condition may not always prevail.

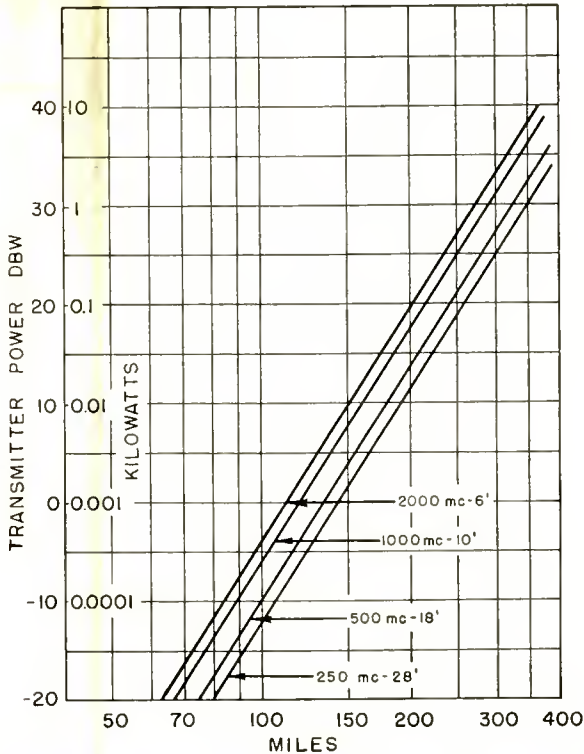


Fig. 16—Transmitter power versus distance and frequency for 1-path 60-words-per-minute frequency-shift teleprinter systems using economical antenna sizes with diversity reception, and following parameters: signal-to-noise ratio 10 decibels 99.9 per cent of time; frequency shift  $\pm 200$  cycles; i-f bandwidth 1000 cycles; received power  $-164$  dbw; diversity gain 10 decibels.

The noise factor used makes no allowance for external noise. A reference value of 10 decibels above the value for an ideal receiver has been used; receiver noise factors higher or lower than 10 decibels will require correspondingly higher or lower transmitter power.

The frequency-modulation parameters used are arbitrary, but

correspond to good balances between spectrum usage, FM improvement and fading margin. The i-f bandwidths are those found desirable to allow system bandwidth for maintaining lowest crosstalk levels. This assumes that all other elements throughout the system are not too selective. In Figure 12, television video signals are also shown transmitted on a vestigial sideband basis, displaced in frequency so that the sound channel, and a block of telephone channels occupy the lower 1 megacycle of the baseband. The required signal-to-noise ratios are best realized this way in an FM system.



Fig. 17—Paraboloid antenna 40 feet in diameter at radiation laboratory on Covey Hill, Quebec, completed in May 1954.

#### ACKNOWLEDGMENT

The unpublished scatter propagation measurements used in this paper are based mainly on the work of H. O. Peterson, G. S. Wickizer, and A. M. Braaten of RCA Laboratories, Riverhead, N. Y. Helpful suggestions and comments were also contributed by J. B. Coleman and H. R. Mathwich of RCA, Camden. G. B. MacKimmie of the RCA Victor Company, Ltd., Montreal, did the electrical design work, and H. Buzzell, of the Dominion Bridge Company, Ltd., did the mechanical design work for the antenna shown in Figure 17.

# EXTENSION OF "THE EFFECT OF INITIAL NOISE CURRENT AND VELOCITY CORRELATION ON THE NOISE FIGURE OF TRAVELING-WAVE TUBES"

BY

W. R. BEAM

Research Laboratory, RCA Laboratories,  
Princeton, N. J.

*Editor's Note:* This material is, as the title states, an extension of the paper which appeared in the June 1955 issue of *RCA Review*.

IN Bloom's recently published article<sup>1</sup> on the effects of correlation of current and velocity fluctuations at a potential minimum of an electron gun, the fluctuations were assumed to originate from three independent (uncorrelated) sources: (1) current fluctuations, (2) velocity fluctuations, (3) directly proportional (positively correlated) current and velocity fluctuations.

It should be pointed out that for completeness, it is necessary to allow the correlation of current and velocity fluctuations of the third wave to have an arbitrary phase relation. It is also desirable to allow the correlated parts of the total mean-square current and velocity to be different fractions of the total, and to express the correlation and non-correlation of the various quantities in a more rigorous fashion.

In accordance with the above, Equation (1) of Bloom's paper is replaced by

$$\begin{aligned}
 \overline{I_{(1)}^2(a)} &= 0, & \overline{V_{(1)}^2(a)} &= (1 - |\kappa_1|^2) \overline{V_a^2}, \\
 \overline{I_{(2)}^2(a)} &= (1 - |\kappa_2|^2) \overline{I_a^2}, & \overline{V_{(2)}^2(a)} &= 0, \\
 \overline{I_{(3)}^2(a)} &= |\kappa_2|^2 \overline{I_a^2}, & \overline{V_{(3)}^2(a)} &= |\kappa_1|^2 \overline{V_a^2}, \\
 I_{(3)}(a) &\equiv V_{(3)}(a) \frac{\kappa_2}{\kappa_1} \sqrt{\frac{\overline{I_a^2}}{\overline{V_a^2}}}.
 \end{aligned} \tag{1}$$

where  $|\kappa_1|^2 \leq 1$ ,  $|\kappa_2|^2 \leq 1$ ,

$$\begin{aligned}
 \overline{V_{(1)}(a) I_{(2)}(a)} &= \overline{V_{(1)}(a) I_{(2)}^*(a)} = \overline{V_{(1)}(a) I_{(3)}(a)} \\
 &= \overline{V_{(1)}(a) I_{(3)}^*(a)} = 0
 \end{aligned}$$

<sup>1</sup> S. Bloom, "The Effect of Initial Noise Current and Velocity Correlation on the Noise Figure of Traveling-Wave Tubes," *RCA Review*, Vol. XVI, pp. 179-196, June, 1955.

The bar indicates mean value, and the quantities involved are narrow-band a-c values, hence the bottom line indicates the absence of correlation between  $V_{(1)}$ ,  $I_{(2)}$  and  $I_{(3)}$ .

Under these assumptions, Equations (2) thru (10) of Bloom's paper retain their form, but Equation (11) becomes

$$W^2 |I_{\max}|^2 |I_{\min}|^2 = \overline{V_a^2} \overline{I_a^2} (1 - 1/4 [\kappa_1 \kappa_2^* - \kappa_1^* \kappa_2]^2). \quad (2)$$

Equations (12) and (13) are correct as written, but now apply to the case  $|\kappa_1| = |\kappa_2| = 1$ . Bloom's quantities  $P_R(a)$  and  $P_X(a)$  become

$$P_R(a) = \frac{\sqrt{\overline{V_a^2} \overline{I_a^2}}}{2} (\kappa_1 \kappa_2^* + \kappa_1^* \kappa_2), \quad (3)$$

$$P_X(a) = \frac{j}{2} \sqrt{\overline{V_a^2} \overline{I_a^2}} (\kappa_1 \kappa_2^* - \kappa_1^* \kappa_2). \quad (4)$$

The minimization of noise figure is not altered by the new choice of parameters, and Equations (28) for minimum noise figure remains correct. If Equations (2), (3), and (4), as given here are substituted,

$$F_{\min} = 1 + \sqrt{\overline{V_a^2} \overline{I_a^2}} \left( \frac{\sqrt{4QCf_a f_i}}{KT \Delta f} \right) \left[ \sqrt{1 - 1/4 [\kappa_1 \kappa_2^* - \kappa_1^* \kappa_2]^2} - 1/2 (\kappa_1 \kappa_2^* + \kappa_1^* \kappa_2) \right] \quad (5)$$

Since only the angle  $\theta$  between  $\kappa_1$  and  $\kappa_2$  is of importance, we can assume  $\kappa_1$  real. Then  $\kappa_2 = |\kappa_2| e^{j\theta} = |\kappa_2| (\cos \theta + j \sin \theta)$ , and Equation (5) reduces to

$$F_{\min} = 1 + \sqrt{\overline{V_a^2} \overline{I_a^2}} \left( \frac{\sqrt{4QCf_a f_i}}{KT \Delta f} \right) \left[ \sqrt{1 - |\kappa_1 \kappa_2|^2 \sin^2 \theta} - |\kappa_1 \kappa_2| \cos \theta \right] \quad (6)$$

A rather interesting method of plotting this result was suggested by R. W. Peter. The construction is shown in Figure 1 and the resulting family of curves in Figure 2. The  $|\kappa_1 \kappa_2|$  and  $\theta$ -dependent factor in Equation (6) may be found by drawing a line from point A to point C, at the intersection of the proper  $|\kappa_1 \kappa_2|$  and  $\theta$  circles. If the length of

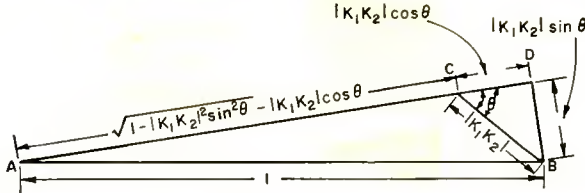


Fig. 1—Geometrical construction for the correlation-dependent factor in  $F_{min}$ .

AB is unity, AC will equal the bracketed factor of Equation (6). Several interesting results of the theory are readily observed:

1. Minimum noise figure is unity for  $-90^\circ \leq \theta \leq +90^\circ$ , and corresponds to full correlation.
2. Full correlation for  $|\theta| > 90^\circ$  results in greater than unity noise figure. At  $\theta = 180^\circ$ , best noise figure is obtained with no correlation.
3. With  $\theta = 90^\circ$  (quadrature correlation), although there is no real noise power in the beam, noise figure varies with  $|\kappa_1 \kappa_2|$  in much the same way as at  $\theta = 0$ .

Aside from the equations mentioned, the changes in variables and notation made herein do not explicitly affect other results in Bloom's paper.

The author wishes to thank R. W. Peter for suggesting the graphical construction of Figures 1 and 2, and R. C. Knechtli, for the discussion which led to this extension. It is also recognized that the treatment of H. A. Haus<sup>2</sup> contains implicitly these same considerations, but since the formalism of Bloom is widely known and understood, the author felt justified in presenting this extension.

$$F_{min} - 1 = \frac{\sqrt{V_a^2 I_a^2}}{KT\Delta f} \sqrt{40Cf_0 f_i} g(K_1 K_2, \theta)$$

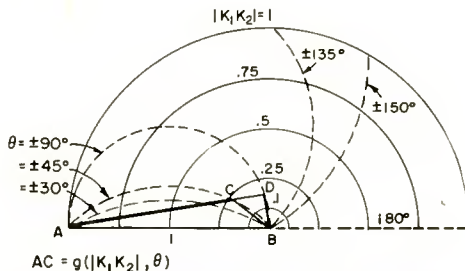


Fig. 2—The correlation-dependent factor in  $F_{min}$  as a function of  $|\kappa_1 \kappa_2|$  and  $\theta$ .

<sup>2</sup> H. A. Haus, "Noise in One-Dimensional Electron Beams," *Jour. Appl. Phys.*, Vol. 26, pp. 560-571, May, 1955.

# ON THE PROBLEM OF OPTIMUM DETECTION OF PULSED SIGNALS IN NOISE\*

BY

A. H. BENNER AND R. F. DRENICK

Engineering Products Division, Radio Corporation of America,  
Camden, N. J.

*Summary*—A detection philosophy is introduced which distinguishes only the presence or absence of a pulsed signal, avoiding the designation of signal location. This so-called interval detector is formulated statistically as a composite hypothesis problem and solved by decision function theory. The optimum decision rule is derived, its superiority in principle to others is proven, and an illustrative mechanization is described. The explicit evaluation of this optimum relative to other detection procedures has been achieved only in special border cases, one of which is included as an example.

## INTRODUCTION

A RECENT series of papers<sup>1-3</sup> dealt with the detection of pulsed signals in noise and apparently treated the problem in a rather exhaustive manner. It is possible, however, to develop an interesting variant on the usual approach and arrive at some new, and at least in principle, better results. This variant arises through the following reasoning. "Detection of a pulsed signal" customarily refers to a statistical decision which establishes the presence or absence of a signal at a specific point of, say, a radar sweep. That is to say, if the decision is negative the presence of a signal is ruled out. If it is positive, it establishes not only the presence but also the location of the signal pulse along the sweep. Statistically, this is a legitimate formulation of the problem.

The new variant arises through the following reasoning. Operationally, the question concerning the presence or absence of a signal often is not coupled with the question concerning the location of the pulse. In fact, the latter is usually irrelevant when it comes to mere detection. In this case the decision to be made is simply whether the

---

\* Decimal Classification: R116.

<sup>1</sup> J. Marcum, "A Statistical Theory of Target Detection by Pulsed Radar," Rand Corporation Report, December, 1947 (unclassified).

<sup>2</sup> D. Middleton, "Statistical Criteria for the Detection of Pulsed Carriers in Noise I, II," *Jour. Appl. Phys.*, Vol. 24, pp. 371-391, April, 1953.

<sup>3</sup> T. G. Slattery, "The Detection of a Sine Wave in the Presence of Noise by the Use of a Nonlinear Filter," *Proc. I.R.E.*, Vol. 40, pp. 1232-1236, October, 1952.

signal pulse is present or absent somewhere in a given surveillance area. The question of location is secondary and can be taken up subsequently and independently. Intuitively, one could expect that to make a decision concerning the mere presence or absence of a signal, regardless of its location, is simpler than the decision involved in the conventional detection process, and that it can accordingly be carried out more efficiently.

The present paper demonstrates the superiority, in principle, of a certain signal-detection scheme of the above sort. This is an optimum scheme, derived by purely theoretical statistical considerations, which runs counter to the intuition of some communications engineers. Signal-detection probabilities to which the optimum procedure leads are apparently only slightly greater than those achieved by other reasonably competitive schemes. Actually, its superiority may easily be lost in the engineering compromises which are always necessary in reducing such schemes to practice. Some scheme resembling the optimum derived here may also be attractive for reasons other than performance: say, for simplicity of mechanization. It is important to know in such a case that performance need not be sacrificed, and that in fact some gain may be achieved.

It will be assumed that detection of a pulse somewhere in a video sweep interval is desired, but that its location is irrelevant. The extension to larger areas of indifference will be quite clear. This process will be referred to as "interval" detection, as distinguished from the conventional "point" detection. Only nonsequential decision processes will be considered; these will be compared on the basis of the detection probabilities to which they lead.

The paper is organized as follows: The interval-detection problem is first formulated, and a solution is derived which is closely related to the minimax solution. The special case of detection of a pulsed signal in video noise is then discussed, is contrasted with the conventional point-detection method, and an illustrative mechanization is suggested. An example is introduced which demonstrates the theoretical superiority of the interval-detection process

#### FORMULATION OF THE INTERVAL-DETECTION PROBLEM

It is assumed here, as it was in References (1)-(3), that the decision concerning the presence or absence of a signal pulse is to be made on the basis of a record of  $n$  successive sweeps of video voltages, all of which contain the signal if it is present. It is also assumed that the record of each sweep consists of  $N$  successive voltage measure-

ments which yield the values  $v_{jk}$  ( $j = 1, 2, \dots, n; k = 1, 2, \dots, N$ ). For simplicity of presentation, a further assumption is made, namely, that the measurements are spaced a pulse width apart; therefore, one and only one voltage measurement in each sweep will contain a record of the signal (if it is present). Finally, it should be mentioned that, in order to retain the parallel to the radar problem, the signal pulse, if it occurs, is assumed to have the same location in all  $n$  sweeps. That is to say, if the  $i^{\text{th}}$  measurement in sweep 1 strikes a signal, the same will be true of the corresponding measurements in all succeeding sweeps.

The joint probability density of the voltages measured if no signal is present is denoted

$$P_o = P_o(v_{11}, v_{12}, \dots, v_{nN})$$

The corresponding density if a signal pulse is present at the location  $i$  in each sweep is

$$P_i = P_i(v_{11}, v_{12}, \dots, v_{nN})$$

For the moment, these probability densities will be left unspecified and the solution will be derived at this level of generality. Later, certain specializations will be introduced.

The statistical decision problem to be solved is, then, that of deciding, on the basis of a specific set of measured voltages,  $v_{jk}$ , whether  $P_o$  is their true distribution, or (since the signal pulse location is irrelevant) whether it is one of the  $P_i$ .

#### STATISTICAL SOLUTION OF THE PROBLEM

The problem of interval detection, in statistical terminology, is a problem of hypothesis testing. However, since the hypothesis of "no signal" is to be tested against  $N$  alternatives, the problem deals with what is called a composite hypothesis. This fact differentiates it from the conventional point-detection problem which deals with a simple hypothesis and for whose solution a well-known and very general method exists, namely, the Neyman-Pearson<sup>4</sup> lemma.

The corresponding solution to the composite hypothesis problem is apparently not as widely known. In this section it will be derived using a line of reasoning which is essentially the same as that em-

<sup>4</sup>J. Neyman and E. S. Pearson, "On the Problem of the Most Efficient Tests of Statistical Hypotheses," *Roy. Soc. Phil. Trans.*, Vol. A231, p. 289, 1933.

ployed by Lehmann and Stein<sup>5</sup>, and by A. Wald<sup>6</sup> in his decision function theory. Their argument, in the terminology of the communications problems under consideration, might run roughly as follows: One assumes first that a set of (a priori) probabilities  $\xi_1, \xi_2, \dots, \xi_n$  is given with which the signal will occur at locations 1, 2,  $\dots, n$ , if it occurs at all. A solution is then derived under that assumption. As will be shown presently, the detection rule which should in this case be adopted is the following: A signal should be declared present after the voltages  $v_{jk}$  have been observed if

$$\lambda P_o (v_{11}, v_{12}, \dots, v_{nN}) \leq \sum_{i=1}^N \xi_i P_i (v_{11}, v_{12}, \dots, v_{nN}) \quad (1)$$

where  $\lambda$  is a constant which is to be determined from the desired false-alarm probability. This detection rule has the disadvantage that the detection probability will in general vary with the location  $i$  of the signal. But it is optimum in the sense that the mean of these local detection probabilities,  $P_{Di}$ , over all locations is maximized.

In practice, however, the a-priori probabilities  $\xi_i$  often will not be given, as has just been assumed, or it will seem altogether artificial and unconvincing to construct them for the mere benefit of such a solution. When this is the case, the method of solution employed above is not patently useful because it rests on such a-priori knowledge; nor is the basis of comparison applicable, because one cannot compute the mean of the detection probabilities. One can, however, salvage the situation by an argument due to A. Wald. He recommends the determination of a special set of a-priori probabilities which will be denoted by  $\xi_i^*$  below, and which lead to an optimal decision rule. This rule is optimum in the sense that the local detection probabilities to which it leads are greater at one location at least, than can be achieved by any other decision rule. One finds in this case a rule very similar to Equation (1), namely,

$$\lambda^* P_o (v_{11}, v_{12}, \dots, v_{nN}) \leq \sum_{i=1}^N P_i (v_{11}, v_{12}, \dots, v_{nN}).$$

The first solution, that is Equation (1), is closely related to what, in the terminology of decision theory, is called the Bayes solution to the present detection problem. The second corresponds to the so-called minimax solution.

<sup>5</sup> E. L. Lehmann and C. Stein, "Most Powerful Tests of Composite Hypothesis I," *Ann. Math. Stat.*, Vol. 19, p. 495, 1948.

<sup>6</sup> A. Wald, "Statistical Decision Functions," John Wiley & Sons, Inc., New York, N. Y., 1950.

## PROOF OF OPTIMIZATION

The above outline of reasoning will now be substantiated on a level of appropriate generality. First, it must be shown that the decision rule (1) is in fact optimum when the set of a-priori probabilities  $\xi_i$  is given, that is to say that it leads to a mean detection probability which cannot be exceeded by any other rule. To understand this, it is well to imagine a sample of space ( $nN$ ) dimensions, spanned by the variables  $v_{jk}$ . In this space the inequality (1) defines a region which shall be denoted by  $w$ . Any other competitive detection rule will define another such region, say  $w'$ . Both are characterized by the fact that a signal is declared present if the point represented by the observed voltages  $v_{jk}$  falls into that region.

These competitive rules will be put on the same footing by requiring that they lead to the same false-alarm probabilities  $P_{FA}$ . This is conveniently expressed by the equation

$$P_{FA} = \int_w P_o(v) dv = \int_{w'} P_o(v) dv$$

where  $v$  has been written generically for all variables  $v_{jk}$ . The rule (1) will be regarded as the better of the two if, as mentioned above, the mean detection probability to which it leads, namely,

$$\overline{P_D} = \sum_{i=1}^N \xi_i P_{Di} = \sum_{i=1}^N \xi_i \int P_i(v) dv, \quad \sum_{i=1}^N \xi_i = 1$$

is greater than that of its competitor

$$\overline{P_D'} = \sum_{i=1}^N \xi_i \int_{w'} P_i(v) dv.$$

The superiority in this sense of (1) can be shown by an argument used by Neyman and Pearson.<sup>4</sup> Denote with  $w''$  the region (if any) which is common to  $w$  and  $w'$ . Then,

$$\begin{aligned} \int_{w-w''} P_o(v) dv &= \int_w P_o(v) dv - \int_{w''} P_o(v) dv = P_{FA} - \int_{w''} P_o(v) dv \\ &= \int_{w'-w''} P_o(v) dv. \end{aligned} \quad (2)$$

Using (1) and (2), one has similarly

$$\begin{aligned} \sum_{i=1}^N \xi_i \int_{w-w''} P_i(v) dv &\geq \lambda \int_{w-w''} P_o(v) dv \\ &= \lambda \int_{w'-w''} P_o(v) dv > \sum_{i=1}^N \xi_i \int_{w'-w''} P_i(v) dv. \end{aligned} \quad (3)$$

The latter inequality is true because the region  $w'-w''$  lies wholly outside the region  $w$  so that

$$\lambda P_o(v) > \sum_{i=1}^N \xi_i P_i(v) \quad \text{in } (w'-w'')$$

One can now add  $\sum_{i=1}^N \xi_i \int_{w''} P_i(v) dv$  to both sides of the inequality (3) and obtain

$$\sum_{i=1}^N \xi_i \int_w P_i(v) dv > \sum_{i=1}^N \xi_i \int_{w'} P_i(v) dv \quad (4)$$

This proves that the decision rule (1) is superior to any other that can be conceived, in the case in which a-priori probabilities  $\xi_i$  are given or can be assumed.

The question remains of what to do when an a-priori knowledge of that nature cannot be safely assumed. As has been mentioned earlier, one can utilize some of the above results if one can find a special set of a-priori probabilities, say,  $\xi_i^*$ . This set will now be introduced, but it will as a matter of convenience, be defined through a certain property which it has.

The decision rule (1), and hence also the region  $w$  in the sample space of the voltages  $v_{jk}$ , depends on the choice of the probabilities  $\xi_i$ . The same is true of the special set of these probabilities, namely,  $\xi_i^*$ , and their corresponding region  $w^*$ . They will be defined here by the requirement that the local detection probabilities to which they lead, namely,

$$P_{Di}^* = \int_{w^*} P_i(v) dv.$$

should be independent of location  $i$ . That is,

$$P_{Di}^* = P_D^* \tag{5}$$

The question of how the  $\xi_i^*$  can be found will be disregarded for the moment. First, it will be shown that they actually have the desired property, namely, that any other set  $\xi_i$  will lead to local detection probabilities  $P_{Di}$  at least one of which is lower than the constant detection probability  $P_D^*$  due to  $\xi_i^*$ . More specifically,

$$P_D^* \cong \inf_i P_{Di} \tag{6}$$

In fact, utilizing (4)

$$P_D^* - \inf_i P_{Di} = (P_D^* - \inf_i P_{Di}) \sum_{i=1}^N \xi_i^* = \sum_{i=1}^N \xi_i^* \left[ \int_{w^*} P_i(v) dv - \inf_i \int_w P_i(v) dv \right] > 0$$

which bears out (6).

Therefore, if one can find such a set  $\xi_i^*$ , the detection probability  $P_D^*$  based on this set will be greater in at least one location than the detection probability obtainable from any other set  $\xi_i$ . It is in this sense an optimum set.

The determination of the set  $\xi_i^*$  is not difficult in the present case if one can assume that  $P_o(v)$  and  $P_i(v)$  are symmetrical in the variables  $v_{jk}$ . When this is true, the set

$$\xi_i^* = 1/N \tag{7}$$

clearly satisfies the requirement (5). In fact, not only are the local detection probabilities equal, as was prescribed, but their mean  $\overline{P_D}$ , which was used as a basis of comparison for the case of a-priori known  $\xi_i$ , becomes also equal to the local probabilities:

$$\overline{P_D^*} = \sum_{i=1}^N \xi_i^* P_{Di}^* = P_D^*$$

It can be concluded, therefore, that the decision rule (1) should, in the absence of a-priori information concerning the location of the signal, be modified according to (7). That is to say, a signal should be declared present when

$$\lambda^* P_o (v_{11}, v_{12}, \dots v_{nN}) \leq \sum_{i=1}^N P_i (v_{11}, v_{12}, \dots v_{nN}), \quad (\lambda^* = N\lambda) \quad (8)$$

If this detection rule is adopted, the detection probability will be greater, at least at one possible signal location, than can be achieved by any other detection rule for given false-alarm probability. This result holds under quite general conditions. It is, in particular, rather independent of the nature and interpretation of the variables  $v_{jk}$  and their distributions  $P_o$  and  $P_i$ , a fact which will be utilized in a special example below, and which has also been made use of in another study.<sup>7</sup>

APPLICATION TO PULSED-SIGNAL DETECTION

The problem under consideration, namely the detection of signal pulses in video noise is complicated by the fact (among others) that no closed expressions have so far been found<sup>8</sup> for  $P_o$  and  $P_i$ . Accordingly, a mathematical model which is a considerable simplification over the true situation, yet retains the main features of the problem, will be constructed.

Thus, it is first assumed that the statistical dependence between the voltages measured at adjacent locations is small enough to be negligible. The probability density of the individual video voltages  $v_{jk}$  is then

$$f_o (v_{jk}) = v_{jk} \exp\left(-\frac{v_{jk}^2}{2}\right)$$

if there is no signal present, and

$$f_s (v_{jk}) = v_{jk} \exp\left(-\frac{a^2 + v_{jk}^2}{2}\right) I_o (a v_{jk})$$

if a signal is present.  $I_o$  is the Bessel function of imaginary argument and zero order. Therefore, in the notation of the preceding,

$$P_o (v_{11}, v_{12}, \dots v_{nN}) = \prod_{j=1}^n \prod_{k=1}^N v_{jk} \exp\left(-\frac{v_{jk}^2}{2}\right)$$

<sup>7</sup> R. Drenick, S. Gartenhaus, and P. Nesbeda, "Coherent and Non-Coherent Detection of Signals in Noise," *Conv. Record I.R.E.*, 1955, to be published.

<sup>8</sup> W. C. Hoffman, "Joint Distribution of  $n$  Successive Outputs of a Linear Detector," *Jour. Appl. Phys.*, Vol. 25, August, 1954.

$$P_i(v_{11}, v_{12}, \dots, v_{nN}) = \exp\left(-\frac{na^2}{2}\right) \prod_{j=1}^n I_0(av_{ji}) \prod_{k=1}^N \prod_{j=1}^n v_{jk} \exp\left(-\frac{v_{jk}^2}{2}\right).$$

In these equations,  $a$  is the input signal-to-noise ratio, and all voltages are measured in multiples of the r-m-s noise. The optimum decision rule (8) can be written

$$\lambda^* \leq \sum_{k=1}^N \prod_{j=1}^n I_0(av_{jk}) = \sum_{k=1}^N \exp\left[\sum_{j=1}^n \log I_0(av_{jk})\right]. \quad (9)$$

The rule contains the expected signal-to-noise ratio  $a$ . This is to say, the decision rule can optimize the detection probability relative to only one such ratio. In an application, this would presumably be smallest signal-to-noise ratio which is considered of interest. For larger values of  $a$ , it is true, the rule would no longer produce strictly optimum results, but this is a circumstance which will not seem too disturbing since the situation grows less critical for stronger signals.

It may be instructive to compare this rule with the one obtained for the case of conventional point detection which is usually given, as in Reference (2):

$$\lambda \leq \sum_{j=1}^n \log I_0(av_{jk}).$$

The basis of comparison will, more particularly, be the following: The point detector will announce the presence and location of a signal, rightly or wrongly, whenever the quantity on the right matches or exceeds the constant on the left. In order to keep the comparison fair, the point detector will be given credit for having correctly announced the presence of the signal even if it announced its location incorrectly. That is to say, it will consider it to have made the correct decision even if it ignored the signal pulse at its actual location if only it sounded a false-alarm at some other location. However, the point detector will be charged with a false-alarm if, in the absence of a signal, it sounds an alarm anywhere in the interval.

Mathematically, this can perhaps be expressed as follows: A function  $\delta_k$  is introduced which is zero when the point-detector output remains below threshold at location  $k$  and unity if it exceeds the threshold. The point detection rule for the total interval can then be written

$$\sum_{k=1}^N \delta_k \left[ \sum_{j=1}^n \log I_o (av_{jk}) - \lambda \right] > 0. \quad (10)$$

This solution, according to the results derived here, is not optimum, a fact which could also be exhibited in principle by calculating the detection probabilities to which it leads, and by comparing to those achieved by the optimum (9). Unfortunately, such calculations are prohibitively laborious for the decision rules (9) and (10). Examples of cases in which such comparative calculations can be carried out are apparently quite rare, and one of the few which have been found is presented in the next section. What is more, the calculations have been somewhat unrewarding.

In all cases which could be evaluated explicitly, the detection probabilities which are obtained from the optimum rule (8) and its various specializations, developed to be only slightly better than those obtained from other common-sense rules. For small signal-to-noise ratios,  $a$ , for instance, which is a much studied special case, rules (9) and (10) can be shown to coincide. Evidence, in other words, circumstantial as it is, does not point to great gains in detection probabilities from using the optimum rule (9).

The two solutions to the detection problem, (9) and (10), can perhaps be also compared profitably in terms of some illustrative mechanizations, as shown in Figure 1. As can be seen, the two mechanizations are identical up to a point. Thus, the second detector should be strictly linear in both cases, and followed by a gain adjustment corresponding to the input signal-to-noise ratio,  $a$ . This should, in turn, be followed by a nonlinear element forming  $\log I_o (av)$ . The device should next record  $N$  points from each sweep, and add corresponding readings of  $n$  sweeps for each point ( $\Sigma_{1k}$ ). This is the point up to which the interval-detecting device is the same as the corresponding device for point detection. Beyond it, however, the data processing differs. For interval detection, the results of these  $N$  additions should be applied, through nonlinear elements ( $E$ ) with exponential transfer characteristics, to another integrator ( $\Sigma_2$ ) which would add these  $N$  sums. A comparison with threshold  $\lambda^*$  would ring the alarm. The threshold setting should be determined to insure the desired false-alarm probability.

For point detection, each sweep-to-sweep integration  $\Sigma'_{1k}$  is followed by a threshold  $\lambda$  and by a relay which closes when the threshold  $\lambda$  is exceeded. Paralleling of relay contacts for the  $N$  points of the sweep represents, in effect, the second summation in (10). Closing of any relay will then sound the alarm.

PERFORMANCE OF THE DEVICE IN A SPECIAL CASE

The idea that the device, called the interval detector above, should operate better than a conventional point detector is intuitively somewhat difficult to accept, especially when the detection interval is rather wide. The offhand reaction to the scheme is that the wider the interval, the more noise there is introduced and the poorer, accordingly, the decisions made.

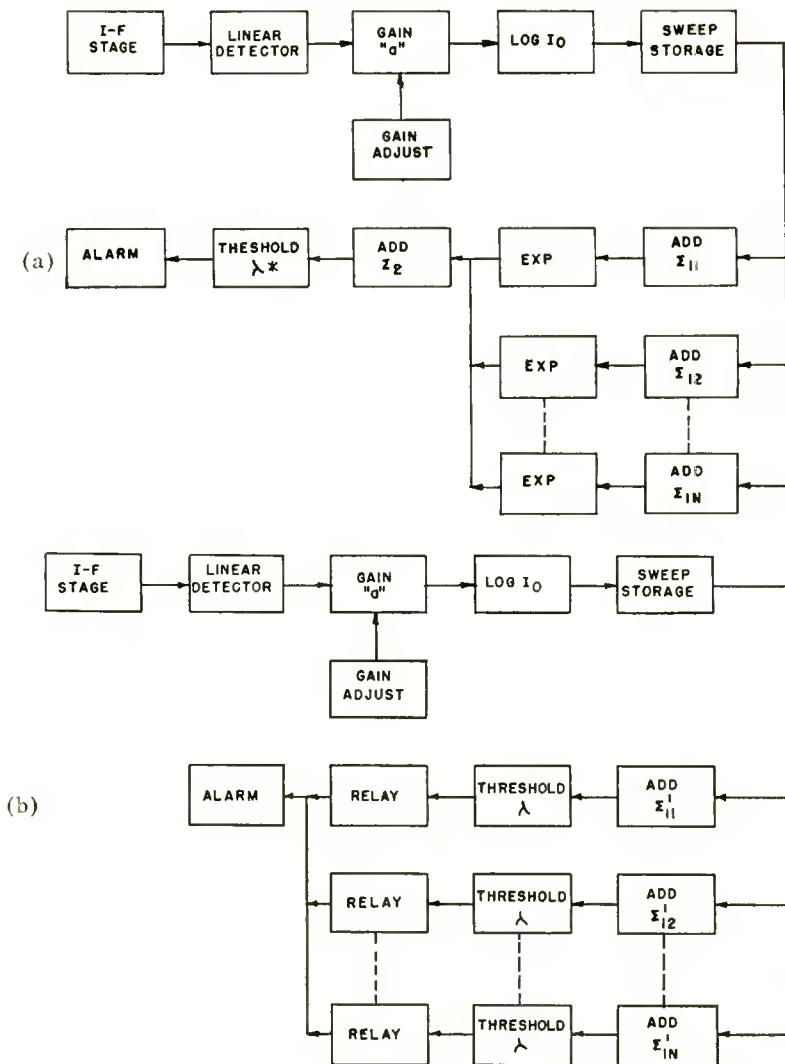


Fig. 1—Simplified video detection: (a) Illustrative mechanization of interval detector; (b) Illustrative mechanization of point detector.

For this reason, a special example will now be presented which shows that better performance can in fact be expected from interval detection than from point detection. The example is admittedly somewhat artificial, but it is apparently one of the few which can be carried through explicitly. It is, more particularly, the example which can be evaluated for the especially controversial case of very wide interval.

The basis of comparison will be the one proposed in the previous section. That is to say, the point detector, as well as the interval detector, will be charged with a false-alarm if it announces a signal somewhere in the interval despite its complete absence. They will both be allowed the same false-alarm probability  $P_{FA}$  and their detection thresholds will be adjusted accordingly. When it comes to detection, the point detector will not be penalized in any way for errors in location.

Also as in the preceding section, the input will be assumed sampled at  $N$  discrete points in each sweep, and the samples so obtained will be assumed statistically independent. The probability densities of the input voltages, however, will be assumed of the form (Type III of the Pearson system)

$$f_o(v_{jk}) = \frac{\beta_o^\alpha}{\Gamma(\alpha)} v_{jk}^{\alpha-1} \exp(-\beta_o v_{jk}), \quad (v_{jk} \geq 0)$$

if no signal is present, and

$$f_s(v_{jk}) = \frac{\beta_s^\alpha}{\Gamma(\alpha)} v_{jk}^{\alpha-1} \exp(-\beta_s v_{jk}), \quad (v_{jk} \geq 0)$$

if a signal is present. These are, of course, not the actual distribution functions of video voltages but can be made at least quite similar in shape if the parameters  $\alpha$  and  $\beta$  are suitably chosen.<sup>1</sup> They have, above all, the advantage of being more manageable, providing only that one can also assume

$$0 < \beta_s < \beta_o < 3/2 \beta_s, \quad n\alpha > 1.$$

Now, the development of the general decision procedure, as outlined by, say, Middleton for the best point-detection procedure, and here for interval detection, is applicable regardless of the specific formula for the probability distribution. One finds from (8) that, for optimum results, one should use

$$\sum_{k=1}^N \delta_k \left[ \sum_{j=1}^n v_{jk} - \lambda \right] > 0 \tag{11}$$

for point detection, and

$$\sum_{k=1}^N \exp \left[ (\beta_o - \beta_s) \sum_{j=1}^n v_{jk} \right] \geq \lambda^* \tag{12}$$

for interval detection.

Equations (11) and (12) imply two illustrative mechanizations which are shown in Figure 2. They are seen to be quite similar to those required for the case of video voltages in Figure 1.

The problem now is that of calculating the detection probabilities for these two decision rules. As mentioned earlier, this is to be done for the case of extremely wide detection intervals, that is to say, for very large  $N$ . The procedure by which the evaluation is carried out, of interest in that it exhibits the sort of difficulties which are encountered in calculations of this nature, is contained in the Appendix.

The result is the following. One finds for the detection probability of the point detector at large values of  $N$  (Equation (17))

$$P_D = P_{FA} - \left[ \frac{(\log N)^\gamma}{N} - \frac{1}{N} \right] (1 - P_{FA}) \log (1 - P_{FA}) + \dots$$

where

$$\gamma = (n\alpha - 1) \frac{\beta_o - \beta_s}{\beta_o}$$

The corresponding expression for the interval detector is (Equation (20))

$$P_D^* = P_{FA} - \frac{1}{\sqrt{2\pi N}} \frac{m_o - m_s}{\sigma_o} \exp \left[ -\frac{(\lambda^* - Nm_o)^2}{\sigma_o^2 N} \right] + \dots$$

where

$$\begin{aligned} m_o &= [\beta_o/\beta_s]^{n\alpha} \\ m_s &= [\beta_s/(2\beta_s - \beta_o)]^{n\alpha} \\ \sigma_o^2 &= m_o (m_s - m_o). \end{aligned}$$

The comparison of  $P_D$  and  $P_D^*$  is this: For  $N = \infty$ , they are equal. They both reduce to  $P_{FA}$ . For large  $N$ ,  $P_D$  decreases to  $P_{FA}$  as  $(\log$

$N)\gamma/N$ , that is, more slowly than the corresponding term in  $P_D^*$  which is proportional to  $N^{-\frac{1}{2}}$ . This is true regardless of the magnitude of  $\gamma$ . Hence  $P_D^*$  will attain higher values at large  $N$  than  $P_D$ .

The conclusion reached is, therefore, the following: For very wide detection intervals (large  $N$ ), that is, for the case which seems intuitively the least plausible, the probability of interval detection is higher than of point detection. This may make the general result obtained above more readily acceptable. The virtue of this sample case, in which  $P_{FA}$  and  $P_D$  necessarily approach equality, lies in its mathematical tractability. No great practical importance is claimed for it.

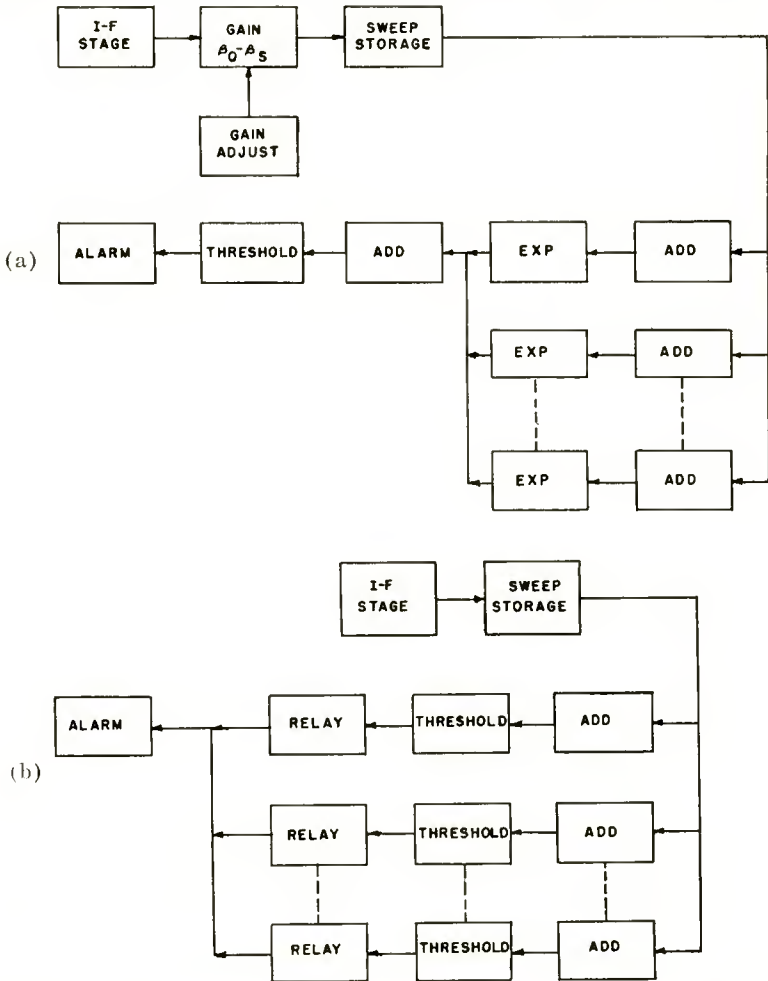


Fig. 2—Special example: (a) Illustrative mechanization of interval detector; (b) Illustrative mechanization of point detector.

## APPENDIX—EVALUATION OF ASYMPTOTIC DETECTION PROBABILITIES FOR SPECIAL EXAMPLE

The problem here is to derive expressions for the detection probabilities encountered in the special examples. The probability densities are assumed of the form

$$f_o(v_{jk}) = \frac{\beta_o^\alpha}{\Gamma(\alpha)} v_{jk}^{\alpha-1} \exp(-\beta_o v_{jk}) \quad (v_{jk} \geq 0)$$

when no signal is present, and

$$f_s(v_{jk}) = \frac{\beta_s^\alpha}{\Gamma(\alpha)} v_{jk}^{\alpha-1} \exp(-\beta_s v_{jk}) \quad (v_{jk} \geq 0)$$

when a signal is present. The constants  $\beta_o$  and  $\beta_s$  are restricted by the relation  $0 < \beta_s < \beta_o < (3/2)\beta_s$ .

The detection rules obtained for this example are

$$\sum_{k=1}^N \delta_k \left[ \sum_{j=1}^n v_{jk} - \lambda \right] > 0 \quad (11)$$

if point detection is used, and

$$\sum_{k=1}^N \exp \left[ (\beta_o - \beta_s) \sum_{j=1}^n v_{jk} \right] \geq \lambda^* \quad (12)$$

if interval detection is relied upon. In both cases, expressions are needed for the detection probabilities for large values of  $N$ . The two procedures will be considered separately, point detection being taken up first.

*Point Detection*

To evaluate the case of point detection, the random variable

$$\mu_k = \sum_{j=1}^n v_{jk}$$

is introduced. This has the distribution function<sup>9</sup>

<sup>9</sup> E.g., H. Cramer, "Mathematical Methods in Statistics," Princeton University Press, p. 234, 1946.

$$F_o(\mu_k) = \frac{\beta_o^{n\alpha}}{\Gamma(n\alpha)} \int_0^{\mu_k} x^{n\alpha-1} \exp(-\beta_o x) dx \quad (13)$$

when no signal is present at the point  $k$  and

$$F_s(\mu_k) = \frac{\beta_s^{n\alpha}}{\Gamma(n\alpha)} \int_0^{\mu_k} x^{n\alpha-1} \exp(-\beta_s x) dx \quad (14)$$

when a signal is present at that point.

Point detection will occur, according to the convention stated in Equation (11), when the inequality

$$\sum_{j=1}^n v_{jk} \geq \lambda$$

is satisfied at least once in the whole interval. This will happen with the (given) false-alarm probability,

$$P_{FA} = 1 - [F_o(\lambda)]^N \quad (15)$$

when no signal is present, and with the detection probability

$$P_D = 1 - [F_o(\lambda)]^{N-1} F_s(\lambda) = 1 - [1 - P_{FA}] \frac{F_s(\lambda)}{F_o(\lambda)} \quad (16)$$

when a signal is present at one of the  $N$  points.

The problem at hand is the investigation of the behavior of  $P_D$  as  $N$  becomes very large. From (16), this is equivalent to the problem of determining the asymptotic behavior of  $F_s(\lambda)/F_o(\lambda)$  as  $N$  in (15) approaches infinity. Now, for large  $N$ ,  $\lambda$  will have to be large in order to maintain Equation (15). In fact, since for large  $\lambda$

$$F_o(\lambda) \simeq 1 - \frac{(\beta_o \lambda)^{n\alpha-1}}{\Gamma(n\alpha)} \exp(-\beta_o \lambda)$$

$$F_s(\lambda) \simeq 1 - \frac{(\beta_s \lambda)^{n\alpha-1}}{\Gamma(n\alpha)} \exp(-\beta_s \lambda)$$

then from Equation (15)

$$\beta_o \lambda \approx \log N - \log [\Gamma(n\alpha) P_{FA}] - (n\alpha - 1) \log \beta_o \lambda \approx \log N.$$

The ratio  $F_s/F_o$  can, for large  $N$ , be represented by

$$\frac{F_s(\lambda)}{F_o(\lambda)} \approx 1 - \frac{1}{\Gamma(n\alpha)} [(\beta_s \lambda)^{n\alpha-1} \exp(-\beta_s \lambda) - (\beta_o \lambda)^{n\alpha-1}$$

$$\exp(-\beta_o \lambda)] = [1 - (1 - P_{FA})^{1/N}] (\beta_o \lambda)^\gamma + [1 - (1 - P_{FA})^{1/N}]$$

where

$$\lambda = (n\alpha - 1) \frac{\beta_o - \beta_s}{\beta_s} > 0.$$

The asymptotic expression required here is, therefore,

$$\frac{F_s(\lambda)}{F_o(\lambda)} = 1 + \left[ \frac{(\log N)^\gamma}{N} - \frac{1}{N} \right] \log(1 - P_{FA}) + \dots$$

The corresponding expression for the detection probability  $P_D$  is

$$P_D = P_{FA} - \left[ \frac{(\log N)^\gamma}{N} - \frac{1}{N} \right] (1 - P_{FA}) \log(1 - P_{FA}) + \dots \quad (17)$$

which shows that, in the limit,  $P_D$  decreases to  $P_{FA}$ , and that the rate of approach will, for large  $N$ , be governed by the term proportional to  $(\log N)^\gamma/N$ . This will be the important term in the comparison with the next case.

### Interval Detection

The decision rule for interval detection is given by (12). Let  $w$  denote the random variable

$$w = \sum_{k=1}^N \exp \left[ (\beta_o - \beta_s) \sum_{j=1}^n v_{jk} \right] \quad (18)$$

and let  $F_o^*(w)$  be the distribution function of  $w$  if no signal is present at any point of the interval, and  $F_s^*(w)$  the distribution when a signal is present, regardless of where. (Asterisks will be used to distinguish quantities which apply to interval detection from their counterparts in the point detection problem.) Then

$$P_{FA} = 1 - F_o^* (\lambda^*)$$

for the false-alarm probability (which, for the purpose of the comparison, is the same numerically as in the case of point detection), and

$$P_D^* = 1 - F_s^* (\lambda^*)$$

for the detection probability. The latter must now be calculated, assuming that the former is given. This will again be done for the case of large  $N$ .

In this case,  $w$  in (18) is the sum of  $N$  independent variables

$$Z_k = \exp (\beta_o - \beta_s) \mu_k$$

where  $\mu_k$  has the same meaning as before and has the distribution functions (13) or (14). The  $z_k$ , therefore, have the distribution functions, respectively,

$$F_s \left( \frac{z_k}{\beta_o - \beta_s} \right) \text{ and } F_o \left( \frac{z_k}{\beta_o - \beta_s} \right)$$

depending on whether or not  $k$  is a point containing a signal pulse. The means and dispersions of these two functions are

$$m_s = \left( \frac{\beta_s}{2\beta_s - \beta_o} \right)^{n\alpha}$$

$$m_o = \left( \frac{\beta_o}{\beta_s} \right)^{n\alpha}$$

$$\sigma_s^2 = m_s \left[ \left( \frac{2\beta_s - \beta_o}{3\beta_s - 2\beta_o} \right)^{n\alpha} - \left( \frac{\beta_s}{2\beta_s - \beta_o} \right)^{n\alpha} \right]$$

$$\sigma_o^2 = m_o \left[ \left( \frac{\beta_s}{2\beta_s - \beta_o} \right)^{n\alpha} - \left( \frac{\beta_o}{\beta_s} \right)^{n\alpha} \right]$$

It is a straightforward matter to convince oneself that, under the restrictions imposed here on  $\beta_o$  and  $\beta_s$ ,

$$m_s - m_o > 0, \quad \sigma_s^2 - \sigma_o^2 > 0. \quad (19)$$

Now, since  $w$  is the sum of a large number of independent variables,

it will be approximately normally distributed. That is, if  $\phi(y)$  represents the standardized gaussian distribution function,

$$P_{FA} = 1 - \phi\left(\frac{\lambda^* - Nm_o}{\sigma_o \sqrt{N}}\right)$$

$$P_D^* = 1 - \phi\left(\frac{\lambda^* - (N-1)m_o - m_s}{\sqrt{(N-1)\sigma_o^2 + \sigma_s^2}}\right)$$

(these should, strictly, be written as Edgeworth series<sup>10</sup>, and could be, without affecting the argument which follows.) The arguments of these functions do not differ by much, relatively, for large  $N$ . In fact if, for brevity, we let

$$\frac{\lambda^* - Nm_o}{\sigma_o \sqrt{N}} = w_o$$

$$\frac{\lambda^* - (N-1)m_o - m_s}{\sqrt{(N-1)\sigma_o^2 + \sigma_s^2}} = w_o + \delta w$$

then

$$\delta w = \frac{m_o - m_s}{\sqrt{N}\sigma_o} + \frac{w_o}{2} \frac{\sigma_o^2 - \sigma_s^2}{N\sigma_o^2} + \dots$$

which, by (18), will be negative for large  $N$ . Hence,

$$P_D^* = P_{FA} - \frac{\delta w}{\sqrt{2\pi}} \exp\left(-\frac{w_o^2}{2}\right) + \dots \quad (20)$$

The detection probability,  $P_D^*$  will, accordingly, decrease to the false-alarm probability, for increasing  $N$  as  $1/\sqrt{N}$ .

This expression, and its counterpart (17), are used in the body of the paper.

<sup>10</sup> Reference (9), p. 228.

## RCA TECHNICAL PAPERS†

Second Quarter, 1955

Any request for copies of papers listed herein should be  
addressed to the publications to which credited.\*

"Additional Nomographs for Significance Tests," C. H. Li, <i>ASTM Bulletin</i> , No. 205 (April) .....	1955
"Antenna System for Missile Telemetry," G. E. Bower and J. B. Wynn, Jr., <i>Electronics</i> (June) .....	1955
"Behind the Phosphor Curtain—A Glimpse of Television Picture Tubes and Color," H. C. Moodey, <i>Smith Alumnae Quarterly</i> (Spring) .....	1955
"Bias and Drive Considerations for Three-Gun Color Kinescopes," R. N. Rhodes and C. G. Seright, <i>RCA Industry Service Laboratory Bulletin LB-984</i> (June 24) .....	1955
"The BK-5A Uniaxial Microphone," J. W. O'Neill and R. M. Carrell, <i>Broadcast News</i> (May) .....	1955
"The BK-6A Microphone," L. M. Wigington and R. M. Carrell, <i>Broadcast News</i> (May) .....	1955
"Color-Video Envelope-Delay Measurement," R. C. Kennedy and H. French, <i>Electronics</i> (June) .....	1955
"Designing 2,000-Mc Components for Communications," N. C. Colby, <i>Electronics</i> (May) .....	1955
"Development of the Premium Ultra-High-Frequency Triode 6J4-WA," G. W. Barclay, <i>RCA Review</i> (June) .....	1955
"Development of the RCA 21-Inch Metal-Envelope Color Kinescope," H. R. Seelen, H. C. Moodey, D. D. VanOrmer, and A. M. Morrell, <i>Elec. Eng.</i> (April) .....	1955
"A Developmental Pocket-Size Broadcast Receiver Employing Transistors," D. D. Holmes, T. O. Stanley, and L. A. Freedman, <i>Proc. I.R.E.</i> (June) .....	1955
"Discharging an Insulator Surface by Secondary Emission Without Redistribution," A. S. Jensen, <i>RCA Review</i> (June) .....	1955
"The Effect of Initial Noise Current and Velocity Correlation on the Noise Figure of Traveling-Wave Tubes," S. Bloom, <i>RCA Review</i> (June) .....	1955
"The Effective Surface Recombination of a Germanium Surface with a Floating Barrier," A. R. Moore and W. M. Webster, <i>Proc. I.R.E.</i> (April) .....	1955
"Electromechanical Filters for 100 KC Carrier and Sideband Selection," R. W. George, <i>RCA Industry Service Laboratory Bulletin LB-981</i> (June 2) .....	1955
"Electron Voltaic Study of Electron Bombardment Damage and its Thresholds in Ge and Si," J. J. Loferski and P. Rappaport, <i>Phys. Rev.</i> (Letter to the Editor) (June 15) .....	1955
"Electronic Music Synthesizer," H. F. Olson and H. Belar, <i>Jour. Acous. Soc. Amer.</i> (May) .....	1955

† Report all corrections or additions to RCA Review, RCA Laboratories, Princeton, N. J.

\* *RCA Industry Service Laboratory Bulletins* are not published and are issued only as a service to licensees of the Radio Corporation of America.

- "An Experimental Automobile Receiver Employing Transistors," L. A. Freedman, T. O. Stanley, and D. D. Holmes, *Proc. I.R.E.* (June) ..... 1955
- "An Experimental High-Speed Photo-Resist Technique for Printed Circuits," M. L. Sugarman, Jr., *RCA Industry Service Laboratory Bulletin LB-978* (May 19) ..... 1955
- "First Microwave System for 2450-2700 Mc.," P. A. Greenmeyer and S. Lapenson, *Radio-Electronic Engineering* (April) ..... 1955
- "Frequency Characteristics of Local Oscillators," W. Y. Pan, *RCA Industry Service Laboratory Bulletin LB-980* (May 25) ..... 1955
- "High-Gain Transistor Amplifier," J. J. Davidson, *RCA Engineer* (June-July) ..... 1955
- "High-Power UHF-TV Uses Grid-Control Tube," L. L. Koros, *Electronics* (April) ..... 1955
- "How to Make an 'Illuminant C' Grey Scale Monitor," E. P. Bertero, *Broadcast News* (May) ..... 1955
- "How to Plan for Color Television Broadcasting—Part III," L. E. Anderson and W. O. Hadlock, *Tele-Tech* (April) ..... 1955
- "An Immittance Chart," H. M. Wasson, *RCA Industry Service Laboratory Bulletin LB-976* (April 6) ..... 1955
- "An Immittance Sweep," R. W. Sonnenfeldt, *RCA Engineer* (June-July) ..... 1955
- "Increasing Creativeness in Engineers," C. D. Tuska, *RCA Engineer* (June-July) ..... 1955
- "Introduction to 'Engineering the World's First 1000-KW TV Station,'" W. O. Hadlock, *RCA Engineer* (June-July) ..... 1955
- "Large-Screen Color-Television Projection," L. L. Evans and R. V. Little, Jr., *Jour. S.M.P.T.E.* (April) ..... 1955
- "Luminous Microflux Standard," R. W. Engstrom, *Rev. Sci. Instr.* (June) ..... 1955
- "Magnetic Head Wear Investigation," M. Rettinger, *Jour. S.M.P.T.E.* (April) ..... 1955
- "Magnetic Properties of Zinc Sulfide and Cadmium Sulfide Phosphors," S. Larach and J. Turkevich, *Phys. Rev.* (May 15) ..... 1955
- "Measurement of Minority Carrier Lifetime and Surface Effects in Junction Devices," S. R. Lederhandler and L. J. Giacoletto, *Proc. I.R.E.* (April) ..... 1955
- "Measurement of Shot Noise in CdS Crystals," C. I. Shulman, *Phys. Rev.* (April 15) ..... 1955
- "The Measurement of Wind Noise in Microphones," R. M. Carrell, *Broadcast News* (May) ..... 1955
- "Motion-Picture Photography in Guided-Missile Research," W. A. Price and Ernest H. Ehling, *Jour. S.M.P.T.E.* (June) ..... 1955
- "New Distribution Amplifiers for Television Broadcasting Studios," R. G. Thomas, *Broadcast News* (May) ..... 1955
- "A New Method for Magnifying Electron Beam Images," W. R. Beam, *RCA Review* (June) ..... 1955
- "New Portable Direction Finder for Pleasure Craft," H. F. Mohr, *RCA Engineer* (June-July) ..... 1955
- "New Techniques in Color Demodulation," W. W. Cook, *Radio-Electronics* (May) ..... 1955
- "A Novel UHF High-Power-Amplifier System," L. L. Koros, *RCA Review* (June) ..... 1955
- "On the Possibility of Amplification in Space-Charge-Potential-Depressed Electron Streams," W. R. Beam, *Proc. I.R.E.* (April) ..... 1955

"The Philosophy of JETEC Tube-Type Designations," R. S. Burnap, <i>RCA Engineer</i> (June-July) .....	1955
"The Planets and TV DX," J. H. Nelson, <i>Radio-Electronics</i> (May) ..	1955
"Plasma Ion Oscillations in Electron Beams," K. G. Hernqvist, <i>Jour.</i> <i>Appl. Phys.</i> (May) .....	1955
"Principles of Light Amplification," D. W. Epstein, <i>RCA Engineer</i> (June-July) .....	1955
"Producing Formed and Inside-Out Grids for UHF Pencil Tubes," H. J. Ackerman, <i>Electronics</i> (May) .....	1955
"Product Quality as Influenced by Field Data," W. J. Zaun, <i>RCA</i> <i>Engineer</i> (June-July) .....	1955
"The Radechon, a Barrier Grid Storage Tube," A. S. Jensen, <i>RCA</i> <i>Review</i> (June) .....	1955
"Radechon Storage Tube Circuits," A. S. Jensen and G. W. Gray, <i>RCA Review</i> (June) .....	1955
"The RCA Model 21CT662U 21-Inch Color Television Receiver," <i>RCA</i> <i>Industry Service Laboratory Bulletin LB-982</i> (June 8) .....	1955
"Re 'Low-Impedance Transmission Lines,'" W. C. Morrison, <i>QST</i> (April) (Letter to the Editor) .....	1955
"Retrograde Motion in Gas Discharge Plasmas," K. G. Hernqvist and E. O. Johnson, <i>Phys. Rev.</i> (June 15) .....	1955
"Ring Type Teflon Gasket," E. C. Giaimo, Jr., <i>Rev. Sci. Instr.</i> (May)	1955
"Russian Vacuum-Tube Terminology," I. G. Maloff, <i>Proc. I.R.E.</i> (April) (Letter to the Editor) .....	1955
"Short-Circuit Protection for Meters," P. Koustas, <i>Rad. and Tele.</i> <i>News</i> (June) .....	1955
"Some Electrical Characteristics of Electrofax Coatings on Metallic and Paper Supports," E. C. Giaimo, Jr., <i>RCA Industry Service</i> <i>Laboratory Bulletin LB-983</i> (June 10) .....	1955
"Sound-Effects Track Noise-Suppressor," J. F. Byrd, <i>Jour. S.M.P.T.E.</i> (June) .....	1955
"Spectrographic Determination of Lead in Oxygen-Free, High-Con- ductivity Copper," S. B. Deal, <i>Analytical Chemistry</i> (May) ..	1955
"Subjective Loudspeaker Testing," H. F. Olson, <i>Proceedings of The</i> <i>Institution of Radio Engineers Australia</i> (April) .....	1955
"Temperature Dependence of the Width of the Band Gap in Several Photoconductors," R. H. Bube, <i>Phys. Rev.</i> (April 15) .....	1955
"Temperature Effects in Circuits Using Junction Transistors," H. C. Lin and A. A. Barco, <i>RCA Industry Service Laboratory Bul-</i> <i>letin LB-979</i> (May 19) .....	1955
"The Transfluxor—A Magnetic Gate with Stored Variable Setting," J. A. Rajchman and A. W. Lo, <i>RCA Review</i> (June) .....	1955
"A UHF-VHF Television Tuner Using Pencil Tubes," W. A. Harris and J. J. Thompson, <i>RCA Review</i> (June) .....	1955
"The Ultra-Gain, High-Power UHF Antenna," E. H. Shively, <i>RCA</i> <i>Engineer</i> (June-July) .....	1955
"Unusual Assembly Methods Used in Developing a New Thyatron," N. R. Goldstein, <i>Ceramic Age</i> (May) .....	1955
"What the Engineer Has Meant to Communication," E. W. Engstrom, <i>Elec. Eng.</i> (April) .....	1955
"Why Engineers Should Write Papers," M. S. Corrington, <i>RCA</i> <i>Engineer</i> (June-July) .....	1955
"Wider Screens in Drive-Ins," R. H. Heacock, <i>International Pro-</i> <i>jectionist</i> (April) .....	1955
"World's First 25-KW UHF Transmitter," J. E. Joy, <i>RCA Engineer</i> (June-July) .....	1955

- "A 15-Kilowatt Beam Power Tube for UHF Service," W. P. Bennett,  
*RCA Engineer* (June-July) ..... 1955
- "144-Megacycle Transmitter (72 Watts Input on 155 Mc with an  
RCA-5894)," R. M. Mendelson, *Ham Tips* (May) ..... 1955

## AUTHORS

W. R. BEAM—(See *RCA Review*, Vol. XVI, No. 2, June 1955, p. 315.)



ARTHUR H. BENNER received the B.S. degree in Electrical Engineering from the University of Kansas in 1944, the M.S. degree in 1948, and the Ph.D. degree in 1951 from Pennsylvania State College. From 1944 to 1946, he served as an officer in the U. S. Army Signal Corps. From 1946 to 1949 he was a research engineer with the Ordnance Research Laboratory, State College, Pa., and from 1949 through 1950 he was associated with the Radio Propagation Laboratory at Pennsylvania State College. He has been with RCA since 1950, and at present is a group leader in the Analytical Group of the

Advanced Development Engineering Section of the Engineering Products Division. Dr. Benner is a member of Sigma Xi and Tau Beta Pi, and a Senior Member of the Institute at Radio Engineers.

WILFRED P. BENNETT received the B.S. degree in Electrical Engineering from Michigan State College in 1944. Upon graduation, he was engaged by the Radio Corporation of America at Lancaster, Pa., where he is at present in the Power Tube Engineering Group working on the design and development of tubes for uhf television and pulse applications. Mr. Bennett is a member of the Institute of Radio Engineers and of Tau Beta Pi.



HAROLD H. BEVERAGE received the B.S. degree in Electrical Engineering in 1915, and Doctor of Engineering in 1938 from the University of Maine. Following his graduation, he was associated with Dr. E. F. W. Alexanderson at Schenectady for four years, transferring to RCA in 1920. He was appointed Chief Research Engineer of RCA Communications, Inc. in 1929, and Vice President in Charge of Research and Development in 1942. The Research and Development activities of RCA Communications, Inc. were consolidated with the RCA

Laboratories in 1942. Dr. Beverage is now Director of Radio Research for RCA Laboratories.

KERN K. N. CHANG—(See *RCA Review*, Vol. XVI, No. 1, March 1955, p. 172.)



C. C. CHENG received the B.S. degree in Electrical Engineering in 1943 from the National Central University of China and the M. Sc. degree in Communication Engineering in 1946 from Harvard University, and has done further graduate study at the Polytechnic Institute of Brooklyn. He was associated with the National Resources Commission of China from 1943 to 1944, and with the Westinghouse Electric Co. and the Central Electric Company of China from 1946 to 1949. In 1952, he joined the Engineering Products Department of the RCA Victor Division in Camden, N. J., where he was engaged in advanced

development work on transistor circuitry and network theory. Since his transfer to the Tube Division in Harrison, N. J. in 1954, he has been working on transistor circuitry and transistor noise theory. Mr. Cheng is the co-author of a book entitled *Transistor Electronics*, to be published by Prentice-Hall, Inc.

R. F. DRENICK graduated from the University of Vienna in 1939 with the degree of Ph.D. in Theoretical Physics. He was assistant professor for mathematics and physics at Villanova College from 1939 to 1944. During his military service, he assisted in the evaluation of captured German documents, particularly of the technical reports dealing with German guided missiles development. From 1946 to 1949, he was employed by the General Electric Co., where he worked on the mathematical problems of a guided missiles project. He has been with RCA, Camden since 1949. Dr. Drenick is now the manager of the Analytical Group of Advanced Development Engineering.



EDMUND A. LAPORT attended Northeastern University, Massachusetts University Extension, and McGill University. In 1924 he joined the Westinghouse Electric and Manufacturing Company of Springfield, Mass., as a radio engineer. From 1933 to 1934 he was with the Paul Godley Company, Montclair, N. J., and from 1934 to 1936 with Wired Radio, Inc., of Ampere, N. J. In 1936 he became associated with the RCA Victor Division, Camden, N. J.; in 1938, Chief Engineer of engineering products in the RCA Victor Company Limited, Montreal; and in 1944, Chief Engineer of the RCA International Division, New

York. Since November 1954 he has been Administrative Engineer—Communications, for the Radio Corporation of America. Mr. Laport is a Fellow of the Institute of Radio Engineers.

ARCH C. LUTHER, JR., received the B.S. degree in Electrical Engineering from the Massachusetts Institute of Technology in 1950. During the summers of 1947 and 1948 he worked for the Philco Corporation, and during the summer of 1949 at station WFIL-TV in Philadelphia. In 1950 he joined the Broadcast Studio Engineering section of RCA in Camden, N. J. where he has worked on live pickup and film color cameras, sync generators, and various military television projects. Mr. Luther is an Associate Member of the Institute of Radio Engineers and a member of the Eta Kappa Nu and Sigma Xi.





WEN YUAN PAN received the E.E. Degree from Stanford University in 1939, and the Ph.D. Degree in Electrical Engineering in 1940. He served in an advisory capacity to the China Defense and Supplies in 1941 and to the Chinese Delegation to the International Civil Aviation Conference in 1944. He was engaged as a research scientist at the Radio Research Laboratory at Cambridge, Massachusetts, during the war years and was invited to be a member of the Advisory Committee of the United Nations Telecommunications in 1946. Since 1945, he has been with the RCA Victor Division at Camden, New

Jersey. Dr. Pan is an honorary member of the Veterans' Wireless Operators Association, a member of Sigma XI and Senior Member of the Institute of Radio Engineers.

JACQUES I. PANKOVE received the B.S. degree in Electrical Engineering in 1944 and the M.S. degree in Electronic Engineering 1948 from the University of California in Berkeley. From 1944 to 1946 he served with the United States Army. Since 1948 he has been engaged in semiconductor research at RCA Laboratories in Princeton, N. J. Mr. Pankove is a Member of Sigma Xi and a Senior Member of the Institute of Radio Engineers.



LEROY C. SIMPSON received the B.S. degree in Electrical Engineering from the University of New Hampshire in 1928. From 1928 to 1934 he was engaged in the design and installation of high power transmitters for the General Electric Company. In 1934 he joined RCA Victor Argentina, S.A. as Manager of the Engineering Products Division, and was concerned with the production, sale and installation of communications equipment. Since 1948 he has been with RCA International Division in New York, N. Y. and Clark, N. J. where he is now Manager of Systems Projects. Mr. Simpson is a Senior

Member of the Institute of Radio Engineers.

JAKOB ZAWELS served an electrical engineering apprenticeship with the South African Iron and Steel Corporation, and received the B. Sc. (Eng.) degree from the University of Cape Town in 1949. In 1950 he joined the General Electric Company in the United States as a member of the Advanced Engineering Program, subsequently receiving the M.S. degree from the Massachusetts Institute of Technology. He then joined the transistor circuit development group of the RCA Victor Division. In 1953 he joined the S. A. Iron and Steel Industrial Corporation in the Union of South Africa where he is engaged in development work. Mr. Zawels is an Associate Member of Sigma Xi and the South African and British Institutes of Electrical Engineers, and a Member of the Institute of Radio Engineers.



